

THESIS

METHODOLOGY FOR UNCERTAINTY-BASED INSPECTION PLANNING OF
CONCRETE BRIDGE DECKS USING MECHANISTIC MODELS OF CRACK FORMATION
AND PROPAGATION

Submitted by

Patrick Sanders

Department of Civil and Environmental Engineering

In partial fulfillment of the requirements

For the Degree of Master of Science

Colorado State University

Fort Collins, Colorado

Summer 2015

Master's Committee:

Advisor: Rebecca Atadero

Co-Advisor: Mehmet Ozbek

Bolivar Senior

Copyright by Patrick Sanders 2015

All Rights Reserved

ABSTRACT

METHODOLOGY FOR UNCERTAINTY-BASED INSPECTION PLANNING OF CONCRETE BRIDGE DECKS USING MECHANISTIC MODELS OF CRACK FORMATION AND PROPAGATION

The bridge inspection program in the United States started in 1971 following the collapse of the Silver Bridge in Ohio. Since then, bridges have generally been inspected every two years. This uniform inspection interval for all bridges is not the most efficient system for conducting inspections because many bridges do not require inspections this frequently, and leads to unnecessary use of inspection resources on bridges that do not require them. Efforts toward changing the bridge inspection program to a risk-based program are being made. Such a program would allow for bridge inspection timing to be based on each particular bridge's need, and each bridge would then be inspected for the components that present the highest risk to the structure.

The research presented herein focuses on using the uncertainty in the current condition of concrete bridge decks to plan inspection timing, and to plan inspection type based on limited resources. A mathematical program called Concrete Deck Cracking Probability Model (CDCPM) is written in MATLAB to model the uncertainty in the occurrence of transverse cracking and delamination in the deck. Through literature review, mechanistic models of the processes that affect cracking are determined and implemented in the program. Using Monte Carlo simulations, the uncertainty in the occurrence of cracking and delamination is analyzed based on the input parameter uncertainty. The effect of different climates and mechanistic models on the prediction of cracking is explored using CDCPM. This model is then applied to a

bridge in Larimer County, Colorado to see how the results compare to actual inspection results, and then the model is used to plan a future delamination inspection on the bridge. Another scenario is investigated where CDCPM is used together with uncertainty forecast plots to allocate inspection resources to two bridge decks.

CDCPM revealed that the uncertainty in the current bridge condition is heavily influenced by the mechanistic models chosen for the analysis, as well as some of the parameters used in the models. The surface chloride content has a large effect on the delamination of the concrete deck, while the relative humidity and ambient temperature for a given location can affect the probability of transverse cracking. Analysis of the Larimer County bridge inspection reports showed that the model can be good indicator of future damage to the deck. The model provides unique insight into inspection planning using uncertainty. Using the model output along with uncertainty forecast plots of different inspection methods, the inspection manager is provided with a useful planning tool that gives information on the effect of inspection methods on bridge condition assessment. Suggestions for implementing the bridge inspection plan for agency use is also provided.

ACKNOWLEDGEMENTS

The author would like to thank his advisors, Dr. Rebecca Atadero and Dr. Mehmet Ozbek, for their continued guidance and support while conducting this research and writing this thesis. Their insight and ideas have been invaluable in ensuring a well-structured and complete project. Also, thank you to Dr. Bolivar Senior for serving on my thesis defense committee.

The author would also like to thank the Mountain Plains Consortium, a United States DOT research program, for funding this project. A special thanks also goes to Mr. Ron Winnie at the Larimer County Engineering Department for providing design drawings and inspection reports for bridge LR 50-0.2-17. The provided information was crucial to the analysis in this research.

A special thanks also goes out to the author's parents, family, and friends that have provided support and encouragement throughout his college experience.

TABLE OF CONTENTS

ABSTRACT.....	ii
ACKNOWLEDGEMENTS.....	iv
TABLE OF CONTENTS.....	v
LIST OF TABLES.....	viii
LIST OF FIGURES.....	ix
LIST OF ACCRONYMS.....	xii
1. INTRODUCTION.....	1
1.1 Background on Bridge Condition and Inspection Planning.....	1
1.2 Research Objectives.....	6
1.3 Research Approach.....	7
1.4 Thesis Structure.....	8
2. LITERATURE REVIEW.....	9
2.1 Probabilistic Representation of Uncertainty.....	9
2.1.1 Sources of Uncertainty in Structural Reliability.....	10
2.1.2 Limit State Functions and Monte Carlo Simulation.....	11
2.1.3 Bayes' Theorem.....	15
2.2 Previous and Current Bridge Inspection Practice.....	16
2.2.1 National Bridge Inspection Standards (NBIS).....	16
2.2.2 FHWA Recording and Coding Guide.....	18
2.2.3 AASHTO Manual for Bridge Evaluation.....	20
2.3 New Approaches to Bridge Inspection Timing and Planning.....	22
2.3.1 Risk-Based Inspection Planning-NCHRP Report 782.....	22
2.3.2 Inspection Planning Based on Statistical Analysis of Past Bridge Condition.....	25
2.3.3 Inspection Time and Maintenance Type Using Markov Chains.....	27
2.4 Analysis and Uncertainty in Concrete Deck Cracking.....	30
2.4.1 Causes of Concrete Deck Cracking.....	31
2.4.2 Subsidence Cracking in Concrete.....	33
2.4.3 Creep and Shrinkage of Concrete.....	34
2.4.4 Temperature.....	37
2.4.5 Freeze/Thaw Cycling of Concrete Pore Water.....	38

2.4.6	Corrosion Model	39
2.4.7	Uncertainty in Model Accuracy and Precision	42
2.4.8	Variance-Based Sensitivity Analysis	42
2.5	Inspection Methods and Testing Uncertainty	44
2.5.1	Visual Inspection	45
2.5.2	Mechanical Sounding.....	46
2.5.3	Ground Penetrating Radar.....	48
2.5.4	Infrared Thermography.....	49
2.5.5	Impact-Echo	50
3.	METHODS	51
3.1	Model Development and Updating	51
3.1.1	Subsidence Cracking Model	53
3.1.2	Temperature Model.....	54
3.1.3	Shrinkage Model.....	56
3.1.4	Creep Model.....	58
3.1.5	Chloride Diffusion Model for Corrosion Initiation	62
3.1.6	Time-to-Cracking Model for Corrosion.....	64
3.1.7	Combining Models to Determine Formation of Vertical Cracks.....	65
3.1.8	Combining Concrete Effects to Determine Delaminations	69
3.2	Modeling of Larimer County Bridge LR 50-0.2-17.....	71
3.3	Incorporating Inspection Results into Model and Projecting the Future Condition	76
3.3.1	Updating the Current Condition with Inspection Results for Delamination.....	76
3.3.2	Projecting the Future Condition Post-Inspection	78
3.4	Sensitivity Analysis for Vertical Cracking and Delamination	79
3.5	Determination of Parameter Values for Climate Analysis.....	81
3.5.1	Humidity Parameters	81
3.5.2	Temperature Parameters	82
3.5.3	Chloride Concentration Parameters	85
3.6	Use of Uncertainty in Inspection Planning	86
3.6.1	Analysis of Past Inspection Results Based on Model Prediction	87
3.6.2	Predicting Future Inspection Strategy.....	88
3.6.3	Inspection Decision between Two Decks	89
4.	RESULTS AND ANALYSIS.....	93
4.1	Development of Uncertainty Forecast Plots.....	93

4.2	Planning Inspections Using Uncertainty	96
4.2.1	Planning Inspection for Vertical Cracking	97
4.2.2	Planning Inspection Timing for Delamination	103
4.2.3	Planning Inspection Method for Delamination.....	111
4.3	Effect of Uncertainty of Parameters on the Deterioration Model	114
4.3.1	Sensitivity Analysis of Vertical Cracking.....	115
4.3.2	Sensitivity Analysis of Delamination	117
4.3.3	Example: Climate Parameter Uncertainty	119
4.3.4	Establishing Important Parameters for Individual Bridges.....	127
4.4	Inspection Planning Scenario Analyses	128
4.4.1	Past Inspection Analysis on Larimer County Bridge LR 50 - 0.2 - 17.....	128
4.4.2	Future Inspection Plan on Larimer County Bridge LR 50 - 0.2 – 17	130
4.4.3	Inspection Planning for Two Bridge Decks.....	135
4.5	Implementing Inspection Plan for Use by Bridge Management Agencies	139
5.	CONCLUSIONS	142
5.1	Summary	142
5.2	Contributions to Bridge Inspection and Maintenance Practice	143
5.3	Further Research	144
6.	REFERENCES	146
7.	APPENDIX.....	154

LIST OF TABLES

Table 2.1. Condition state description for NBI reporting (FHWA, 1995).....	19
Table 2.2. Condition states for CoRe element 12: concrete deck–bare (CDOT, 1998)	21
Table 2.3. Description of occurrence factor and how it relates to likelihood-NCHRP Report 782	23
Table 2.4. Description of consequence factor-NCHRP Report 782	24
Table 2.5. Secondary loads and effects that affect deck cracking	31
Table 2.6. Factors affecting cracking of concrete bridge decks (Krauss & Rogalla, 1996)	32
Table 2.7. Applicable ranges on creep and shrinkage for models considered (Goel et al., 2007)	36
Table 3.1. Geometry and material parameters for bridge LR 50-0.2-17	74
Table 3.2. Deterioration and professional factor parameters for bridge LR 50-0.2-17	75
Table 3.3. Variable parameters used in both cracking models for sensitivity study	80
Table 3.4. Seasonal temperature differential from the bottom of the deck to the top of the deck (Kennedy & Soliman, 1987).....	83
Table 3.5. Mean, standard deviation, and Type I distribution parameters for annual minimum temperatures at various locations.....	85
Table 3.6. Chloride content statistics by % weight of mortar from various state DOTs (Cady & Weyers, 1983).....	86
Table 3.7. AASHTO CoRe element and NBI inspection ratings for LR50-0.7-17 from 1996 to 2002.....	87
Table 3.8. Bias, standard deviation, and smallest detectible area values for various NDE inspections for delamination.....	89
Table 3.9. Minimum detectable ADL for each bridge deck for each inspection method.....	90
Table 4.1. Statistics of prior distribution created using CDCPM	93
Table 4.2. Statistical results of transverse crack width and spacing from CDCPM.....	99
Table 4.3. Condition states for crack width and spacing, from AASHTO Smartflag 358	99
Table 4.4. Maximum inspection interval for vertical crack inspection	100
Table 4.5. Additional inspection time for bridges that show little increase in probability of occurrence.....	101
Table 4.6. Definition of condition states for deck delamination.....	104
Table 4.7. Inspection interval based on allowable spread in prediction at condition state 3.....	107
Table 4.8. Inspection interval based on probability of change in condition state from 3 to 4....	108
Table 4.9. Maximum standard deviation of ADL for each condition state	109
Table 4.10. Statistics for the high-spread and close to condition state change prior distributions	112
Table 4.11. Seasonal maximum tensile stress in the deck for Fort Collins, CO from temperature sub model.....	121
Table 4.12. Maximum tensile stress in winter for various locations from temperature sub model	122
Table 4.13. Initial ADL statistics for severely delaminated deck.....	132
Table 4.14. Statistics of the two concrete bridge deck at the current time	135
Table A.1. NBI condition rating statistical evaluation (Graybeal et al., 2002).....	154

LIST OF FIGURES

Figure 2.1. Visualization of second-moment reliability analysis on probability space for two variables	13
Figure 2.2. Comparison of regular Monte-Carlo (left) and Latin hypercube (right) probability space coverage	14
Figure 2.3. Bayes' Theorem applied to deterioration PDFs (Enright & Frangopol, 1999)	16
Figure 2.4. Risk matrix example used in NCHRP Report 782 (Washer et al., 2014)	24
Figure 2.5. Weibull PDFs for time-to-condition change for concrete girders (Nasrollahi & Washer, 2014)	26
Figure 2.6. Typical transition matrix in Markov chain deterioration model (Li et al., 2014)	28
Figure 2.7. Illustration of subsidence crack formation (Emmons, 1993)	34
Figure 2.8. Relative volumes of corrosion products to iron (Liu & Weyers, 1998)	41
Figure 2.9. Delamination inspection study by mechanical sounding (Graybeal et al., 2002)	47
Figure 3.1. Flowchart of CDCPM order of operations	52
Figure 3.2. Temperature profiles for uniform temperature (left) and linear temperature (right) in the deck	55
Figure 3.3. Location of forces used in analyzing deck and girder for temperature	56
Figure 3.4. Shrinkage strain model for determining deck stresses (Krauss & Rogalla, 1996)	58
Figure 3.5. Creep stages in concrete	59
Figure 3.6. CDF of rebar depth to determine percent of rebar above chloride concentration threshold	63
Figure 3.7. Normal probability plot of tensile stress output for various times	66
Figure 3.8. Visualization of the reliability index calculation	67
Figure 3.9. Plan view of bridge LR50-0.2-17 in Larimer County, CO	72
Figure 3.10. Cross sections of the concrete girder (left) and steel girder (right) used in analysis	72
Figure 3.11. Visualization of Bayesian updating using bins	77
Figure 3.12. Four temperature profiles used in deck stress analysis	83
Figure 3.13. Probability plots of minimum annual temperature in Fort Collins, CO for Type I (left) and normal (right) distributions	84
Figure 3.14. Design drawings of sample decks for inspection planning comparison	91
Figure 4.1. Uncertainty forecast plot for mean ADL based on inspection result for various levels of inspection precision	94
Figure 4.2. Uncertainty forecast plot for standard deviation of ADL based on inspection result for various levels of precision	94
Figure 4.3. Probability of transverse cracking over the service life of a bridge in Fort Collins, CO	98
Figure 4.4. Flowchart of methodology for vertical crack inspection timing	103
Figure 4.5. Projection of standard deviation of ADL for various initial mean and standard deviation values	105
Figure 4.6. Projection of ADL for various mean and percentile values at 1% initial standard deviation	106
Figure 4.7. Flowchart of inspection timing plan for delaminations	110

Figure 4.8. Updated standard deviation in ADL from the high-spread prior distribution for various inspection precisions	112
Figure 4.9. Updated mean ADL for the condition state change prior distribution for various inspection precisions.....	113
Figure 4.10. First-order sensitivity indices of the vertical cracking model for the first year of bridge service	115
Figure 4.11. First-order sensitivity indices of the vertical cracking model projected for 50 years of service.....	116
Figure 4.12. First-order sensitivity indices for the delamination model during the first 30 years of bridge service.....	117
Figure 4.13. First-order sensitivity indices for the delamination model for years 30 to 100 of bridge service.....	118
Figure 4.14. Probability of cracking at different standard deviations-60% mean relative humidity	120
Figure 4.15. Probability of cracking at different mean values - 10% standard deviation.....	120
Figure 4.16. Probability of cracking comparison of various locations when deck surface is warmer than bottom in winter.....	122
Figure 4.17. Probability of cracking comparison for various locations when the deck surface is cooler than bottom in winter	123
Figure 4.18. 90 th percentile ADL projection based on surface chloride content levels for various states.....	124
Figure 4.19. Projected standard deviation of ADL based on surface chloride content levels for various states.....	124
Figure 4.20. Comparison of variability in surface chloride content on the standard deviation of ADL	126
Figure 4.21. Projection of standard deviation of ADL for bridge LR 50-0.2-17 from 1996 to 2002	129
Figure 4.22. Projection of 90 th percentile ADL value for bridge LR 50-0.2-17 from 1996 to 2002	129
Figure 4.23. Projected standard deviation of ADL for bridge LR 50-0.2-17	131
Figure 4.24. Projected 90 th percentile ADL for bridge LR 50-0.2-17	131
Figure 4.25. Uncertainty forecast plot of the updated standard deviation in ADL for various inspection methods in 2019	132
Figure 4.26. Standard deviation of ADL projection for severely delaminated bridge deck.....	133
Figure 4.27. 90 th percentile ADL projection for severely delaminated bridge deck	133
Figure 4.28. Uncertainty forecast plot of the mean ADL for the severely delaminated concrete deck.....	134
Figure 4.29. Uncertainty forecasting plot for the mean updated ADL – Deck A.....	136
Figure 4.30. Uncertainty forecasting plot for the mean updated ADL – Deck B	136
Figure 4.31. Uncertainty forecasting plot for the standard deviation of updated ADL – Deck A	137
Figure 4.32. Uncertainty forecasting plot for the standard deviation of updated ADL – Deck B	137
Figure A.1. Probability plots of annual minimum temperatures for Santa Barbara, CA-Type I (left) and normal (right).....	160

Figure A.2. Probability plots of annual minimum temperatures for Clemson, SC-Type I (left) and normal (right)..... 160

Figure A.3. Probability plots of annual minimum temperature for Ann Arbor, MI-Type I (left) and normal (right)..... 160

Figure A.4. Probability plots of annual maximum temperature in Fort Collins, CO-Type I (left) and normal (right)..... 161

Figure A.5. Probability plot of annual mean temperature in Fort Collins, CO-normal..... 161

LIST OF ACCRONYMS

AASHTO.....	American Association of State Highway and Transportation Officials
ADL.....	Percent Deck Area Delaminated
ASCE.....	American Society of Civil Engineers
ASTM.....	American Society for Testing and Materials
BMS.....	Bridge Management System
CDCPM.....	Concrete Deck Cracking Probability Model
CDF.....	Cumulative Distribution Function
CI.....	Confidence Interval
DOT.....	Department of Transportation
FHWA.....	Federal Highway Administration
FOSI.....	First-Order Sensitivity Index
FOSM.....	First-Order Second Moment
GPR.....	Ground Penetrating Radar
LRFD.....	Load and Resistance Factor Design
MCS.....	Monte Carlo Simulation
NBI.....	National Bridge Inventory
NBIS.....	National Bridge Inspection Standards
NCHRP.....	National Cooperative Highway Research Program
NDE.....	Nondestructive Evaluation
PDF.....	Probability Density Function
RAP.....	Reliability Assessment Panel

SEI.....Structural Engineering Institute
SNBIBE.....Specification for the National Bridge Inventory Bridge Elements
TSI.....Total Sensitivity Index

1. INTRODUCTION

1.1 Background on Bridge Condition and Inspection Planning

The condition of the bridges in the United States has been a major point of concern in recent years, as many of these bridges are reaching the later years of their useful life. According to Rens et al (2005), there were two periods of heavy bridge construction in the United States: first in the 1930's and second in the 1950's to 1960's. According to Ramey et al (1997), these bridges were most likely designed for a service life of 50 years, although the writers also state that these older bridges were not designed to a specific target design life. The current American Association of State Highway and Transportation Officials (AASHTO) *LRFD Bridge Design Specifications* (2012) states that new bridges must be designed for a 75-year design life, and recommendations for even longer design lives have been made (Azizinamini et al., 2014; Ramey et al., 1997). While this longer design life should ensure that newer bridges are designed and constructed with durability in mind, all bridges require periodic maintenance and inspection. With tight federal, state and local budgets, it is important that funds for maintenance and inspection are used effectively. This thesis focuses on improved allocation of inspection resources in particular.

The first bridge inspection system was implemented as a response to the collapse of the Silver Bridge, which spanned the Ohio River between Point Pleasant, WV and Gallipolis, OH, in December 1967 (Lichtenstein, 1993). This failure was caused by an eyebar in the bridge's truss system that developed a cleavage fracture. Because there were no routine inspection measures in place at the time, this fracture, which was 4 inches in length prior to collapse, was never discovered and therefore led to a redistribution of stresses that overburdened the steel truss

system. The result of this tragedy was the development of the National Bridge Inspection Standards (NBIS) in 1971, the first federal standard for bridge inspections in the United States (Ryan, Mann, Chill, & Ott, 2012). Since this time, the standard has evolved and expanded. Currently, three manuals exist to present a unified approach to bridge inspection in compliance with NBIS; the AASHTO *Manual for Bridge Evaluation* (2014), the Federal Highway Administration (FHWA) *Recording and Coding Guide* (1995), and the *Bridge Inspector's Reference Manual* (Ryan et al., 2012). NBIS established a general maximum of twenty-four months between routine inspections in 1971, and this is still the current practice. Using a twenty-four month interval for all bridges means that newer bridges that are designed for longer lifespans are inspected with the same frequency as older bridges that deteriorate at a faster pace. Therefore, the need for an inspection-timing policy that accounts for an individual bridge's needs while also staying within the limited budget available for inspections is necessary to ensure that bridges will be properly maintained to the best our resources can provide.

Other issues are present when looking at how bridge inspections are scheduled in the United States. Some of these issues are outlined by the American Society of Civil Engineers Structural Engineering Institute (ASCE/SEI)-AASHTO Ad-Hoc Group on Bridge Inspection, Rating, Rehabilitation, and Replacement's paper, *White Paper on Bridge Inspection and Rating* (2009). In regard to inspection timing, AASHTO references bridge inspection practices in Europe, where intervals longer than two years are normal, and can extend to 6 years for some bridges. While variable timing would make for a more complicated inspection system, they suggest that more in-depth inspections conducted less frequently will allow a better understanding of the current bridge condition.

The ASCE/SEI-AASHTO Ad-Hoc Group white paper not only the need for a change from a uniform inspection timing policy, but the need for better inspection quality. For example, Phares et al (2004) studied the reliability of visual inspections on bridges based on the National Bridge Inventory (NBI) condition rating system presented in the FHWA *Recording and Coding Guide* (1995) They observed a fairly large amount of variability arising from the subjectivity of inspectors. Another point of inconsistency is in how bridge conditions are reported to different agencies. In comparison to the NBI condition rating system, AASHTO uses element-level data collection to provide a more detailed and uniform system for use in any bridge management system (BMS). Consistency in inspection reporting and documentation is important in reducing the uncertainty in inspection results, which leads to a more reliable inspection program.

To address the problems of inspection timing and quality, Washer et al. (2014) recently published the National Cooperative Highway Research Program (NCHRP) Report 782 *Proposed Guideline for Reliability-Based Bridge Inspection Practices*, which is the culmination of research done in recent years to develop an inspection plan based on the risk of deterioration of bridge components. Here, risk is separated into two components: occurrence and consequence. The occurrence is the likelihood that the bridge element will fail sometime during a specified time period, and the consequence describes the expected outcome of that failure. This system would allow for variable timing of inspections, as well as allocating inspection resources to specific elements that are at risk of failing or have major consequences from a potential failure. Washer's methodology, as well as other reliability-based models, is described in the literature review in more depth.

Washer's plan (Washer et al., 2014) addresses inspection timing and planning based on expert opinion and qualitative assessment, and states that use of quantitative reliability models

are a viable option to base these decisions. For example, the occurrence factor is determined by identifying damage modes and attributes to these modes, and predictions are made using past performance of similar attributes and current knowledge of how a component may fail. However, the writers caution multiple times that past performance of a component may not be the best indicator of future performance, especially when visual inspection results are used. An alternative to using past data is to make future predictions based on mechanistic deterioration models, however these models introduce their own sources of uncertainty. Some past researchers have implemented reliability in deterioration modelling, which analyzes the model with an associated degree of uncertainty in the factors involved. However, such models have not been used for the purpose of inspection planning and they have considered only a limited number of deterioration modes such as loading and corrosion (Estes & Frangopol, 2003; Stewart & Rosowsky, 1998a; Val & Melchers, 1997). Washer's risk-based plan does not include much for the assessment of risk outside of a quantitative assessment made by a panel of professionals, and the use of reliability-based mechanistic models can provide a powerful tool for understanding the risk of a bridge component due to uncertainty.

Understanding the current condition of a bridge requires an understanding of the uncertainty in the factors that affect the component. The research presented here starts from the premise that inspections should be carried out when there is a large enough uncertainty in the condition of a component to warrant efforts to collect more accurate data. The actual condition state is then used to plan maintenance or repair for the bridge. To fully utilize the uncertainty in the bridge's condition as an inspection planning indicator, an understanding of the deterioration processes, material behavior, modeling accuracy, and inspection accuracy is needed. This thesis addresses gaps in past research which has not explicitly considered the interaction of uncertainty

between deterioration modeling and bridge inspection findings, and aims to model the effect of inspection quality, as well as schedule future inspections based on uncertainty. This modelling includes many different components of the bridge, identifying the possible failure criteria of individual components and system failure, accuracy of available models to describe these events, and inclusion of inspection results to improve the model over time. A complete, useable model would take extensive research of each component type and material, as well as available deterioration models. For this reason, a demonstration of this uncertainty based approach to inspection planning is done for bridge deck cracking and delamination only.

Concrete deck cracking will showcase both the interaction of various deterioration modes to project the uncertainty in the bridge deck, and use various inspection procedures to evaluate the deck. Deterioration from thermal and drying shrinkage combined with other factors such as creep and subsidence will affect the formation of vertical transverse cracks in the deck (Krauss & Rogalla, 1996). Another form of cracking is delamination, where the concrete cracks inside the deck on planes parallel to the deck surface. They can be the result of debonding between layers or corrosion of embedded reinforcement. This type of deterioration cannot be seen through visual inspection, and presents major serviceability concerns (Vu & Stewart, 2005). The development of nondestructive evaluation (NDE) technology is making a big impact on how concrete bridge decks are inspected for cracks and delaminations. Delaminations can only be investigated by drilling cores in the deck or by using NDE methods since they are not visible from the surface. However, the NDE methods available all come with their own cost for equipment and implementation, as well as differences in accuracy of results. Therefore, the variability in testing should be considered and weighed versus the cost of the test.

1.2 Research Objectives

The goal of this research is to use the uncertainty in the knowledge of the current bridge condition to plan inspection timing and method. In order to describe this methodology, the following research will focus solely on concrete bridge decks and the failure modes associated with deck cracking. By understanding the sources and extent of uncertainty in the cracking of the deck from deterioration models and inspection results, an efficient inspection plan can be developed such that the inspection results will yield the greatest improvement to the current knowledge of the deck condition. This goal is achieved by examining the following objectives:

- 1) Explain how can uncertainty in the knowledge of the bridge condition identified through deterioration models and inspection results can be used to plan inspection timing and method.
- 2) Identify the parameters that contribute the most to uncertainty in the bridge condition.
- 3) Give examples of how the parameters that affect uncertainty in bridge deterioration can be managed.
- 4) Provide examples of how the proposed bridge inspection planning method can be applied to different bridge management scenarios.

These objectives establish the scope for this thesis, and together help to analyze how uncertainty plays a role in our understanding of concrete bridge deck cracking. While other concerns may be present for a given bridge deck, the objectives above provide a base for analyzing uncertainties that pertain to every bridge deck, and show how this uncertainty can be managed through inspection.

1.3 Research Approach

This research seeks to establish an inspection plan based on the knowledge of the bridge condition, using concrete bridge decks as an example. The current inspection methodology in the United States and current risk-based inspection planning tools are researched and reviewed in the literature review. Also in the literature review, important factors that drive cracking and delamination of concrete bridge decks are identified, and current knowledge on the uncertainty in the evaluation of cracks through NDE is examined.

Uncertainty is analyzed using mechanistic deterioration models in this research, so appropriate mechanistic models to describe the processes behind cracking and delamination are identified and reviewed based on the modeling approach and uncertainty of results. Models that are included in this study describe the probability of subsidence cracking, creep and shrinkage of concrete over time, and the cracking caused by corrosion of embedded steel reinforcement. All of the models are coded in MATLAB in order to simulate the condition and uncertainty in the amount of cracking that occurs in the lifespan of a concrete bridge deck. The interaction of these models was investigated so that two estimates of cracking are determined: 1) transverse vertical cracks and 2) delamination at the level of rebar. The delamination model is modified to allow for inspection updating. The inspection methods that are analyzed in this thesis are mechanical sounding, impact-echo, and ground penetrating radar.

Separate inspection plans for vertical cracking and delamination are developed based on the analysis provided from the mechanistic model, appropriate limits on uncertainty in cracking are found. A sensitivity study is then conducted on the mechanistic model to identify the important input parameters, and insight on how to manage these parameters is given. The inspection plan is then applied to a real bridge, and is subjected to a bridge management scenario

involving two bridge decks to show how this plan can be implemented for bridge inspection management decisions.

1.4 Thesis Structure

This thesis presents four additional chapters to explain the methods and results. Chapter 2 will cover the literature review regarding: the current research on improving inspections based on reliability principles, the factors that are most important in controlling concrete deck cracking, the models that have been developed to predict concrete properties over time, and the current NDE methods that can be implemented to determine the percent of a concrete deck that is cracked or delaminated. This information is used to develop a combined, interactive model to represent the bridge deck condition over time. Chapter 3 introduces the methodology and explanation behind the model, and the various scenarios used to address the objectives of this research. The developed inspection plans, identification of important sources of uncertainty, and results of the example cases are presented in chapter 4. Chapter 5 presents the conclusions drawn from this study, as well as areas of further research on developing this inspection plan, and understanding how to manage uncertainty. An appendix section is also included with other relevant information.

2. LITERATURE REVIEW

An extensive literature review was conducted to understand the current inspection practices in the United States as well as to examine current research in developing an improved inspection strategies. This review also aims to better understand the role of uncertainty as it relates to deterioration modelling and inspection results for concrete bridge decks. The uncertain knowledge about a bridge component is analyzed through probability theory. Therefore, an overview of probabilistic representation of uncertainty is described in Section 2.1. Past and current inspection timing and planning strategies in the United States are presented in Section 2.2. There are current research projects that aim to move towards a risk-based inspection strategy for bridges, and some of their approaches are summarized in Section 2.3. The modelling approaches and associated uncertainty in representing the time-dependent properties and deterioration modes of concrete bridge decks are discussed in Section 2.4. Common visual and NDE inspection methods for concrete bridge decks, and research on their uncertainty, are presented in Section 2.5.

2.1 Probabilistic Representation of Uncertainty

Uncertainty is an attribute of information (Zadeh, 2006), which implies that most information used for developing and analyzing a model is uncertain in nature, and any new information from the model is also uncertain. For design codes, uncertainty is accounted for by using factors on input and output values to achieve a target level of reliability, which is called Load and Resistance Factor Design (LRFD). In analysis problems, the uncertainty can be examined through a reliability analysis by numerical evaluation or simulation of random variables (Melchers, 1999).

2.1.1 Sources of Uncertainty in Structural Reliability

There are two categories of uncertainty in a structural analysis: 1) aleatoric and 2) epistemic. Aleatoric uncertainty arises from the inherent randomness of an event. Natural events such as wind loads or earthquakes are examples of aleatoric uncertainty, and the uncertainty in the event cannot be reduced. Epistemic uncertainty arises from a lack of knowledge about an event. For instance, the model developed for an analysis may be uncertain due to simplifications of the process. This type of uncertainty can be reduced through research, experimentation, and less simplification to a model.

Uncertainties may arise in several ways. Melchers (1999) has summarized the sources of uncertainty present in any structural analysis, and they can be classified as follows:

- Phenomenological Uncertainty

This is the uncertainty associated with an ‘unimaginable’ event that would cause structural failure. Such uncertainty is particularly important for new designs that attempt to extend the ‘state of the art,’ where the performance of such designs is not well-known.

- Decision Uncertainty

Decision uncertainty arises when deciding if a particular event has occurred. For instance, the decision as to whether a fatigue crack has exceeded an allowable amount at a connection on a steel girder may be uncertain.

- Modeling Uncertainty

The model that represents an event may be uncertain depending on the number of simplifications and assumptions made in developing the model. Most of this uncertainty is due to epistemic uncertainty surrounding the event, or through human intervention in the modelling process.

- Prediction Uncertainty

When an analysis is performed to predict the future state of a structure, prediction uncertainty is introduced. The prediction of future events, such as the occurrence of an extreme weather event, may contribute as well as the knowledge of performance of similar structures in the past.

- Physical Uncertainty

Physical uncertainty is the uncertainty in the basic random variables of an analysis. Some examples are concrete compressive strength, traffic loading, corrosion rate, and structural dimensions.

- Statistical Uncertainty

Uncertainty is typically represented by probability, which uses mean and standard deviation values. However, the accuracy of these values is also uncertain based on sample size and bias. This leads to uncertainty in the statistical parameters involved.

- Uncertainty from Human Factors

Human factors can be separated into two categories: 1) human error and 2) human intervention. Human error may arise from ignorance, mistakes in design drawings, and misuse of the structure among others. Human intervention occurs from a broad range of factors, including education, reduction of complexity in design, and inspections.

2.1.2 Limit State Functions and Monte Carlo Simulation

In structural reliability, the performance of a structure is analyzed as a probability of failure. This is determined by preserving the uncertainty in the basic variables of a problem so that the uncertainty in the results may be analyzed. In order to determine the probability of

failure for a structure, a limit state equation must be established. All limit state equations take the following general form as shown in equation 1 below.

$$G(\bar{X}) = R(\bar{X}) - S(\bar{X}) \quad (1)$$

The parameters that determine the resistance of the structure will determine R, and the parameters that determine the applied loading will determine S. When the safety margin, G, is less than zero, the structure has failed. When the parameters that determine R and S are uncertain, the safety margin G is also uncertain. The probability that G is less than zero is also known as the probability of failure. The application of limit states to bridge decks will be discussed later.

Evaluation of limit states may be carried out either through numerical evaluation or sampling (Melchers, 1999). Numerical evaluation has the advantage of providing approximate results for probability of failure while also being efficient in terms of computational time for problems with few variables. However, once the solution depends on more than approximately 5 variables, the mathematical evaluation of the limit state becomes very difficult, and in many cases, closed form solutions are not attainable (Melchers, 1999). One popular numerical procedure for evaluating limit states is first-order second moment reliability theory (Cornell, 1969).

First-order second moment (FOSM) reliability analysis uses the first two moments of the distributions of input data, such as the mean and standard deviation for a normal distribution, to estimate the probability of failure for a system or component (Melchers, 1999). For example, consider the joint probability density function (PDF) of two normally distributed random variables, S and R. The area under the PDF is always equal to 1, which represents the entire probability space. The probability of failure is defined as the area under the pdf for values that

fall in the failure region. Figure 2.1 shows a visual of the safety index (β) when both variables are standard. Any normal distribution can be standardized using the Hasofer-Lind transformation (Hasofer & Lind, 1974). Then, the probability of failure can be determined by equation 2 below.

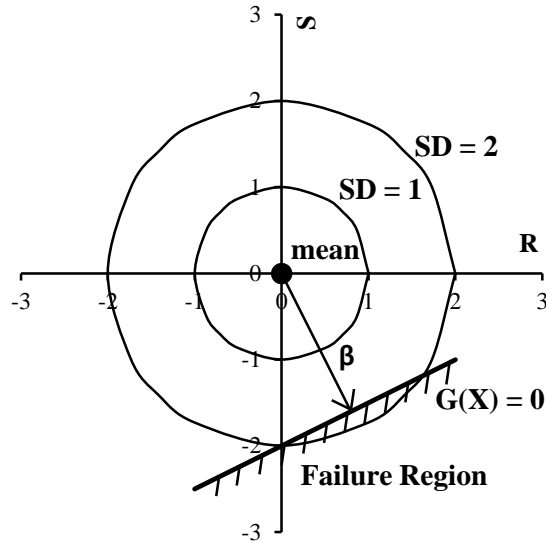


Figure 2.1. Visualization of second-moment reliability analysis on probability space for two variables

$$p_f = \Phi(-\beta) \quad (2)$$

- $\Phi(-)$ = standard normal distribution function

For limit states that depend on many variables, the only known solution for an accurate estimation of the probability of failure is Monte Carlo simulation (MCS) (Gavin & Yau, 2008). This is a numerical experiment where each random variable is sampled many times from its associated cumulative distribution function (CDF), and the limit state function is evaluated once for each sample. The number of failures is then divided by the number of simulations to obtain an approximation of the probability of failure. This process is very common in research where many variables are considered (Beck & Au, 2002; Stewart & Rosowsky, 1998b).

Monte Carlo simulation may be computationally expensive due to the random nature of samples, and the possibility of sample clustering means that more simulations must be performed

for the probability of failure value to converge. To solve this, stratified sampling and variance reduction techniques may be implemented to reduce clustering and converge on the probability of failure value sooner (Melchers, 1999). One of these techniques is Latin hypercube sampling. This stratified sampling technique breaks the probability space into a number of equivalent ranges equal to the number of simulations. Each variable is sampled randomly within each range, and each range is sampled only once. This ensures that the probability space is fully covered. Figure 2.2 below shows a comparison of regular Monte Carlo simulation versus Latin Hypercube sampling.

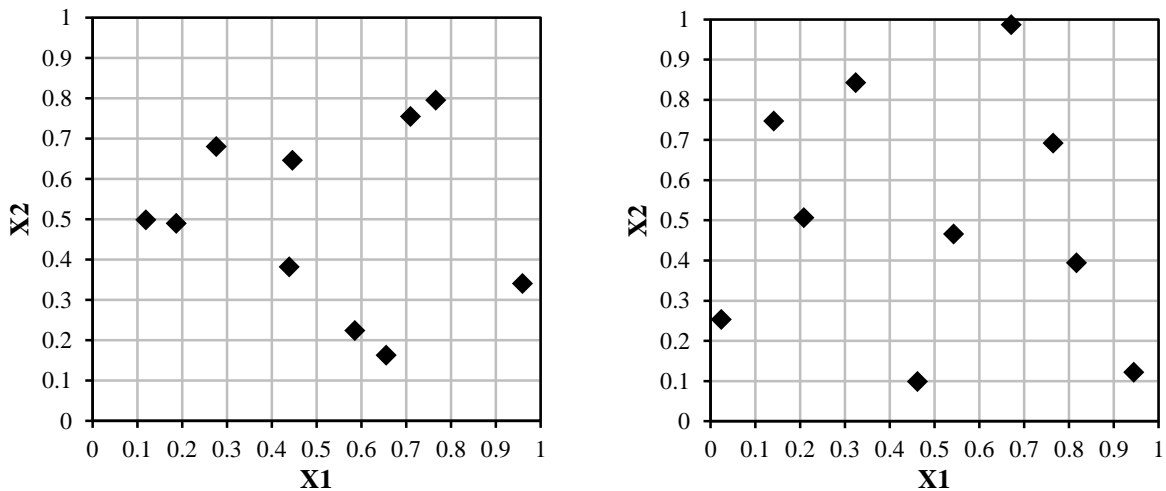


Figure 2.2. Comparison of regular Monte-Carlo (left) and Latin hypercube (right) probability space coverage

The Monte Carlo simulation has the possibility of sampling in groups, and leaving large spaces without sampling. For instance, the variable X2 is not sampled above 0.8 during the regular Monte-Carlo simulation in Figure 2.2. Latin Hypercube sampling ensures that this does not happen. With more coverage of the probability space, less samples need to be run for the output of the model to converge.

2.1.3 Bayes' Theorem

Bayes' theorem, which was first introduced by Thomas Bayes (Bayes & Price, 1763), is a unique approach to understanding interactions of probabilities. There is a subset of statistics called Bayesian statistics, where a measure of belief is determined based on supporting evidence. Many improvements and clarifications of his idea have been made, and his theorem can best be described as shown in equation 3.

$$P[A|B] = \frac{P[B|A] * P[A]}{\sum\{P[B|A_i] * P[A_i]\}} \quad (3)$$

In the equation, the event A is the event that we are interested in learning more about, or updating. Event B is the event that we know to have occurred, and gives some supporting evidence for or against our belief in event A . The expression $P[A|B]$, and similar expressions, is a conditional probability where the probability of event A is based on the known occurrence of event B . This equation uses a prior distribution, $P[A]$, takes a set of new, relevant sample data, B , and updates the distribution to a new posterior distribution, $P[A|B]$. Bayes' Theorem has found many applications to structural reliability (Enright & Frangopol, 1999; Igusa, Buonopane, & Ellingwood, 2002).

Bayes' Theorem is particularly useful for updating the condition of a bridge using inspection data (Enright & Frangopol, 1999). While deterioration models may predict the future state of the bridge component, they will not be perfect, and the prediction uncertainty will grow larger with time. The deterioration model is the prior distribution in the analysis, and inspection data is the new information from which the posterior distribution is determined (Enright & Frangopol, 1999). However, inspection data is also uncertain, and this must be included in the analysis as well to gain a true representation of uncertainty (Moses, 1996). The result of these two sources of information is the posterior distribution, which shows the updated and more

certain belief in the current condition of the structure. Figure 2.3 below shows an example using PDFs.

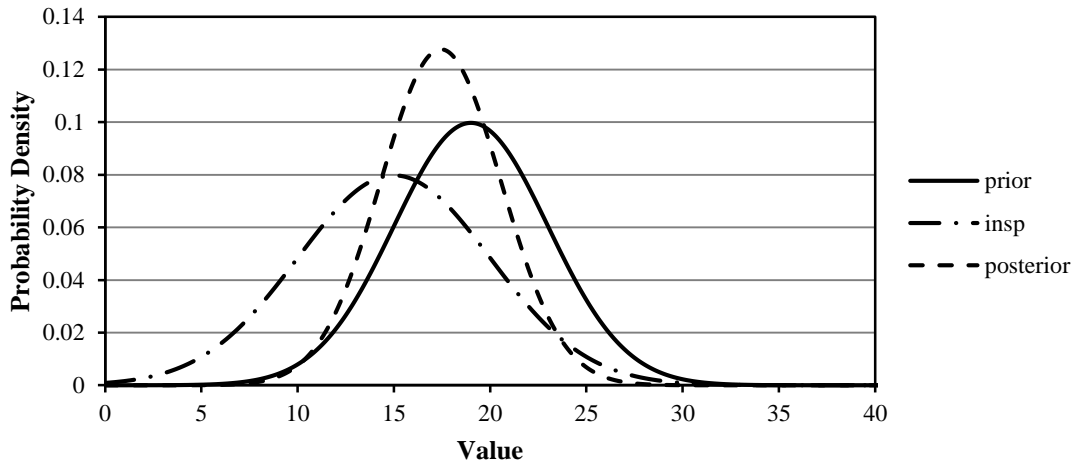


Figure 2.3. Bayes' Theorem applied to deterioration PDFs (Enright & Frangopol, 1999)

2.2 Previous and Current Bridge Inspection Practice

As a result of the Silver Bridge collapse, the first national bridge inspection program in the United States was implemented as the National Bridge Inspection Standards (NBIS). Since this time, many ideas have been explored for conducting these inspections, including the level of detail and the proper way to record the inspection data. The results from inspections are used as a basis for management decisions for bridges when it comes to repair and maintenance. This thesis will focus on the inspection practice in the United States such that an understanding of the growth of inspection program as well as the current state of the inspection program may be understood.

2.2.1 National Bridge Inspection Standards (NBIS)

In 1971, the NBIS established the criteria by which bridge inspections should be timed and conducted, personnel should be trained, and data should be collected and reported. The current standard requires inspection intervals no longer than twenty-four months for most

elements, and no longer than sixty months for underwater elements, unless the bridge has written approval from the Federal Highway Administration (FHWA) to have a longer interval. These inspection procedures are outlined in the *American Association of State Highway and Transportation Officials (AASHTO) Manual for Bridge Evaluation* (2014), which is discussed later. The NBIS establishes the qualifications and expectations of inspection personnel in terms of their training and experience, and these inspectors are provided with guidance on conducting the inspections through the *Bridge Inspector's Reference Manual* (2012). The format of inspection reporting to the National Bridge Inventory (NBI) is laid out in the *FHWA Recording and Coding Guide for the Structure Inventory and Appraisal of the Nation's Bridges* (1995).

Many of the pitfalls of the current NBIS system are outlined in a report by the American Society of Engineers/Structures Engineering Institute (ASCE/SEI)-AASHTO Ad-Hoc Group on Bridge Inspection, Rating, Rehabilitation, and Replacement (2009). The timing of inspections is one of the major concerns brought forth. The common twenty-four month inspection interval is not the most efficient strategy in that many bridges are being inspected too often, and those resources are no longer available for bridges that require closer monitoring. For example, older bridges that contain fracture-critical details are inspected at the same 2 year interval as newer bridges that do not contain these details. A more rational approach would vary these inspection intervals to address the failure risk associated with a fracture-critical member. A survey of inspection intervals in European agencies indicated that intervals beyond two years were common, and may be as long as six years in some cases.

Another concern addressed by the ASCE/SEI-AASHTO Ad-Hoc Group (2009) is the quality control in how inspections are conducted. The uncertainty in the consistency of data obtained for the NBI arises from the differences in state bridge management systems (BMS)

recording procedures and the training and consistency of bridge inspectors. Each state develops a management plan within the standards set by the NBIS, but the plan for complex bridges or special situations such as fracture-critical bridges left for each state to decide itself. Therefore, the practice within each state may lead to inconsistencies when reporting to the FHWA, which has a unified system for rating bridge components. Examples of different state inspection recording practices are shown in a study by Phares et al (2004). While the FHWA *Recording and Coding Guide* (1995) emphasizes that the condition ratings are meant to represent the overall condition of the bridge component, each inspector may view this differently during an inspection (B. M. Phares, Rolander, Graybeal, & Washer, 2001). Such uncertainty can be reduced through evaluation and certification of bridge inspectors. Other issues that are addressed are use of non-destructive evaluation (NDE) methods and lack of available deterioration data.

2.2.2 FHWA Recording and Coding Guide

The FHWA requires that all inspection results be reported to the NBI in accordance with the *FHWA Recording and Coding Guide for the Structure Inventory and Appraisal of the Nation's Bridges* (FHWA, 1995). This guide provides the entire documentation procedure for the report, which includes location, traffic, and condition state information. In regard to reporting condition states of bridge components, the only components needed for a typical bridge is the deck, superstructure, and substructure overall condition. Each condition is reported as a value between 0 and 9, with 9 being a newly constructed structure and 0 being the structure is failed. A condition state of 4 or lower is classified as structurally deficient. Table 2.1 shows the description of each condition state.

Table 2.1. Condition state description for NBI reporting (FHWA, 1995)

Condition State	Description
9	EXCELLENT CONDITION
8	VERY GOOD CONDITION - No problems noted
7	GOOD CONDITION - Some minor problems
6	SATISFACTORY CONDITION - Structural Elements show some minor deterioration
5	FAIR CONDITION - all primary structural elements are sound, but may have minor section loss, cracking, spalling, or scour
4	POOR CONDITION - advanced section loss, deterioration, spalling, or scour
3	SERIOUS CONDITION - loss of section, deterioration, spalling, or scour have seriously affected primary structural components. Local failures are possible. Fatigue cracks in steel and shear cracks in concrete may be present.
2	CRITICAL CONDITION - advanced deterioration of primary structural elements. Fatigue cracks in steel or shear cracks in concrete may be present or scour may have removed substructure support. Unless closely monitored, it may be necessary to close the bridge until corrective action is taken.
1	“IMMINENT” FAILURE CONDITION - major deterioration or section loss present in critical structural components, or obvious vertical or horizontal movement affecting structural stability. Bridge is closed to traffic, but corrective action may put back in light service.
0	FAILED CONDITION - out of service, beyond corrective action.

This information is collected in the NBI, and is used to evaluate the general state of the bridge inventory in the United States. Due to the collection of data on many different bridges, this inventory is popular for conducting statistical analysis (Bolukbasi, Mohammadi, & Ardit, 2004; Nasrollahi & Washer, 2014). The generality of the components being assessed does limit the knowledge about specific components of the bridge, and leads to uncertainty in the source of the condition rating. Therefore, any of the analysis conducted using this data set give general trends in the overall deterioration, but information on deterioration of specific elements is lost.

Currently, the FHWA is working to update the condition rating system to be an element-level system, which would include not only data on individual elements, but also the location of any noted deterioration. This new system is outlined in the *Specification for the National Bridge*

Inventory Bridge Elements (SNBIBE) (2014). This increase in data collection will expand the knowledge base for deterioration of a particular bridge, and it would help increase the capability of bridge management system (BMS) software. This would also allow for a large bank of historical data in the NBI from which deterioration modelling based on past performance can be developed at the element-level instead of the general sense.

2.2.3 AASHTO Manual for Bridge Evaluation

AASHTO developed the *Manual for Condition Evaluation of Bridges (MCE)* (1994), which outlined procedures and policy for determining the current condition, maintenance actions, and load capacities for the nation's bridges. Around the same time, AASHTO developed a BMS software called PONTIS, which is now called AASHTOware Bridge Management (BrM), to provide management information for bridges based on cost and condition assessment. This provided unified guidance for condition assessment that satisfies the NBIS, and created a base for management decisions on a particular bridge. However, the MCE did not present a unified system for assigning ratings. In 1997, AASHTO developed a common system for assigning condition ratings to commonly recognized (CoRe) structural elements, which can be used as inputs for BMS software (AASHTO, 1997). Using the CoRe elements, BrM determines information on optimal management strategies and can predict future conditions for inspection and maintenance planning.

The CoRe elements describe the elements that may be commonly found on bridges. Each element is rated on a condition range spanning 3 to 5 condition states, depending on the element. While there are less condition states than the NBI uses, this may reduce the uncertainty in ratings that is present in NBI data (B. Phares et al., 2004). This is also advantageous compared to condition rating in the NBI, because the condition ratings relate to specific components instead

of the overall structure. A table of the condition state ratings for a bare concrete bridge deck is shown in Table 2.2 below.

Table 2.2. Condition states for CoRe element 12: concrete deck–bare (CDOT, 1998)

Condition State	Condition Description	Feasible Maintenance Actions
1	Surfacing on deck has no repaired areas, and there are no potholes in this surfacing.	1) Do nothing (DN)
2	Repaired areas and/or spalls/delaminations exist. Combined area is less than 2% of total deck area.	1) DN 2) Repair spalled/delam areas 3) Add a protective system
3	Repaired areas and/or spalls/delaminations exist. Combined area is less than 10% of total deck area.	1) DN 2) Repair spalled/delam areas 3) Repair spalled areas and add a protective system
4	Repaired areas and/or spalls/delaminations exist. Combined area is more than 10% of total deck area, but less than 25% of deck area.	1) DN 2) Repair spalled/delam areas 3) Repair spalled areas and add a protective system
5	Repaired areas and/or spalls/delaminations exist. Combined area is more than 25% of total deck area.	1) DN 2) Repair spalled/delam areas and/or add a protective system 3) Replace deck

Currently, since the FHWA still requires inspection condition reporting for the NBI on the 0 – 9 scale, the AASHTO CoRe elements do not lend themselves to direct reporting to the FHWA. However, in 1997, the FHWA approved a computer program that translates CoRe element data into NBI data so that both of the data requirements can be met (FHWA, 2012). This has helped to make the process more efficient in that inspections can be conducted by using AASHTO CoRe elements and then use the program to report to the FHWA. However, these are still two different systems for describing the bridge condition.

2.3 New Approaches to Bridge Inspection Timing and Planning

2.3.1 *Risk-Based Inspection Planning-NCHRP Report 782*

Risk is defined as a function of the probability of occurrence of an event and the consequence of that event on the system. For bridges, the occurrence can be any number of possible deterioration modes, and the consequence looks at the impact this deterioration has on the structure and the surrounding environment. In order to better evaluate and report the current condition of bridges, the National Cooperative Highway Research Program (NCHRP) has funded research into developing a risk-based inspection program and the results are reported in NCHRP Report 782 (Washer et al., 2014). The appeal of this approach is that it considers both occurrence and consequence factors in determining the risk an event poses to a bridge.

The approach used in NCHRP Report 782 for determining the risk of a structural failure for a bridge component uses the combination of an occurrence factor and a consequence factor. Both factors are defined between 1 and 4, with 1 being the ‘low-risk’ end and 4 being the ‘high-risk’ end. Each factor is assigned to a bridge based on the decision of a Reliability Assessment Panel (RAP), and they describe a particular event for the bridge. An event can be defined as a particular deterioration mode such as steel corrosion, or can be defined as a system level failure such as moment collapse of a girder. The RAP consists of experienced engineers, inspectors, and bridge managers that make the ultimate decisions about what constitutes a particular occurrence or consequence factor. They may use a reliability analysis to aid in their decision-making, as well as past statistical analysis, deterioration models, and personal judgement in determining the appropriate factors. Both factors are combined using a risk matrix to give an overall condition rating for the bridge component.

The occurrence factor for a particular event describes the likelihood that the event will occur. It can be defined through a reliability analysis resulting in a probability of failure, but is ultimately assigned by the RAP. A reliability analysis will give the probability of failure (POF), also defined as the likelihood, that the event will occur. NCHRP Report 782 gives general guidance on how to convert the likelihood of an event into an appropriate occurrence factor using Table 2.3 below.

Table 2.3. Description of occurrence factor and how it relates to likelihood-NCHRP Report 782

Occurrence Factor	Qualitative Rating	Description	Likelihood (POF)	Expressed as a percentage
1	Remote	Remote probability of occurrence, unreasonable to expect failure will occur	$\leq 1/10,000$	0.01% or less
2	Low	Low likelihood of occurrence	$1/1,000 - 1/10,000$	0.1% or less
3	Medium	Moderate likelihood of occurrence	$1/100 - 1/1,000$	1% or less
4	High	High likelihood of occurrence	$> 1/100$	$> 1\%$

The consequence factor is based on cost of repairs, serviceability impact, traffic impact, and structural safety. This factor is used to prioritize different bridges for inspection planning by considering the ‘worst-case’ event for the particular failure mode (Washer et al., 2014). Such events are never expected to occur for any bridge, but they do give an indication of the level of consequence. This would be events such as moment failure of a girder or complete delamination within the deck that should be addressed prior to actually occurring. Again, the ultimate decision on the consequence factor for a situation is decided on by the RAP. Here, structural stability analysis and examination of the bridge environment may be the best tools for determining the potential consequences. For example, a bridge that spans over a roadway may have higher consequence factor for moment collapse due to impact on the traffic below than for the same

bridge that spans a river. The relative importance of an event is generally described as shown in Table 2.4 below.

Table 2.4. Description of consequence factor-NCHRP Report 782

Level	Category	Consequence on Safety	Consequence on Serviceability	Summary Description
1	Low	None	Minor	Minor effect on serviceability, no effect on safety
2	Moderate	Minor	Moderate	Moderate effect on serviceability, minor effect on safety
3	High	Moderate	Major	Major effect on serviceability, moderate effect on safety
4	Severe	Major	Major	Structural collapse/loss of life

Once the occurrence and the consequence of an event are determined, the result is compared to a risk matrix, which groups the event into a risk category (I – V). This category can be used to determine appropriate inspection intervals and maintenance actions for each event considered. A risk category of (V) would imply that the bridge has a very low risk of failure for a particular component, while a risk category of (I) indicates there is a high risk of failure for the component with potentially major ramifications. An example of the risk matrix developed for NCHRP Report 782 is shown in Figure 2.4 below.

Occurrence Factor	4	III	II	II	I
	3	III	III	II	II
	2	IV	IV	III	II
	1	V	IV	III	III
	/	1	2	3	4
		Consequence Factor			

Figure 2.4. Risk matrix example used in NCHRP Report 782 (Washer et al., 2014)

NCHRP Report 782 uses mostly human judgement with the aid of analytical tools to evaluate the bridge condition through defining the factors described above. This human reliance on judgement also may introduce variability in how each person analyzes a situation, similar to previous visual inspection rating which also uses human judgement (B. Phares et al., 2004). This system is also very complicated for the number of bridges that must be considered. Considering there are over 600,000 bridges in the United States subject to the NBIS, determining the appropriate occurrence and consequence factor guidelines for these events for each bridge is a very time-intensive process. Also, the outline given to describe this program is vague, and can be interpreted in a variety of ways by different DOTs or management agencies. This does allow for adjustments for local conditions, but will also create a spread in the variability of assessment results for the FHWA as addressed earlier. In this sense, there are still issues present here that are also present in current inspection practice.

2.3.2 Inspection Planning Based on Statistical Analysis of Past Bridge Condition

One of the more common approaches to inspection planning uses past inspection performance of a bridge to project the future performance. The most complete and oldest set of condition state data is found in the NBI, so this is the most popular data set to use for such an analysis (Mishalani & Madanat, 2002; Nasrollahi & Washer, 2014; Prozzi & Madanat, 2003). When running a statistical study on this data set, the Weibull distribution appears to be the best-fit distribution for condition state deterioration (Kobayashi, Kaito, & Lethanh, 2010; Nasrollahi & Washer, 2014).

One proposed method for using past inspection data estimates the probability that the condition state has changed since the last inspection (Nasrollahi & Washer, 2014). In a study of the past 20-years of condition ratings from the NBI for bridges in Oregon, Nasrollahi and

Washer attempted to determine the Weibull distribution of the time for a bridge superstructure in one condition state to drop to the next lowest condition state. Therefore, the time to failure is the summation of all failure time distributions between the current state and the failure state. For example, they found that, on average, a pre-stressed concrete superstructure in condition state 8 (very good) would have a 5% chance of reaching a condition state of 4 (poor) in 11.4 years or less. Figure 2.5 below shows example PDFs for the time-to-condition change.

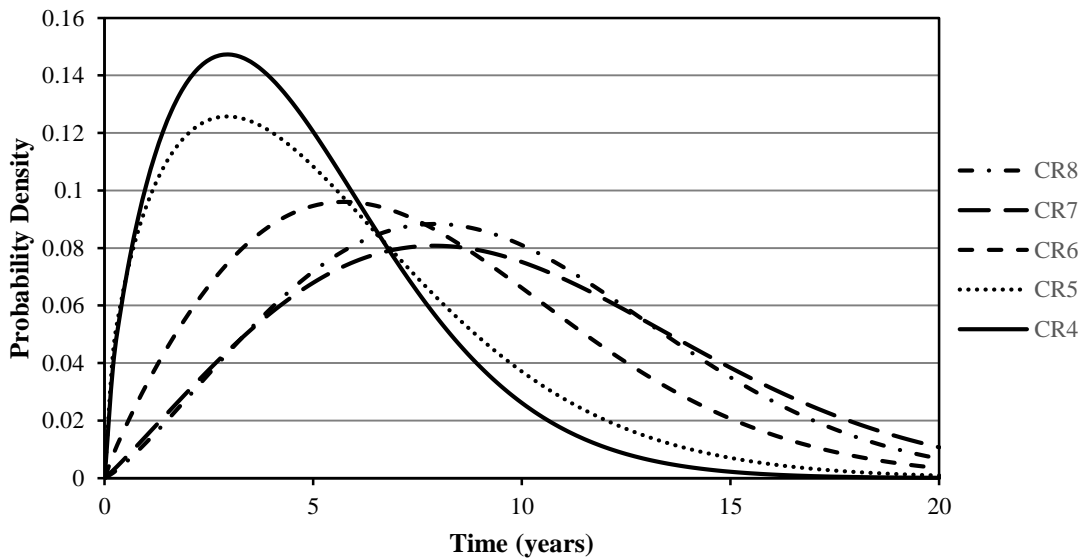


Figure 2.5. Weibull PDFs for time-to-condition change for concrete girders (Nasrollahi & Washer, 2014)

Other models look at using the Weibull hazard function to determine the probability of a condition state change (Kobayashi et al., 2010; Mishalani & Madanat, 2002). The hazard function of any distribution describes the probability that an event in a state will transition to some other state at a specified time (Lancaster, 1992). Prozzi and Madanat (2003) argue that it can be advantageous to estimate the hazard function for an event directly, and then differentiate to determine the survival function. The survival function, when plotted for time, describes the probability that an event, X , will remain unchanged at some time, t . Such a model for predicting failure times has proven to match experimental data better than deterministic models (Prozzi &

Madanat, 2003). The survival function is directly related to the cumulative distribution function by equation 4.

$$S(X(t)) = 1 - F(X(t)) \quad (4)$$

Such a model allows for the determination of inspection intervals based on probability of changing condition states. This can be done by defining a threshold probability depending on what the next lowest condition state would be. A bridge that is deteriorating into condition state 7 versus condition state 3 could have a higher probability threshold due to the relatively little deterioration defined by condition state 7.

Some challenges would have to be overcome in order to implement this type of bridge management system. Many of these Weibull distributions would have to be developed for location specific analysis, and research on updating this model with experimental or inspection data is very limited. The Nasrollahi and Washer model based the time to condition state change on past statistical data, and includes bridge data in Oregon alone. The causes of deterioration in Oregon may differ from the causes in Florida or Minnesota, and therefore, the distributions would have to be fit to region specific data. Also, each bridge may differ in the construction type and quality, which affects the initial condition and deterioration rate of the bridge, as shown later in this thesis. By including physical processes that change a components condition, a better representation of future performance may be achievable.

2.3.3 Inspection Time and Maintenance Type Using Markov Chains

Markov chain models are a popular way to model how multiple condition states can deteriorate over time, and therefore plan when future inspections should be conducted. Many attempts to use Markov chains to estimate the condition of a bridge throughout its useful life have been made (Cesare, Santamarina, Turkstra, & Vanmarcke, 1992; Li, Sun, & Ning, 2014;

Robelin & Madanat, 2007), and computer management programs PONTIS and BRIDGEIT use first-order Markov chains to predict the future condition for inspection planning (Morcoux, 2006). In a first-order Markov process, the current condition state is input and the future condition is determined through a transition matrix. An example of a transition matrix is shown below in Figure 2.6.

$$P = \begin{bmatrix} p_{11} & \cdots & p_{1j} \\ \vdots & \ddots & \vdots \\ p_{i1} & \cdots & p_{ij} \end{bmatrix}$$

$$0 \leq p_{ij} \leq 1$$

$$\sum_{row} p_{ij} = 1$$

Figure 2.6. Typical transition matrix in Markov chain deterioration model (Li et al., 2014)

Each value within the matrix represents the probability that a component in condition i will transition to condition j . This means that this is a statistics based approach, where the probabilities are determined from analysis of bridge data. For bridge deterioration, the matrix is usually simplified to be an upper triangular matrix, because the assumption that the bridge condition will not improve without intervention in the deterioration process is valid (Cesare et al., 1992). To find the potential state for times longer than one interval, the transition matrix can be raised to the power of how many time intervals will pass to the desired year. This is shown in equation 5 below, where C is a vector of condition state quantities.

$$C(t) = P^t \times C(0) \tag{5}$$

Inspection intervals can then be determined based on the results. Like the Weibull PDF approach, when the probability that the condition state has worsened reaches a particular threshold, the inspection should be conducted. This probability can be calculated as the sum of all the probabilities at and below the condition state in question.

One of the drawbacks of a first-order Markov chain is that the analysis disregards the history of information and events that lead to the current state, which ignores useful information. Although transition probabilities may be determined from deterioration behavior from the past, the information specific to the bridge in question is not accounted for or updated (Li et al., 2014). This means that a future model is predicted based on the performance of similar bridges, but not the particular bridge in question. Another drawback of Markov chain analysis is the transition times must be evenly spaced. In the current PONTIS model, the program requires a constant inspection interval, such as two years, to run a reliable analysis (Morcous, 2006). In the framework of a reliability-based inspection plan where the inspection interval will vary based on the reliability of structural components, the inspection interval will not be constant. The validity of modeling bridge deterioration as a Markov process has also come under scrutiny for not representing the physical causes of deterioration (Mishalani & Madanat, 2002; Scherer & Glagola, 1994).

However, attempts have been made to adjust Markov chains to correct the aforementioned issues (Robelin & Madanat, 2007). Robelin and Madanat use a Markov chain, where the transition probabilities can be adjusted using Monte Carlo simulations of each time step and implementing three new variables that represent maintenance, inspection, and deterioration of the bridge. Their results showed that this newer model would reduce the chance at requiring expensive repair measures due to more regular maintenance actions. Another attempt to incorporate past data in the analysis uses Weibull hazard curves for each condition state (Mishalani & Madanat, 2002). Such curves are capable of incorporating uncertainty in the Markov process as related to when the bridge condition may transition to a lower state.

2.4 Analysis and Uncertainty in Concrete Deck Cracking

Concrete is a heterogeneous material, where multiple constituent materials interact to determine the properties of the concrete overall. Concrete is also subject to time-dependent material changes that can affect the loads acting on the structure. For crack formation in concrete bridge decks, the tensile forces on the bridge are important when determining the possibility of deck cracking. Two types of cracking are of primary concern in concrete decks: 1) vertical cracking of the cross-section and 2) delamination at the level of rebar. Delamination is the debonding of concrete layers, typically due to separate concrete pours or corrosion of embedded reinforcement. Delamination occurs below the deck surface, and typically cannot be examined through routine visual inspection. Therefore, delamination is much more serious and tougher to quantify. This section will address current models and theories for the modeling of deterioration modes that affect concrete cracking.

For bridge decks, the stresses that cause cracking are typically not due to the primary loads, but the secondary loads caused by self-straining actions and material changes (Krauss & Rogalla, 1996). Primary loads are major sustained or periodic loads that arise due to self-weight, structural function, or environmental phenomena. Secondary stresses arise in concrete for many reasons, and some are more obvious than others (Davis-McDaniel, Chowdhury, Pang, & Dey, 2012; Krauss & Rogalla, 1996). Secondary stresses are the leading cause of concrete deck cracking, and therefore are the focus of this section. In order to account for secondary stresses, appropriate mechanistic models must be used that predict the stresses based on influencing factors. Table 2.5 below shows the types of secondary loads and effects that affect deck cracking. As described in section 2.1.2, limit state equations can be used to analyze the probability that these stresses will cause cracking of the concrete deck.

Table 2.5. Secondary loads and effects that affect deck cracking

Vertical Cracking	Delamination
<ul style="list-style-type: none"> • Shrinkage • Temperature • Creep 	<ul style="list-style-type: none"> • Subsidence • Corrosion • Creep

2.4.1 Causes of Concrete Deck Cracking

Cracking in concrete can occur very early in the lifespan of the bridge deck, and can be caused by several factors related to conditions experienced during construction and curing. One type of cracking that occurs early in the bridge's lifespan is transverse cracking (Hadidi, Ala Saadeghvaziri, & Thomas Hsu, 2003; Krauss & Rogalla, 1996). In NCHRP Report 380 (Krauss & Rogalla, 1996), the causes of concrete deck cracking from design factors, material types and properties, and construction practice and conditions are identified and ranked as having a major, moderate, minor, or no influence on the potential for cracking. This ranking is shown in Table 2.6 below. They also developed equations for determining the stress in a concrete deck due to temperature changes in the deck and girder material based on strain and curvature compatibility between the deck, girder, and reinforcement. These equations are the basis of the structural analysis for thermal and shrinkage effects in the present study. This model is chosen for determining the stresses due to temperature and shrinkage strains because it is adaptable for different girder sizes and materials, as well as capable of incorporating multiple steel reinforcement layers.

Table 2.6. Factors affecting cracking of concrete bridge decks (Krauss & Rogalla, 1996)

Factors	Effect on Cracking			
	Major	Moderate	Minor	None
Design				
-Restraint	X			
-Continuous/simple span		X		
-Deck thickness		X		
-Girder type		X		
-Girder size		X		
-Alignment of top and bottom reinforcement bars		X		
-Form type			X	
-Concrete cover			X	
-Girder spacing			X	
-Quantity of reinforcement			X	
-Reinforcement bar sizes			X	
-Dead-load deflections during casting			X	
-Stud spacing			X	
-Span length			X	
-Bar type-epoxy coated			X	
-Skew			X	
-Traffic volume				X
-Frequency of traffic-induced vibrations				X
Materials				
-Modulus of elasticity	X			
-Creep	X			
-Heat of hydration	X			
-Aggregate type	X			
-Cement content and type	X			
-Coefficient of thermal expansion		X		
-Paste volume-free shrinkage		X		
-Water-cement ratio		X		
-Shrinkage-compensating cement		X		
-Silica fume admixture		X		
-Early compressive strength			X	
-High range water reducing admixture			X	
-Accelerating admixtures			X	
-Retarding admixtures			X	
-Aggregate size			X	
-Diffusivity			X	
-Poisson's ratio			X	
-Fly ash				X
-Air content				X
-Slump (in typical ranges)				X
-Water content				X
Construction				
-Weather	X			
-Time of Casting	X			
-Curing period and method		X		
-Finishing procedures		X		
-Vibration of fresh concrete			X	
-Pour length and sequence			X	
-Reinforcement ties				X
-Construction loads				X
-Traffic-induced vibrations				X
-Revolutions in concrete truck				X

Issa (1999) determined that cracking was observed in decks soon after construction, and gave ideas about the possible cause of the cracking. This was done through a questionnaire sent

to different state DOTs. Then, an experiment and analysis was conducted to better understand what factors affect the chance of cracking in a deck. He concluded that a high evaporation rate, a high concrete slump, and a high amount of water in the concrete have the greatest chance of causing early cracking. This early cracking is the result of subsidence, extreme shrinkage in the concrete from heat of hydration (Krauss & Rogalla, 1996).

Delaminations form as the result of corrosion of the embedded steel rebar (Liu & Weyers, 1998). Once the rebar starts to corrode, the iron in the steel will corrode to rust. All rust products are less dense than the steel was, so the conservation of mass means that the volume of the rust will be larger than that of the steel. Once this volume exceeds the available pore space around the rebar, the rust will exert pressure on the surrounding concrete. This pressure will be compressive in the radial direction relative to the rebar, but the tangential direction will experience a tensile hoop stress. Due to the lack of tensile strength in concrete, the concrete will crack from the hoop stress. Such cracks will usually form on the plane of the reinforcement, and will therefore be invisible from the surface of the concrete. These hidden cracks are known as delaminations.

2.4.2 Subsidence Cracking in Concrete

Subsidence cracking is one of the most important types of vertical cracking on concrete bridge decks because they form directly over and parallel to the steel reinforcement (Cady & Weyers, 1983). Subsidence cracking occurs very early in the concrete's life when the concrete mix is hardening. As the concrete solidifies around the reinforcement, the concrete mix will subside while the rebar stay in place. This creates a small void below the rebar and creates tensile forces above the rebar, as shown in Figure 2.7 below.

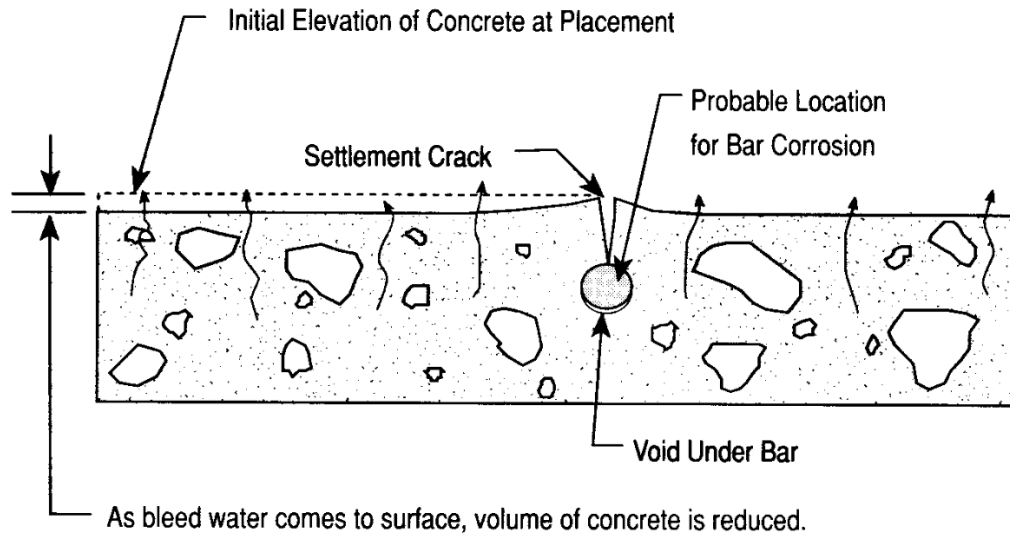


Figure 2.7. Illustration of subsidence crack formation (Emmons, 1993)

Dakhil et al (1975) developed an empirical model for determining the probability of subsidence cracking depending on the concrete cover, rebar diameter, and the concrete slump. This model has been used in other research to determine the area that is subject to early vertical cracking due to subsidence (Cady & Weyers, 1983; Krauss & Rogalla, 1996).

2.4.3 Creep and Shrinkage of Concrete

The two most researched causes of secondary stresses that may contribute to cracking of concrete components are creep and shrinkage. Shrinkage changes the volume of the concrete deck, and when this change is restricted, strain develops in the concrete, which also develops stress. Creep is the increase in strain over time under constant applied stress in the concrete. In contrast, creep also causes stress relaxation in concrete held under constant strain (Zdenek P. Bazant & Kim, 1979). While the two processes have different effects on the concrete, the models that have been developed to describe them are typically presented together.

There are four models that have been used extensively in previous research related to creep and shrinkage effects on concrete. These models will be referred to as ACI-209 (Carreira & Branson, 1982), CEB-FIP (CEB-FIP, 1993), B3 (Z. P. Bazant & Baweja, 1995a), and GL2000

(Gardner & Lockman, 2001). All of these models attempt to predict the strain in concrete due to shrinkage deformation, and the creep coefficient or creep compliance. Each model takes a different approach to determining these effects, and thus they differ in the input parameters and the model uncertainty.

The ACI-209 model determines an ultimate shrinkage and ultimate creep coefficient based on standard conditions, and then this value is adjusted through correction factors for conditions other than standard. The CEB-FIP model uses fitted equations, to estimate shrinkage and creep in concrete. CEB-FIP also uses fewer parameters than ACI-209 to make its predictions. B3 uses the most parameters, and the equations were developed based on many studies of experimental data. The GL2000 model evolved from an earlier model developed by Gardner and Zhao (1993), which was developed based on equations fit to data from multiple tests banks with more than three years of data. The basic variables were chosen based on availability at time of curing and use in previous models including ACI 209 and CEB-FIP 1990. A comparison of the applicability of each model is shown in Table 2.7 below. This applicability was determined either from the appropriate model paper, or the comparison paper by Goel et al (2007).

Table 2.7. Applicable ranges on creep and shrinkage for models considered (Goel et al., 2007)

Parameter	ACI-209 ²	CEB-FIP	B3	GL2000
Concrete and cement type	Normal and lightweight, type I and III cement	ordinary structural concretes	Portland cement concretes	All types
28-day concrete compressive strength [psi]	NL ¹	1,700-11,600	2,500 - 10,100	< 10,100
Curing method and duration	moist cure: 7 days steam cure: 1-3 days	NL	NL	NL
Slump [in]	2.75	NL	NL	NL
Water-cement ratio [by weight] (-)	NL	NL	0.3 - 0.85	0.4 - 0.6
Fine aggregates [% of concrete by weight]	50	NL	NL	NL
Cement content in concrete [pcf]	17.5 - 28	NL	10 - 45	NL
Aggregate-cement ratio (by weight) [-]	NL	NL	2.5 - 13.5	NL
Air content [%]	≤ 6	NL	NL	NL
Curing humidity [%]	>95	NL	NL	NL
Relative humidity [%]	40	40 - 100	NL	NL
Concrete temperature [°F]	70 - 77	41 - 86	NL	NL
Concrete age at loading [days]	load applied same day as end of curing	NL	NL	NL
Volume-surface ratio [in]	1.5	NL	NL	NL

¹NL = No Limit

²ACI-209 limits are the definition of the standard condition. For violation of these conditions, a correction factor is applied

Studies of the relative accuracy of these models and their fit to experimental data have been carried out by previous researchers (Al-Manaseer & Lakshmikantan, 1999; Bazant & Baweja, 1995b; Goel et al., 2007). Bazant and Baweja determined many coefficients of variation for the ACI-209, CEB-FIP, and B3 models based on the time of analysis (the GL2000 model was not introduced yet). The most comprehensive comparison was done by Goel et al (2007). He compares the four models listed above as well as the Muller model, which is an adaptation of the CEB-FIP model to expand its applicability. The models are compared to data from the International Union of Laboratories and Experts in Construction Materials, Systems and Structures (RELIM, from the French translation) test bank as well as from a study conducted on

a 13-story high-rise concrete building (Russel & Larson, 1989). Goel et al concluded that, in most instances, the GL2000 model provided the best prediction of creep and shrinkage as compared to the test bank and the study by Russel and Larson. While there are not many other comparative studies that include the GL2000 model, most agree that the ACI-209 model has the highest variation from experiment of the models examined (Bažant & Baweja, 1995b; Goel et al., 2007).

2.4.4 Temperature

Temperature is also addressed by ACI Committee 209 and NCHRP Report 380 (Krauss & Rogalla, 1996). For any structure, a change in the material's temperature will cause the material to shorten or elongate. For a one-dimensional analysis, the elongation will follow the following expression in equation 6.

$$\epsilon_t = \alpha * (T_f - T_i) \quad (6)$$

The value α is a material property that relates the amount of elongation to the temperature change directly, and is known as the coefficient of thermal expansion. Notice that an increase in temperature will lengthen the component. If the material is allowed to make this change in length as the temperature fluctuates, then no stress will be applied. However, when there is restraint, temperature changes will induce a stress from the restrained strain.

One of the most common restraints for a bridge structure is the restraint of the deck caused by the girders (Krauss & Rogalla, 1996). If the deck is fully connected along the span of the bridge to the girder, then the difference in the elongation between the girder and the deck will cause residual stress in the deck. For a concrete deck, the most severe residual stress may be caused by the heat of hydration during concrete curing and the subsequent cooling (Krauss & Rogalla, 1996). As the concrete cools down, it would like to shrink relative to the girder. If the

deck is restrained from doing so, then deck will experience tensile stress, which leads to a danger of cracking. Seasonal temperature changes may also cause cracking, but since the girder and deck typically expand and contract together, the restraint is reduced, especially if the material's coefficient of thermal expansions are similar between the girder and the deck.

2.4.5 Freeze/Thaw Cycling of Concrete Pore Water

Due to the porous nature of concrete and the trapped water within these pores, freezing and thawing of water is another form of secondary loading. Unlike many materials, water will actually expand when frozen from a liquid to a volume approximately 9% larger as a solid (Penttala, 1998). Based on this fact, it was first thought that keeping the degree of saturation below 91% would eliminate freeze-thaw deterioration in concrete. However, there is no observed direct connection between the expansion of freezing water to the damage in concrete due to freeze-thaw (Everett, 1961). Since this time, numerous other theories have been developed to explain the actual causes of deterioration due to freeze-thaw cycling of concrete pore water (Fagerlund, 1977; Powers & Helmuth, 1953; Setzer, 1999).

Powers (1953) introduced the hydraulic theory of freeze-thaw damage. This theory states that the deterioration of concrete under repeated cycles is the result of successive hydrostatic and osmotic pressures exerted on the concrete as water attempts to move through very small capillary voids. This would only occur if the large pores are saturated such that during freezing, the formation of ice forces water into smaller voids, creating hydrostatic pressure on the surrounding concrete. During thawing, the reduction of ice to water would suck water from these voids into the large pores through osmotic pressure. To solve this, a common practice is to use air-entrainment to create additional pore space in the concrete for which water can be transported as the void water freezes (Zdenek P. Bazant, Chern, Rosenberg, & Gaidis, 1988). Bazant also

brings up how this practice can affect the concrete strength when too many voids are present, and that depending on the size of the cross-section, this may not be necessary.

Researchers have also developed other theories that pertain to freeze-thaw cycle deterioration of concrete. Powers and Helmuth (1953) presented a theory where the capillary void water freezes due to diffusion of water from the cement gel. After conducting tests on cement mortars, they noticed that the rate of freezing had a significant impact on the amount of diffused water that enters the capillary voids. Under slow freezing rates, the diffusion of water may cause drying shrinkage in the concrete, whereas fast freezing rates do not allow for the diffusion process to take place and the hydraulic pressure is the predominant form of pressure on the concrete (Penttala, 1998). Other theories have been made to take other observed phenomena into account such as the curvature of the ice-water interface (Everett, 1961), the role of pore surface stresses that hinder ice crystal formation (Litvan, 1976), and the increase in degree of saturation due to the intake of external water, known as the micro ice lens pump (Setzer, 1999). Theories that give the framework for a fatigue-type problem have also been formulated (Chen & Qiao, 2014; Cho, 2007).

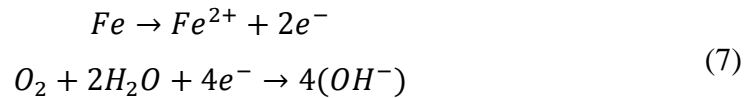
Even with the available research, the exact knowledge of how freeze-thaw works within the pore structure of concrete is not known, and the modelling of this phenomenon is very difficult. The available models do not lend themselves to integration with the other processes that occur in concrete already described. Therefore, this model is not included in the analysis that is presented in the methods section.

2.4.6 Corrosion Model

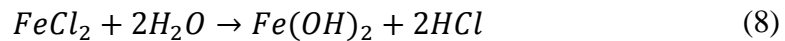
Corrosion occurs due to the reaction of iron in steel with water and oxygen in the presence of chlorides from de-icing salts on roadways or in the atmosphere near salt water

(Stewart & Rosowsky, 1998a). There have been many research studies to better understand the mechanism of corrosion (Zdenek P. Bazant & Oh, 1984; Sommer, Nowak, & Thoft-Christensen, 1993), the movement of chlorides through concrete to rebar, (Dakhil et al., 1975; Page, Short, & El Tarras, 1981) and how this translates to concrete cover cracking and delamination (Liu & Weyers, 1998; Page et al., 1981; Pantazopoulou & Papoulia, 2001).

Corrosion occurs due to a chemical reaction between the iron in the steel and the surrounding atmospheric elements. As stated by Cady and Weyers (1983), corrosion can only occur in the presence of iron, oxygen, water, and a solute of anions. Examples of possible corrosion enablers would be chlorides, such as salt, or carbonates, such as carbon dioxide. Rust formation is an electrochemical oxidation-reduction reaction, where the iron anode gives up electrons that combine with the surrounding oxygen and water within the concrete to form the cathode (Ma, 2012). This is shown by the reaction in equation 7 below.



This creates the necessary environment for the corrosion reaction to occur. The now positively charged iron in the steel attracts the chloride anions and reacts with the water, which then forms the rust product, as shown in the reaction in equation 8 below.



The iron (II) hydroxide product is the rust. For rebar in concrete members, the protective film around the rebar and the concrete layer above the rebar provides protection, but the thickness of the concrete layer also plays an important role in protecting the rebar.

Corrosion of rebar embedded in concrete leads to concrete cracking and delamination, and each corrosion product may affect the time to cracking in a different way. As shown by Liu

and Weyers (1998), each product has a different relative density, all of which are less dense than the iron from the steel. This is illustrated in Figure 2.8 below as the relative volume of the corrosion products for a unit mass and volume of iron. Since the mass is conserved in the chemical reaction, the volume of the product will be larger than that of the steel. This expansion in volume is what exerts pressure on the concrete, creating a tensile hoop stress effect (Pantazopoulou & Papoulia, 2001). This tensile stress is what will lead to cracking when a critical weight of steel has corroded. The time to this critical weight corroded is determined based on the model by Liu and Weyers (1998) in this thesis.

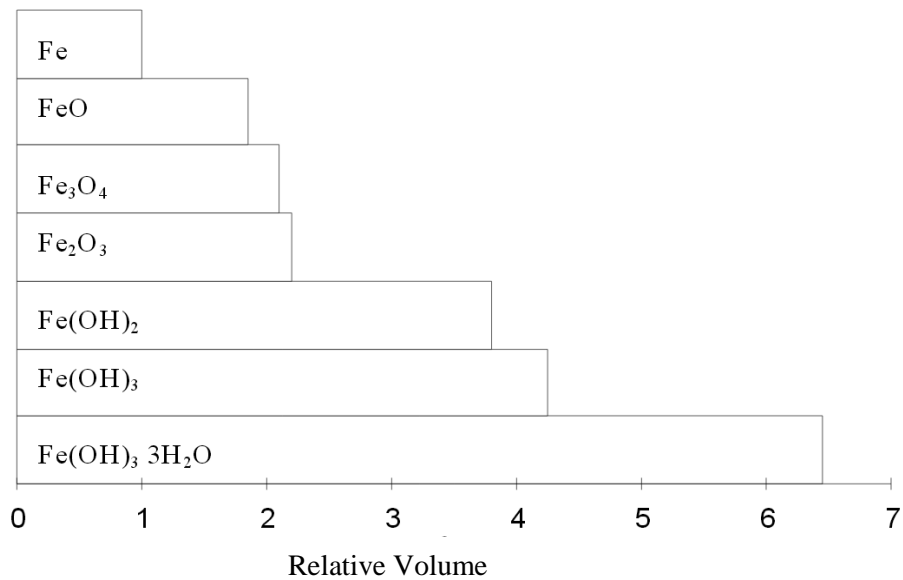


Figure 2.8. Relative volumes of corrosion products to iron (Liu & Weyers, 1998)

One of the previous studies of the reliability of a concrete bridge deck subjected to corrosion has been conducted by Stewart and Rosowsky (1998b). This study looked at the deterioration of concrete decks due to corrosion, with consideration of transverse cracking from temperature, shrinkage, and flexural loads. They examined two limit states; flexural strength, and spalling. They look mostly at probabilities that events related to these limit states will occur, such as the probability of spalling at a particular time, or the probability of structural collapse by

flexural failure given that spalling occurred at a particular time. However, this only provides a general picture of the occurrence of spalling in the deck, and is hard to translate into an inspection program. The model also did not account for creep of concrete, which may relax some of the early stress from dead loading, or could exaggerate the crack width, creating a higher chance of spalling at the surface.

2.4.7 Uncertainty in Model Accuracy and Precision

All of the aforementioned models can be used to describe and simulate real loads and processes that affect the deterioration of a bridge deck. However, they will also come with uncertainty, whether it is in the applicability of the model to a particular situation, the fit of equations to experimental data, or the accuracy and precision of input information. To account for this variability, any of these models that are included in a reliability analysis should have the output screened by a bias, or professional, factor. This is a factor that takes on an average value near one and has an associated coefficient of variation. The average value represents the accuracy of the model in predicting experimental results, and can only be determined in relation to real-life test data. The coefficient of variation accounts for the precision of the model. Previous research has provided some statistical values to the models described above, and will be applied in the example described in the methods section (Ellingwood & Galambos, 1983; Stewart & Rosowsky, 1998a).

2.4.8 Variance-Based Sensitivity Analysis

One cause of uncertainty in the output data of any model is due to the uncertainty in the input parameters. Some parameters will have more weight on the uncertainty in the output than others due to amount of variability in the parameter and the use of the parameter within the

model. One of the most practical ways of analyzing the sensitivity of the output to changes in the input parameters is through a variance-based sensitivity study (Chan, Saltelli, & Tarantola, 1997). Such a study examines the effect of the input uncertainty on the uncertainty in the output parameter. This is useful in locating the cause of the uncertainty in the output among the input parameters. Then, if possible, efforts to reduce the uncertainty in the parameter can be made, which in turn will reduce uncertainty in the output data. There are two types of indices that describe this effect: 1) first-order sensitivity index (FOSI) and 2) total sensitivity index (TSI).

Each sensitivity index provides a different context on how the uncertainty in one part of the model affects the end result. The first-order sensitivity index describes the effect of an individual parameter variability on the entire output variability. The term “first-order” means that all higher order effects, which includes the uncertainty caused by varying multiple parameters at the same time to analyze their effect, is neglected in the analysis. The first-order sensitivity index may also be interpreted as the relative expected reduction in the output variance when the parameter in question is fixed and all other parameters are kept variable (Saltelli et al., 2010). Equation 9 below describes the concept of this index. The calculation is performed for a set of random variables X such that $Y=f(X_1, X_2\dots)$.

$$S_i = \frac{V_{x_i} \left(E_{X_{\sim i}}(Y|X_i) \right)}{V(Y)} \quad (9)$$

- $E(X)$ = expected value of parameter X
- $V(X)$ = variance of parameter X
- X_i = the i^{th} parameter
- $X_{\sim i}$ = all parameters except for the i^{th} parameter

The total sensitivity index encompasses the effect of a particular parameter for all orders of analysis on the overall output. This includes not only the parameter uncertainty itself, but how its uncertainty combined with uncertainty in other parameters affects the overall output. Saltelli

et al (2010) also describe the total sensitivity index as the expected variance in the output if all values except the parameter in question are fixed. Therefore, the entire uncertainty due to a particular parameter is accounted for. Equation 10 below describes this index, and the parameters used are the same as for those used in the previous equation.

$$S_{Ti} = \frac{E_{x_{\sim i}}(V_{X_i}(Y|X_{\sim i}))}{V(Y)} \quad (10)$$

For models that depend on many input variables, the most efficient way to evaluate the sensitivity index is through Monte Carlo simulation (Saltelli et al., 2010). Saltelli et al examined many simulation-based evaluation methods for each parameter as well as simulation techniques to determine the most efficient and reliable method. They concluded that for either sensitivity index, the approximation by Jansen (1999) is the most reliable and accurate Monte Carlo estimator for the index. This estimation is described in detail in section 3.4.

2.5 Inspection Methods and Testing Uncertainty

Inspections are important in determining more information about the current condition of a bridge decks. Typically, inspections provide strong evidence of what condition state a bridge deck falls under, and help in deciding what the future maintenance actions should be. However, no method will provide perfectly accurate and precise results. Inspection types are broken into 5 different categories: 1) initial inspection, 2) routine inspection, 3) in-depth inspection, 4) damage inspection and 5) special inspection (Moore, Phares, Graybeal, Rolander, & Washer, 2001). The initial inspection is performed on a new bridge to obtain structure and appraisal data and to identify any current or potential problem areas. Routine inspections are conducted every two years, and aim to satisfy the NBIS using mostly visual inspection. In-depth inspections also satisfy the NBIS, but may incorporate the use of NDE methods and typically are more intensive

and time-consuming. Damage and special inspections typically do not satisfy the NBIS, but are conducted with a particular section of the bridge in mind to learn more of the current condition and if maintenance is required. This section will focus on routine visual inspections for concrete bridge decks, and later sections will focus on NDE technology for use in in-depth inspections.

2.5.1 Visual Inspection

The oldest and most common form of inspection is visual inspection. This is an inspection where the condition of a bridge is determined through mostly qualitative recording, with quantitative data recorded when accessible, of bridge components. Examples of quantitative data that may be recorded are deck geometry and size of deteriorated portions. Such inspections are completed from areas that are easily accessed, such as deck, ground, or water level or from nearby permanent structures. Visual inspections are conducted in accordance with the NBIS requirements for both inspection timing and inspector qualification (B. Phares et al., 2004).

In 2001, the first major assessment of the reliability of visual inspections in the United States was performed by Wiss, Janney, Elstner Associates, Inc under sponsorship from the FHWA NDE Validation Center (NDEVC) (Moore et al., 2001). After conducting a study of inspection results for eight bridges by 49 inspectors from 25 different states, they concluded that there is high variability among visual inspection results. Of the 49 condition ratings assigned to a particular bridge component, the assigned ratings would span 5 of the possible 10 condition states. A summary of the NBI condition rating assessment can be found in Table A.1 in the Appendix.

The study by Phares et al also covered element-level inspection accuracy using the AASHTO CoRe Element Guide (1997). During an inspection of the Van Buren Bridge in northern Virginia, the inspection teams were asked to evaluate the bridge at an element-level in

accordance with inspection practice from their own state. Out of 16 teams that completed this inspection, two of them did not report inspection results in accordance with the CoRe Element Guide. Phares et al noticed some large inconsistency in recording delamination uncertainty for a concrete deck. Three out of fourteen inspection teams subdivided the deck area into multiple condition states, and five teams reported condition states that did not match the AASHTO CoRe Element Guide for their reported percent deck area delaminated.

The qualitative uncertainty associated with element-level inspections was also high. Due to each inspector conducting the inspection in accordance with their state program, the elements used in the inspection varied greatly. Generally, agreement for elements dealing with the major components such as the deck, girders, bearings, and piers, were similar. However, the other elements were recorded under many different designations, the most inconsistent of which were joints. There was also a high variability in the use of non-CoRe elements that are designated by individual states. Another source of uncertainty found was the recording of information in consistent units. A mix of metric and English units were used depending on the inspection group, and some values were reported as total values as opposed to percentages.

2.5.2 Mechanical Sounding

Mechanical sounding procedures have been used to inspect decks longer than most other procedures, and can be relatively cheap to perform. The basis of these procedures is that when the deck is struck by a metal object, the resulting sound will be dull or hollow if a delamination is present. There are different techniques to conducting such an evaluation, but ASTM International outlines procedures for three different methods: 1) electro-mechanical sounding device, 2) chain drag and 3) rotary percussion. Many of the newer NDE techniques are compared to these practices when determining accuracy in detecting delaminations or spalls (Rens et al.,

2005; Scott et al., 2003). This may be due to familiarity of these methods among bridge inspectors compared to other methods.

The electro-mechanical sounding test is carried out using an electric powered tapping device and receiver mounted on a cart. This cart makes passes across the bridge deck and records data on areas of potential discontinuities in the deck. The chain drag method is run by dragging a length of steel chains across the deck in multiple passes, and listening for changes in the sound of the chains against the concrete. A rotary percussion is a dual-wheeled cart that contains multiple “teeth” on the wheels. This cart makes several passes on the bridge deck, and the user listens for sound changes to indicate areas of possible delamination. An important note about mechanical sounding is that it will not work for bridges with an asphalt overlay on the deck (Rens et al., 2005).

Graybeal et al (2002) reported their findings on mechanical sounding inspection results for the Van Buren Bridge deck in northern Virginia. Through an NDEVC study verified by 8 drilled core samples, the deck was determined to be 19% delaminated over the area. The results of the delamination study is shown in Figure 2.9 below.

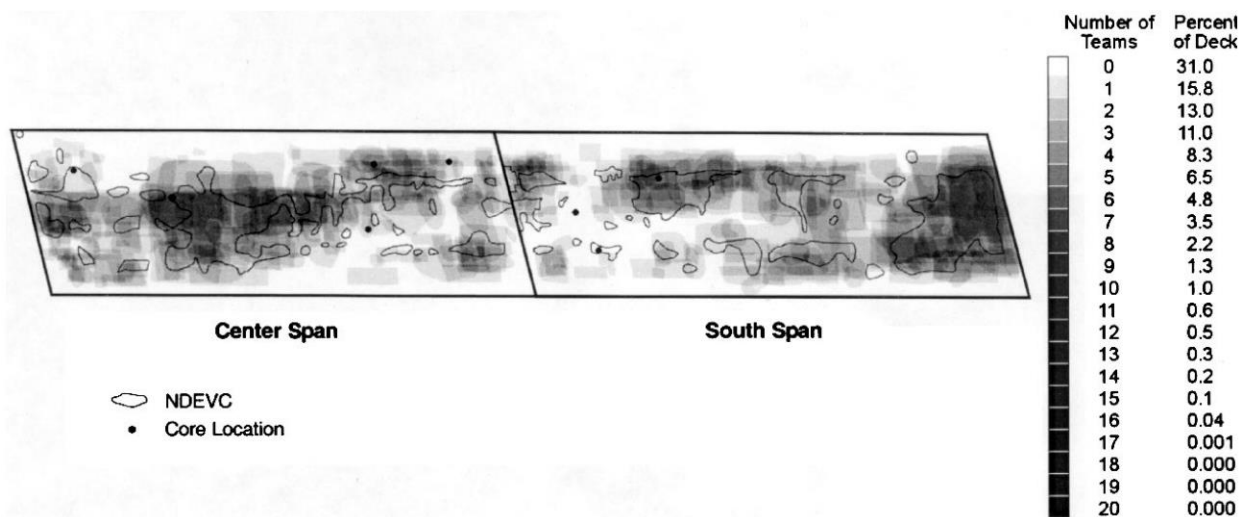


Figure 2.9. Delamination inspection study by mechanical sounding (Graybeal et al., 2002)

The researchers found that out of 22 inspection teams that reported numerical values of percent delamination area, 14 were within 10% of the actual percent deck area delaminated, and three teams estimated the deck area delaminated within 5% of the actual value. Of the 20 inspectors that reported maps of the delaminations as well, only 0.25% of the deck area delaminated was indicated by at least 15 inspectors. While inspectors did a good job of finding major areas of delaminations, the smaller pockets were often overlooked. This could go back to the reduction in reliability of inspection results based on the multiple locations examined (Moore et al., 2001). Therefore, the larger the deck area, the more likely that small pockets of delamination are missed.

2.5.3 Ground Penetrating Radar

Ground penetrating radar (GPR) is a test for detecting delaminations, and is particularly useful in areas that may be subject to rebar corrosion, which is the leading cause of delaminations in concrete bridge decks. This method is also desirable because it can be conducted from a vehicle moving at traffic speeds and is effective through asphalt layers (Barnes & Trottier, 2000). Essentially, this is an electromagnetic method where a signal is sent from a transmitter and then picked up by the receiver. For concrete, this signal may be manipulated by the presence of voids or delaminations in the concrete, and this is detected by the receiver and included in the output data (Maierhofer, Reinhardt, & Dobmann, 2010).

Many procedures for this test as applied to bridge decks are outlined in ASTM D6087 (2008). There are two main types of GPR systems: 1) ground-coupled systems and 2) air-launched systems (Roberts, 2015). Ground-coupled systems operate using an antenna and must operate at slower speeds. Air launch systems operate about 15 to 20 inches above the surface and can work even at speeds of 65 mph. Being able to operate at traffic speeds and ability to work

through an asphalt overlay make this method one of the most efficient methods for determining delamination (Rens et al., 2005). According to ASTM International, this is the only reliable test for delaminations in a concrete deck with an asphalt overlay. However, the interpretation of the signal response results can be complex, and may require destructive testing to get an accurate representation of the delamination (Yehia, Abudayyeh, Nabulsi, & Abdelqader, 2007).

2.5.4 Infrared Thermography

Another widely-used inspection method for determining voids and delaminations in concrete is infrared thermography. This process involves using an infrared camera to determine the areas where discontinuities interrupt the transfer of heat through the concrete (Maierhofer et al., 2010). The data can be presented in a map showing the temperature gradient between possible delaminations and solid concrete. However, like the chain drag method, this is not a viable option for concrete decks with asphalt overlays because the overlay lowers the temperature differential at the delamination, and may cause other thermal anomalies due to debonding between the asphalt and concrete (K. R. Maser & Roddis, 1990).

ASTM has also developed a standard by which to conduct the infrared thermography procedure (ASTM-D4788, 2013). Unlike other tests, infrared thermography is particularly sensitive to the environment in which the test is conducted. One of the main issues is that the time of day in which the test is conducted contributes to the output, and some seasons and times may prove impossible for conducting this test. Yehia et al (2007) found that consistent results could be determined from 10am to 3pm during a mild day with temperatures between 68°F and 78°F, but no flaws could be detected for tests run between 3pm and midnight. Also, the presence of water instead of air in the voids or delaminations will skew the results due to the water's thermal conductivity. Another limitation of this procedure is the depth of the supposed defect. If

the defect is too deep in the deck, the camera may not detect the cooler void, which leads to an underrepresentation of the defect's size (Yehia et al., 2007).

2.5.5 Impact-Echo

Impact-echo was developed as an ASTM standard in 1997 (ASTM-C1383, 2010), and uses the dynamic properties of the material to detect the thickness of the concrete deck. This is how the ASTM standard describes the test, but it can be used in detecting the location and depth of delaminations. When a delamination is present in the deck, the signal response will reveal a smaller thickness, and therefore indicate the location of the delamination (Maierhofer et al., 2010). The procedure is conducted by striking the concrete, creating an impact load that sends vibrations through the material. This wave moves to the bottom of the deck and then rebounds, or echoes, back to a receiver placed on the top of the deck. Using the dynamic properties of the concrete, the thickness can then be calculated.

The results of the test are highly dependent on the impact duration, and therefore, the test must be calibrated for the P-wave speed through the material before conducting the inspection (M. Sansalone & Streett, 1997). It has also been shown that the accuracy of results can be affected by the presence of steel rebar in the deck, which is common with many bridges (Watanabe, Morita, Hashimoto, & Ohtsu, 2004). However, some reports also claim this is not much of an issue (Yehia et al., 2007). This method is reliable for bridges that contain overlays, which greatly increases the applicability of the method (Mary Sansalone & Carino, 1989).

3. METHODS

This section outlines the specific models used in developing the mechanistic model code for analyzing bridge deck cracking and the uncertainty in the cracking. The purpose of developing a model is to provide a tool for analyzing the uncertainty in the current condition as well as the projecting the uncertainty in the future condition for inspection planning. First, the deterioration model is developed using mechanistic equations from the literature review. The models are run through multiple Monte Carlo simulations to examine variability. The model is adapted to update with inspection results at the time of inspection. Once the model is completed, the method used in executing the sensitivity study is presented. Next, the collection and representation of climate parameters is explained, followed by the set-up of example scenarios.

3.1 Model Development and Updating

Both delamination and vertical cracking are represented by probability distributions to examine the uncertainty in each condition. Vertical cracking is the result of excessive tensile stresses in the concrete deck. The probability of cracking is determined by a limit state, and the model also estimated crack width and spacing to gauge the consequence of crack formation. The delamination model determines the percent area of concrete deck that is delaminated (ADL) using the appropriate models. Fick's second law of diffusion, along with the time-to-corrosion cracking model, are used to estimate the delamination within the deck.

To analyze both model, a code was developed in the mathematical software program MATLAB, and the name of this code is Concrete Deck Cracking Probability Model (CDCPM). A flow chart that explains the model execution is shown in Figure 3.1 below. The individual models are then described in the following section.

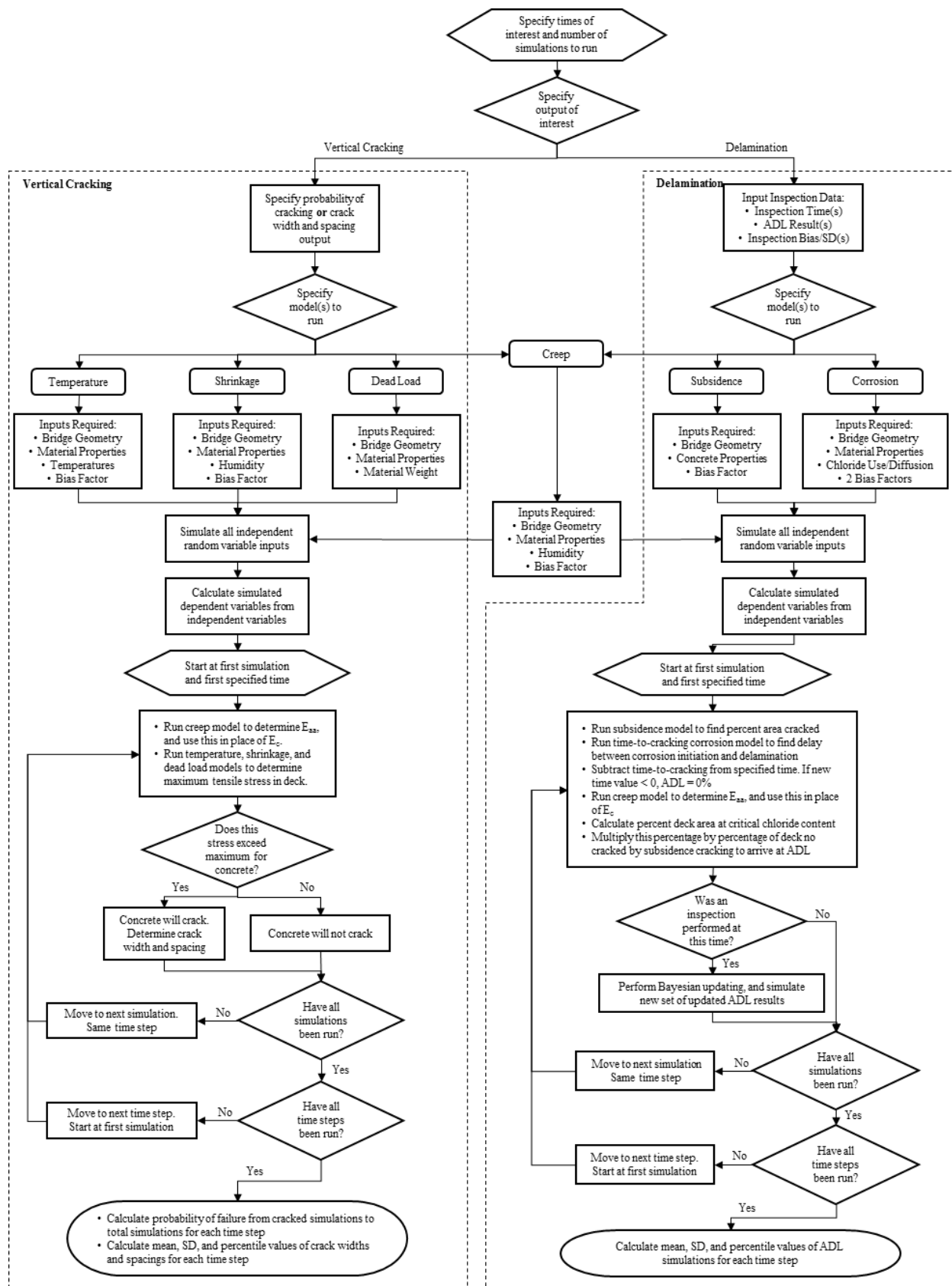


Figure 3.1. Flowchart of CDCPM order of operations

CDCPM uses Monte Carlo simulations to evaluate the uncertainty in the crack width and spacing for vertical cracks and ADL for delaminations. Monte Carlo simulation involves the calculation of multiple scenarios of a complex model based on simulated values. CDCPM first simulates each variable from its underlying probability distribution to create a vector of representative values for each parameter. Next, parameters that are dependent on the input parameters are calculated. This assumes that all variables are either uncorrelated (direct inputs) or fully correlated (calculated from a direct input).

Once all the necessary variables are available, CDCPM can be run through multiple simulations. This is done using two “for” loops, which will run the same process multiple times, changing a single variable for each iteration. This variable is an indexing term such that each run through will use a different value from the simulated input vectors. The outer loop is run for each time of interest in the model, and the inner loop is run for each simulation in the model. The reason for running the time loop on the outside is that all simulations are needed to run the inspection update, and the update must be performed at a specific time. Therefore, the number of model runs for any given simulation is equal to the time steps multiplied by the number of simulations. The output deterioration data consists of a matrix, where each row contains the output of each simulation and each column contains the results for each time step.

3.1.1 Subsidence Cracking Model

Subsidence cracking occurs when the concrete surrounding embedded rebar settles shortly after curing. Dakhil et al (1975) developed an equation that relates the probability of subsidence cracking based on the rebar cover, rebar diameter, and concrete slump. After conducting experiments on three sets of rebar embedded concrete samples with 3 slumps, 4 rebar covers, and 3 rebar sizes (108 total samples), they determined an equation to fit the data based on

multiple regression analyses of combinations of the variables using linear and curvilinear relationships. The resulting best-fit equation is shown in equation 11 below.

$$y = 1.37 - 0.58 * d_c - 0.56 * \frac{d_c}{D_r} + 0.27 * slump \quad (11)$$

$$p_c = \frac{1.5 * e^y - 0.5}{1 + e^y}$$

- d_c = rebar cover (in)
- D_r = rebar diameter (in)
- $slump$ = concrete slump (in)
- p_c = probability of subsidence cracking

This equation is empirical, where the dimensions are not consistent, but it has shown to be an accurate predictor of subsidence cracking when compared to the aforementioned experiments. The probability of subsidence cracking increases as the value of y increases. This means that higher slumps, lower rebar cover and larger rebar diameters will increase the probability of cracking. For use in CDCPM, the probability of cracking can be assumed to represent the overall percent of a bridge deck that will experience this type of cracking. For example, if there is a 2% probability that subsidence cracking will occur, then over an entire deck area, 2% of the deck area will experience cracking from subsidence. This interpretation was used in another study on corrosion effects on concrete bridge decks (Cady & Weyers, 1983).

3.1.2 Temperature Model

The effects of temperature variations in both time and location can have a large effect on a concrete deck if the deck is restrained from moving. There are many ways in which temperature may affect the deck. First, the rise and subsequent drop in temperature due to the heat of hydration of concrete as it cures may cause significant residual strain, especially for concrete with high early strength. After this, temperature variation may be present due to daily or

seasonal temperature variations or from the temperature differential within the deck. By analyzing the region-specific temperature history, estimates of the annual mean, minimum, and maximum temperature probability distributions are made. If the deck is restrained from moving with these temperature fluctuations by the girder, steel rebar, or fixed end conditions, the strains induced will cause stress in the girder.

Krauss and Rogalla (1996) present a model for analyzing the stresses in the top and bottom of a concrete deck embedded with rebar and acting compositely with the girder such that strain compatibility exists between the bottom of the deck and the top of the girder. Two temperature model profiles are presented in their analysis: 1) a uniform temperature change in the deck and uniform temperature change in the girder, or 2) a linear temperature change profile from the top to the bottom of the deck and a uniform temperature change in the girder. Both models are shown in Figure 3.2, and either one may be valid depending on the situation.

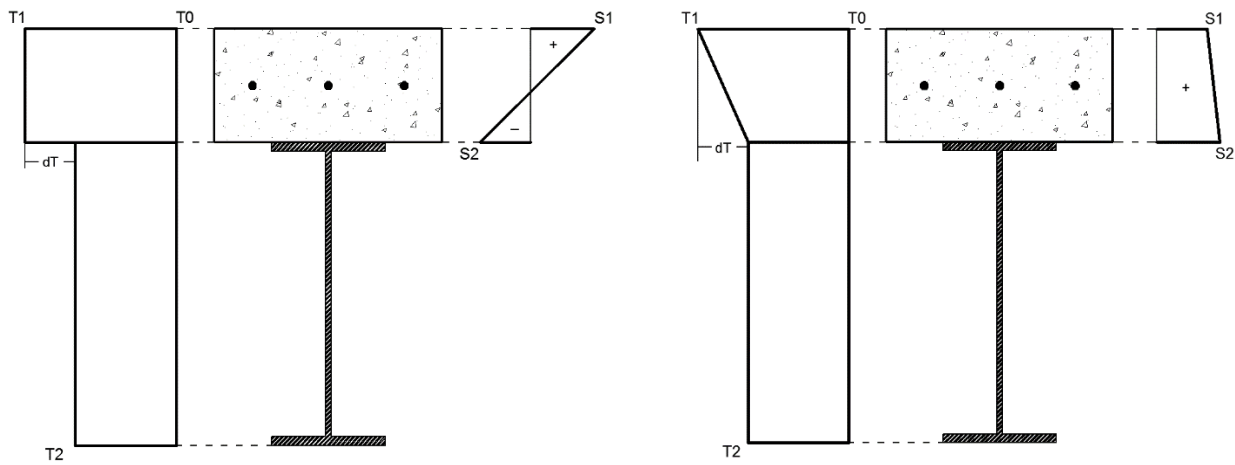


Figure 3.2. Temperature profiles for uniform temperature (left) and linear temperature (right) in the deck

The equations are developed based on structural analysis of the composite system with three unknowns: 1) axial force at the deck soffit, 2) bending moment in the deck, and 3) axial force in the steel rebar embedded in the deck. The locations of these forces are illustrated in Figure 3.3 below.

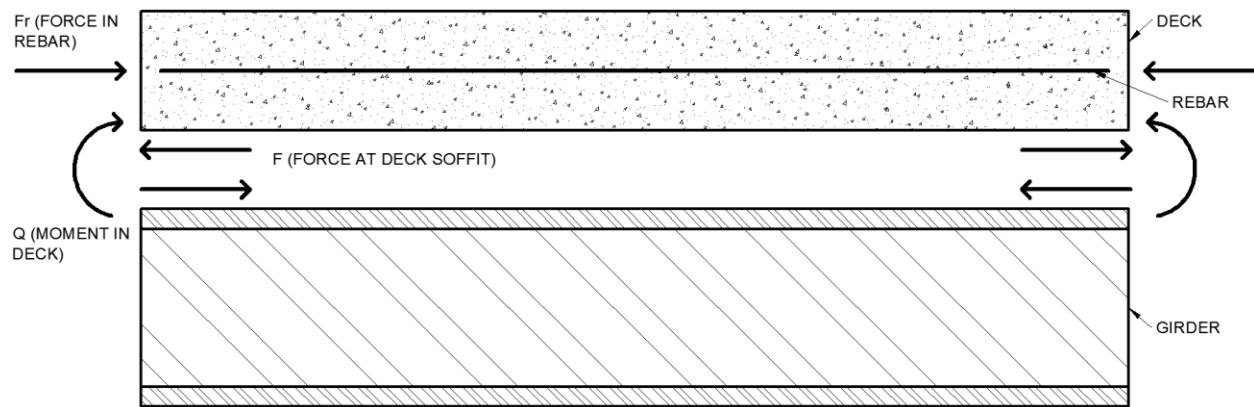


Figure 3.3. Location of forces used in analyzing deck and girder for temperature

To solve for three unknowns, three compatibility equations are formulated: 1) strain compatibility between the bottom of the deck and the top of the girder, 2) curvature compatibility between the bottom of the deck and top of the girder, and 3) strain compatibility between the steel reinforcement and the concrete at the level of reinforcement. All of these equations for both the uniform temperature change and linear temperature change are presented in the Appendix. After solving the equations for the unknown forces, the stress in the top and the bottom of the deck can be calculated. This is the model implemented in CDCPM.

3.1.3 Shrinkage Model

The shrinkage of concrete occurs due to the drying and temperature changes the concrete experiences over time. The temperature shrinkage was discussed in section 3.1.2. The GL2000 model developed by Gardner and Lockman (2001) is used in the present deterioration model due to its practical input parameters. As explained in section 2.4.3, the GL2000 Model provides a superior prediction over the ACI-209, CEP-FIB, and B3 models as shown by Goel et al (2007), and the model uses only inputs available at the time of deck curing, which are easily obtainable.

The GL2000 model predicts the shrinkage strain of the concrete at a specified time based on the concrete strength, relative humidity, volume-to-surface area ratio of the concrete member,

and curing time. After determining the ultimate shrinkage value based on the concrete compressive strength and cement type, the model uses two adjustment factors: 1) humidity factor and 2) time factor. The humidity factor accounts for the difference in humidity between the concrete and the surrounding atmosphere. The concrete is assumed to have 100% pore humidity after curing, and this water will evaporate into the atmosphere over time. The more evaporation, the more shrinkage strain will be induced. The time factor adjusts the ultimate shrinkage depending on the time since curing. The more time that passes after curing, the more shrinkage will be induced up to the ultimate shrinkage strain. The ultimate shrinkage strain is then multiplied by the product of these factors to obtain the approximate shrinkage at any given time after curing. The prediction equations for shrinkage are shown in the Appendix.

To find subsequent stresses imposed on the deck due to shrinkage, the shrinkage strain is represented as an equivalent temperature change, and the aforementioned uniform temperature structural analysis model is used to find the stresses as discussed in section 3.1.2. The equivalent temperature drop is determined by solving the temperature strain relationship for the final temperature, and applying this to the uniform temperature profile model by Krauss and Rogalla (1996). The entire girder below the deck is assumed to have no temperature gradient, and the deck section is assumed to have a uniform temperature decrease such that the imposed strain is equivalent to the shrinkage strain. Figure 3.4 below shows this profile as well as the shrinkage strain transformation. This provides a consistency in the analysis of drying and temperature shrinkage for the combination of concrete effects in section 3.1.7.

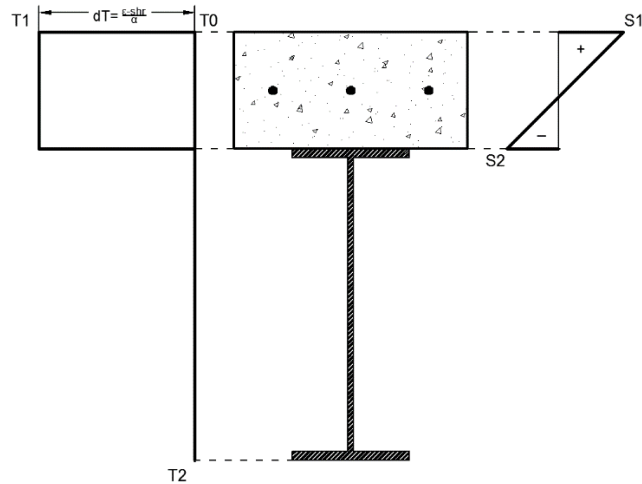


Figure 3.4. Shrinkage strain model for determining deck stresses (Krauss & Rogalla, 1996)

3.1.4 Creep Model

The creep model has similar calculations to the shrinkage model, since these two processes are often discussed together, but the implementation is very different. In addition to the variables used in the shrinkage model, the creep model also depends on the time of load application and the compressive strength and modulus of elasticity at the loading time. The creep coefficient, which is the ratio of total strain with creep to the initial elastic strain, is estimated in two stages: 1) drying creep and 2) basic creep. The drying creep occurs after curing and is usually a small part of the total creep. The basic creep occurs under a sustained, constant load, and is quantified by the creep coefficient. The stages of creep strain increase can be divided into three stages: 1) primary, 2) secondary, and 3) tertiary creep. A figure illustrating the trends of each stage is shown in Figure 3.5 below.

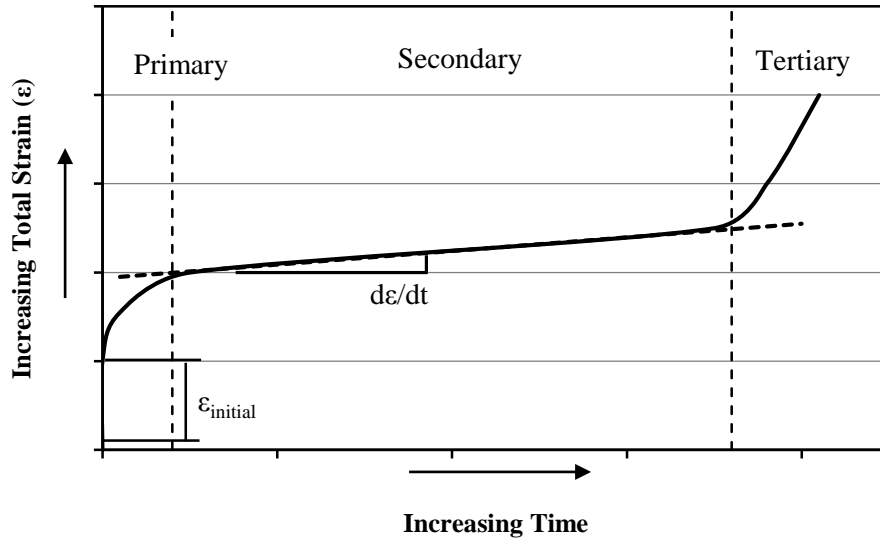


Figure 3.5. Creep stages in concrete

The GL2000 model models the creep strain within the primary and secondary stages. The effect of tertiary creep is ignored in the analysis by Gardner and Lockman, and is not considered here. In most cases, tertiary creep will not take effect unless the load is within 90% of the maximum load (Mazzotti & Savoia, 2003). Therefore, the time model for creep used by Gardner and Lockman predicts the primary quick increase in creep that decreases as time passes. For large values of time, the rate of change in the creep strain approaches a constant value.

In structural analysis, the most common numerical representation of creep is through the creep coefficient. The change in the coefficient with time depends on two factors: 1) time of interest in the analysis (t) and 2) time that the stress was initially applied (t'). The GL 2000 equations for estimating the creep coefficient are given in the Appendix. While this representation is easy to interpret and compare, the creep coefficient is difficult to implement in an analysis and does not give an accurate representation of stress relaxation or aging in strain-controlled processes such as shrinkage. Therefore, the creep is implemented into the rest of the model as an age-adjusted effective modulus of elasticity (Zdenek P. Bazant & L'Hermite, 1988).

The following steps outline the procedure for determining the age-adjusted effective modulus for creep analysis as done in CDCPM:

- 1) Calculate the creep coefficient from the GL 2000 model.
- 2) Calculate the creep compliance from the creep coefficient and concrete modulus of elasticity.
- 3) Estimate the relaxation function at a particular time from the creep compliance.
- 4) Estimate the age-adjusted effective modulus of elasticity from the relaxation function and creep coefficient.

Creep compliance is the same as the compliance used in typical structural analysis, except that it depends on the time of analysis and the time that the concrete was first loaded. This relation is shown in the equation below for concrete that has a sustained constant loading first applied at time. The units of the creep compliance are consistent with the inverse of the stress unit used. The creep compliance $[J(t, t')]$ is related to the creep coefficient (ϕ) for modelling purposes by the modulus of elasticity as shown in equation 12 below.

$$J(t, t') = \frac{1}{E(28)} + \frac{\phi(t, t')}{E(t')} \quad (12)$$

Bazant developed a representation of the effective modulus that accounts for variable stress histories and concrete aging using the age-adjusted effective modulus (Zdenek P. Bazant, 1972). Concrete aging occurs from the continuous nature of the hydration process, which continually changes the properties of concrete with time. The age-adjusted effective modulus is determined according to equation 13 below.

$$E_{aa}(t, t') = \frac{E(t') - R(t, t')}{\phi(t, t')} \quad (13)$$

The modulus of elasticity and the creep coefficient are considered, but the adjustment for aging and stress histories is accounted for in the relaxation function, $R(t, t')$. The relaxation function is related to the creep compliance, and describes the stress relaxation at a constant strain. The creep compliance and relaxation function are complementary to each other, which means if one of them is known, then the other one can be determined directly. An exact solution involves solving multiple integrals of the material stress-strain curve for different levels of creep to arrive at the relaxation function. However, Bazant and Kim (1979) developed an algebraic formula for estimating the relaxation function using only the creep compliance function. This function is shown in the equation 14 below.

$$R(t, t') = \frac{0.992}{J(t, t')} - \frac{0.115}{J(t, t-1)} \left(\frac{J(t-\Delta, t')}{J(t, t'+\Delta)} - 1 \right) \quad (14)$$

$$\Delta = \frac{(t - t')}{2}$$

According to Bazant and Kim, this equation can predict the relaxation function within 2% of the exact theoretical solution from numerical integration. Due to computational efficiency of using the algebraic function, this is used to represent the relaxation function for the age-adjusted effective modulus calculation.

Creep is incorporated into the other models, because it does not cause a stress or strain in the concrete. When creep is applied to the shrinkage and temperature models, the stress is reduced due to the controlled strain condition over time. The dead load in the concrete is also calculated, because it is a constant, sustained load in the deck. The dead load stress is calculated using structural analysis of the simply-supported composite deck and girder section. Creep is then applied to this load, and results in increasing strain over time.

3.1.5 Chloride Diffusion Model for Corrosion Initiation

Corrosion of the steel rebar embedded in the deck is the main cause of delamination, which is one of the more serious forms of deterioration for concrete decks. Corrosion occurs when chlorides reach the rebar, erode the protective film around the rebar, and reduce the alkalinity such that the corrosion reaction can occur. Chlorides can reach the rebar through either vertical cracks along the rebar or by diffusion through the concrete pore structure. The formation of vertical cracks provides a direct path for chlorides to reach the reinforcement, which is a nearly instant process. This section focuses on the diffusion model that can lead to much more extensive delamination later in the bridge's service life.

The most common model for diffusion of particles through a medium is Fick's second law of diffusion, and this is the common model used among researchers for chloride diffusion through concrete (Basheer, Chidiact, & Long, 1996; Cady & Weyers, 1983; Stewart & Rosowsky, 1998a). Fick's second law of diffusion estimates the concentration of a solute at a specified depth and time based on the surface concentration and diffusion rate. The differential equation and the analytical solution are given in equations 15 and 16 below, respectively, for one-dimensional diffusion in a semi-infinite solid.

$$\frac{\partial C}{\partial t} = D \frac{\partial^2 C}{\partial x^2} \quad (15)$$

$$C(x, t) = C_o \left[1 - \operatorname{erf} \left(\frac{x}{2\sqrt{tD}} \right) \right] \quad (16)$$

- C_o = chloride concentration at deck surface (kg/m^3)
- D = diffusion rate (cm^2/s)
- x = depth of interest below surface, cover depth for concrete decks (cm)
- t = time since diffusion initiation (s)
- $\operatorname{erf}(X)$ = error function

This model assumes a constant diffusion rate and chloride concentration at the surface with time. Over time, the chloride concentration will build at the level of the rebar, and will eventually initiate corrosion in the rebar once the concentration reaches a threshold for corrosion initiation. This threshold has been examined through experiment (Cady & Weyers, 1983; Clear, 1974).

This equation can be used to estimate the percentage of the deck that has chloride-induced corrosion at a specified time by using the variability in the rebar depth across the bridge. While the rebar is placed at an average depth over the entire deck, there is always variability in the actual distance between the deck surface and the rebar. The rebar closest to the surface will start corroding first, assuming that the chloride concentration on the surface is uniform and the diffusion rate is the same at all locations on the deck. Under these assumptions, the percent area of the deck with corroding rebar is equal to the percent of rebar at a depth above the chloride threshold. Figure 3.6 shows this concept. This assumption has been used in other research (Cady & Weyers, 1983; Stewart & Rosowsky, 1998b), and is applicable to practical bridge inspection since the deck contains rebar uniformly distributed over the area.

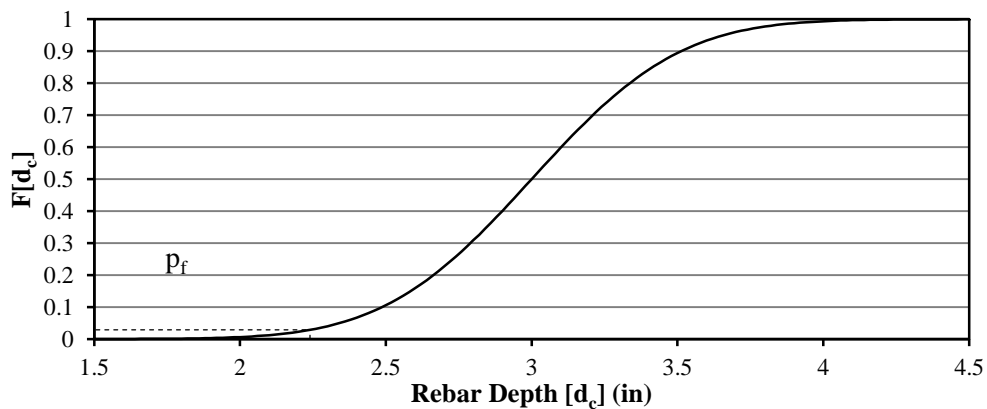


Figure 3.6. CDF of rebar depth to determine percent of rebar above chloride concentration threshold

3.1.6 Time-to-Cracking Model for Corrosion

Liu and Weyers (1998) developed a model that predicts the time between when the corrosion first initiates and when the concrete cover around the rebar first cracks. Their approach uses the critical weight of corrosion products to initiate cracking (W_{crit}) and the corrosion rate (i_{corr}) to determine the time to cracking of the concrete cover. This relation is shown in equations 17 and 18 below.

$$t_{cr} = \frac{W_{crit}^2}{2k_p} \quad (17)$$

$$k_p = 0.098(1/\alpha)\pi D_r i_{corr} \quad (18)$$

- α = ratio of the mass of rust to the mass of steel per unit volume
- D_r = initial diameter of steel rebar (in)

The critical weight of corrosion products is determined based on the structural analysis of a thick-walled concrete cylinder with embedded rebar at its center. The analysis presented by Liu and Weyers allows for an effective pore space around the steel, where corrosion products can build without causing pressure on the concrete. Equation 19 below is used to describe the critical weight of corrosion products.

$$W_{crit} = \rho_{rust} \left(\pi \left[\frac{d_c f'_t}{E_{aa}(t, t')} \left(\frac{a^2 + b^2}{b^2 - a^2} + \nu_c \right) + d_{pore} \right] D_r + \frac{W_{st}}{\rho_{st}} \right) \quad (19)$$

- ρ_{rust} = density of rust (lb/in³)
- f'_t = tensile strength of concrete (psi)
- a = inner radius of concrete cylinder model (in)
- b = outer radius of concrete cylinder model (in)
- d_{pore} = equivalent pore thickness around steel reinforcement (in)
- W_{st} = weight of steel corroded (lbs)
- ρ_{st} = density of steel (lb/in³)

This allows for an estimate of the time-to-cracking based mostly on input that can be measured directly or obtained from experimental results of similar conditions. While values such

as equivalent pore space and mass of rust product are used, they can be fit to experimental numbers and be modelled with a larger coefficient of variation. The combination of equations 17 through 19 can model the state of delamination with time.

3.1.7 Combining Models to Determine Formation of Vertical Cracks

The formation of vertical cracks in concrete is the result of residual tensile stress in the deck caused by restraint. The predominant stress direction for concrete bridge decks over simple spans is parallel to the flow of traffic, because the girders below the deck restrain deformation in this direction. Therefore, the model for vertical crack formation considers transverse cracking due to temperature and shrinkage strains with stress relaxation due to creep, as well as dead load stresses with creep. For inspections, vertical cracks are quantified by their width and spacing if they exist, so the following model attempts to estimate the probability of cracking, and the crack width and spacing if they occur.

All four models are combined together to get an idea of the overall state of stress in the deck. Creep is implemented in the model as the age-adjusted effective modulus of concrete, and is input into each model in place of the concrete modulus of elasticity. Since tensile stress is the determining factor for cracking, the stress caused by shrinkage, temperature, and dead load at the top and bottom of the deck are superimposed to arrive at the total stress in the concrete deck.

Once the total stress in the deck is estimated, this value is compared to the concrete tensile strength to determine the probability of cracking. This is done by running Monte Carlo simulations on the limit state function shown in equation 20 below.

$$G(X) = \sigma_{applied}(X) - f'_t \quad (20)$$

The Monte Carlo simulations are performed based on simulation of the input data from their estimated probability distributions. For some models, this probability may be very small and many simulations may need to run to arrive at a value for probability of cracking. Therefore, an analysis was performed to estimate the distributions of both parts of the limit state to use in a FOSM analysis of two variables. The distribution of the tensile strength is lognormal, based on past research (Ellingwood & Galambos, 1983). The output data for the total applied tensile stress was determined to fit a normal distribution based on probability plotting at different times. An example plot is shown in Figure 3.7 below.

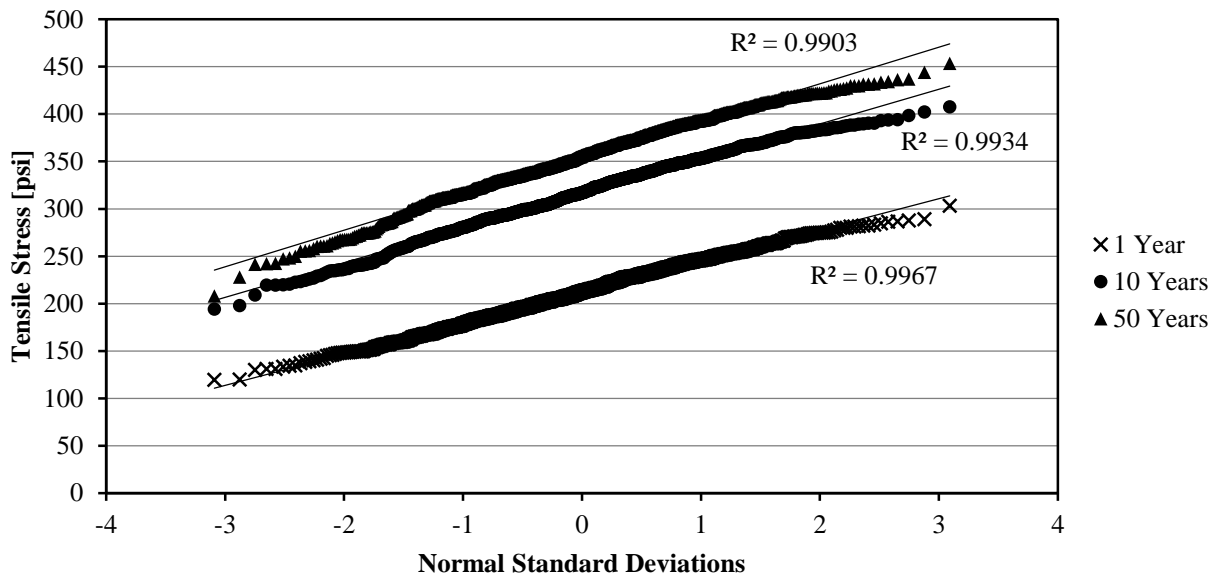


Figure 3.7. Normal probability plot of tensile stress output for various times

Regardless of the time of analysis, the tensile stress shows a close fit to a normal distribution. This may be explained by the central limit theorem (Von Bahr, 1965), which states that the sum of a large number of distributions approaches a normal distribution. The total stress is the summation of three other stress distributions, so the result is approaching a normal distribution.

From here, the probability of failure is determined using numerical evaluation of the limit state for the reliability index, β , and then transforming this into the probability of failure using the standard normal distribution (Melchers, 1999). This is also known as a first-order second-moment reliability analysis. The following steps are taken to perform this analysis:

- 1) The distributions of applied stress and tensile strength of concrete are both transformed to their respective standard distributions using equation 21.

$$\bar{\sigma}_{applied} = \frac{\sigma_{applied} - \mu}{SD}, \quad \bar{f}'_t = \frac{\ln(f'_t) - \lambda}{\zeta} \quad (21)$$

- μ, SD = mean and standard deviation of the data set
- λ, ζ = mean and standard deviation of the associated normal distribution for a log-normal data set

- 2) The number of standard deviations to failure is determined for both probability distributions, where the input point is set as the mean of the other distribution. This is done using equation 22 below.

$$a_{\sigma_{app}} = \frac{\mu_{f'_t} - \mu_{\sigma_{app}}}{SD_{\sigma_{app}}}, \quad a_{f'_t} = \frac{\ln(\mu_{\sigma_{app}}) - \lambda_{f'_t}}{\zeta_{f'_t}} \quad (22)$$

- 3) Using trigonometry, the reliability index can be calculated by equation 23. Figure 3.8 provides a visual representation of the reliability index.

$$\beta = a_{f'_t} * \cos \left[\tan^{-1} \left(\frac{a_{f'_t}}{a_{\sigma_{app}}} \right) \right] \quad (23)$$

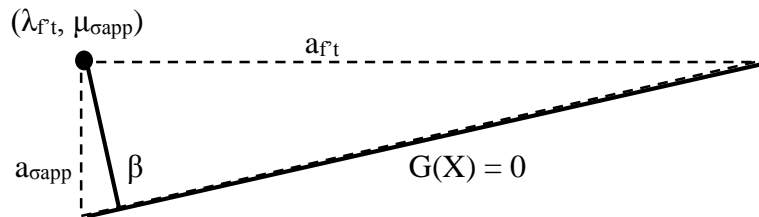


Figure 3.8. Visualization of the reliability index calculation

- 4) The probability of failure is calculated from the standard normal distribution (see section 2.1.2).

If the bridge deck cracks, the way that the severity of the cracking is quantified is through the crack spacing and crack width. The estimation of crack spacing is related to the bond slip distance of the rebar when the rupture occurs (Allam, Shoukry, Rashad, & Hassan, 2012). Bond slip occurs when the rebar slips past the surrounding concrete at a crack, eliminating the force transfer between the rebar and the concrete. Once this occurs, the concrete is incapable of carrying any load at the crack surface, so the entire load is carried by the reinforcement. As the distance away from the crack increases, the concrete will bear more of the tensile force up to the point where the rebar-concrete interface is fully bonded. This distance is known as the bond slip distance. One such equation to predict crack spacing is presented in the CEB-FIP code (Bhide & Collins, 1989), and is used in this model. Note that the crack spacing is not dependent on the stress in the concrete, but on the deck geometry. Equation 24 shows this.

$$S_{cr} = 2 \left(d_c + \frac{S_{rebar}}{10} \right) + 0.1 \frac{D_r}{\rho_r} \quad (24)$$

- S_r = spacing of longitudinal reinforcement (in)
- ρ_r = reinforcement ratio, [= $A_r/(b_c t_c)$]
- A_r = area of reinforcement (in²)
- b_c, t_c = width and thickness of concrete deck, respectively.

The prediction of the crack width is based on the strain in the concrete. Most codified equations estimate crack widths for flexure, where the width will be different due to the curvature developed in the beam. The concrete deck is typically curved as well due to the restraint on the bottom of the deck, but the equations from ACI 318 and BS 8110 are not appropriate for decks. Therefore, a simple analysis of the tensile strain in concrete is used to

estimate crack widths based on the calculated spacing. Equation 25 is adopted to estimate the crack width based on the strain and crack spacing (Bhide & Collins, 1989).

$$w_{cr} = S_{cr} * \varepsilon_t \quad (25)$$

- w_{cr} = crack width (in)
- S_{cr} = spacing of cracks (in)
- ε_t = maximum concrete strain at tensile failure (in/in)

Most equations to analyze vertical cracks exist to provide designers a reliable means to estimating the approximate spacing and maximum crack width, which tends to be a very conservative estimate (Allam et al., 2012). The model can project the probability of cracking and the approximate values of any existing cracks. The probability of cracking is a good indicator of when an inspection may be needed. The crack width and spacing, while useful, are less reliable in terms of actual value. Due to the high uncertainty in the mechanism of vertical cracking and the relative ease of measuring these crack parameters in the field, an inspection will provide the best knowledge of the current cracking condition. Further projections for crack width and spacing do not depend on time-dependent variables, so no future prediction of these parameters are made in the model post-inspection.

3.1.8 Combining Concrete Effects to Determine Delaminations

Delamination is the more serious form of concrete deck deterioration. Delaminations occur due to either corrosion of the steel rebar within the deck or debonding between deck concrete layers. Corrosion is the primary cause of delamination, and may occur in any bridge deck that contains layers of reinforcement embedded in the deck. The present model considers delamination from corrosion only.

Chlorides may penetrate to the level of reinforcement in three ways. 1) Through cracks created during subsidence, 2) through vertical cracks caused by shrinkage of the concrete, and 3)

diffusion through the concrete pores. Vertical cracking due to concrete shrinkage did not show much alignment with transverse rebar (Gergely, 1981), and therefore, the area of rebar affected is only that of the longitudinal bars that the cracks cross. This is a very small area compared to the entire deck, so this effect is neglected in the analysis. This also greatly improves the efficiency of the delamination model by neglecting the temperature and shrinkage models in the analysis, which are very time-consuming to solve. Therefore, only subsidence and diffusion are considered.

First, the percent deck area with chloride-contaminated reinforcement (ADCL) is determined. The ADCL is estimated differently depending on the path of ingress to the reinforcement. According to Gergely (1981), vertical cracks must reach a minimum width of 0.002 inches in order for chlorides to directly infiltrate to the reinforcement. As shown by Kyle (2001), the cracks created by subsidence usually are wider than this value, and therefore the ADCL is equal to the percent area subjected to subsidence cracking that is calculated as shown in section 3.1.1. Diffusion is the most probable cause of ADCL, and it usually occurs later in the bridge's lifespan due to the time it takes to reach the reinforcement layer. The ADCL from diffusion is equal to the percentage of reinforcement above the threshold level at the time of analysis.

The concrete delamination is determined by using the ADCL and time-to-cracking (t_{cr}) model explained in section 3.1.6. For a given time of analysis, the percent area delaminated (ADL) is determined as the ADCL at a time of t_{cr} before the analysis time. This accounts for the time delay between when the rebar is first critically chlorinated before corrosion occurs, and when the corrosion products build to the point where the concrete cracks. When the bridge is

younger than t_{cr} , no delamination is present in the deck. The chloride diffusion model is run at the current time minus the time-to-cracking, and this area is set as the ADL.

3.2 Modeling of Larimer County Bridge LR 50-0.2-17

In order to show the capability and effectiveness of this model for bridge inspection timing and quality, a real bridge deck was chosen to use in all analyses for this model. The sample deck and girder is modeled after bridge LR50-0.2-17, which is located in Larimer County, Colorado just north of the city of Fort Collins. This bridge was originally built in 1936 as a simple span cast-in-place reinforced concrete bridge. In 1962, the bridge underwent a major reconstruction where it was widened with a steel girder superstructure and cast-in-place concrete deck, which is still attached to the original structure today. The reconstruction also changed the direction of traffic over the bridge. Due to the presence of both steel and concrete girders on the bridge, this bridge was ideal to analyze two types of bridge deck and girder combinations. The deck does have an asphalt overlay. Each analysis is performed on the sample sections shown in Figure 3.9 and Figure 3.10. It should be noted that this bridge is scheduled for replacement in 2016.

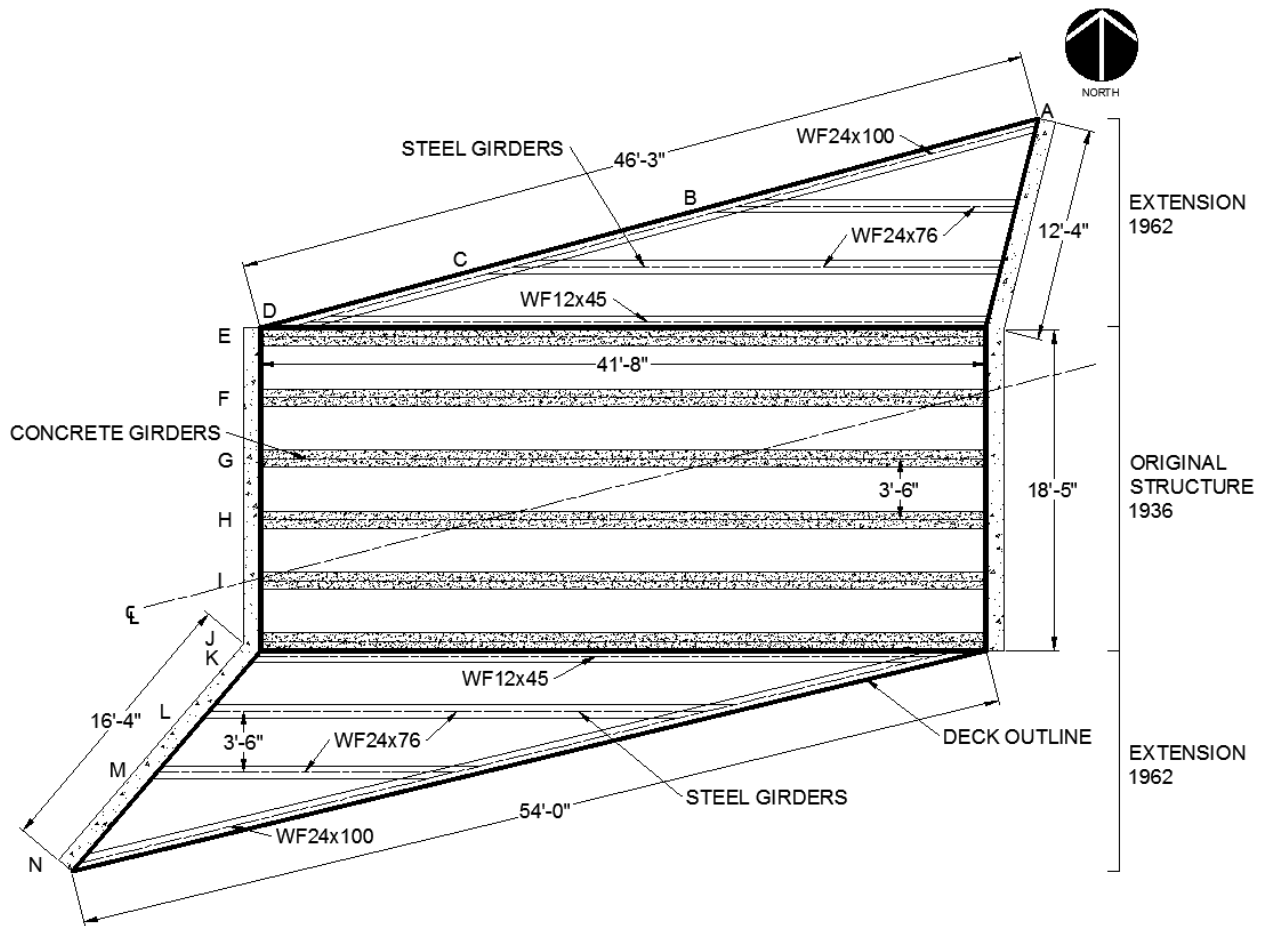


Figure 3.9. Plan view of bridge LR50-0.2-17 in Larimer County, CO

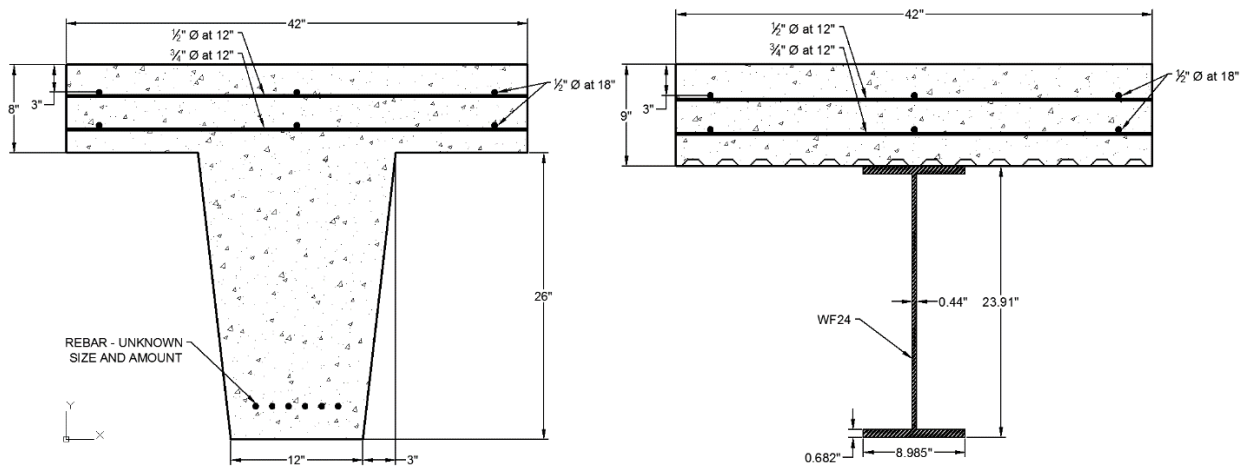


Figure 3.10. Cross sections of the concrete girder (left) and steel girder (right) used in analysis

Figure 3.10 shows a typical composite deck and girder arrangement for this bridge. The concrete sections all have the same length of 41'-8", but the steel sections can vary depending on which girder is examined. For analysis, this section is assumed to span 30', which is the

approximate length of girder C in Figure 3.9. Each section is assumed to be simply supported at the ends, which introduces uncertainty in the results due to the real section not being ideally simply-supported. Further uncertainty is introduced in the model of the actual bridge in that the original drawings of the reinforcement in the concrete girder section no longer exist. Therefore, the size, quantity, and placement of reinforcing steel in this section is unknown. The reinforcement is modeled as the same as the steel section, but the coefficient of variation is augmented to reflect more uncertainty. The rebar size and quantity in the girder is not important for analysis of the deck.

To begin, all of the input parameters must be defined by their second moment representation. Table 3.1 and Table 3.2 show the quantities applied to the parameters in the analysis for bias and coefficient of variation, along with the source of the values, if applicable. The mean values are obtained from the design drawings, or typical values reported in literature.

Table 3.1. Geometry and material parameters for bridge LR 50-0.2-17

Parameter	Unit	Distribution Type	Statistics		Reference or Source of Bias and Variation Information
			Bias	Coefficient of Variation	
Geometry-Concrete Deck					
Slab Thickness	in	Normal	1	0.5*	Nowak et al (1994)
Effective Slab Width	in	Normal	1	0.5*	Adapted: Nowak et al (1994)
Geometry-Steel Girder					
Distance from Centroid to Deck Soffit	in	Normal	1	0.35*	Adapted: Nowak et al (1994)
Total Height	in	Normal	1	0.7*	Nowak et al (1994)
Cross-Sectional Area	in ²	Normal	1	1*	Adapted: Nowak et al (1994)
Moment of Inertia	in ⁴	Normal	1	50*	Adapted: Nowak et al (1994)
Geometry-Steel Reinforcement					
Cover Depth from Surface	in	Normal	1	0.4*	Nowak et al (1994)
Diameter	in	Normal	1	0.011	Adapted: Nowak et al (1994)
Bar C-C Spacing	in	Normal	1	0.4*	Nowak et al (1994)
Material Properties-Concrete					
Compressive Strength at 28 Days	psi	Log-Normal	0.85	0.18	Mirza et al (1979)
Modulus of Elasticity at 28 Days	psi	Log-Normal	0.92 [^]	0.08 [^]	Adapted: Mirza et al (1979)
Tensile Strength at 28 Days	psi	Log-Normal	0.92 [^]	0.09 [^]	Adapted: Mirza et al (1979)
Unit Weight	pcf	Normal	1	0.05	Estes and Frangopol (2003)
Poisson's Ratio	-	Normal	1	0.05	Estimated
Coefficient of Thermal Expansion	in/in/F	Normal	1	0.1	Adapted: FHWA (2011)
Water-Cement Ratio	-	Normal	1	0.05	Estimated
Slump	in	Normal	1	0.1	Estimated
Material Properties-Steel					
Tensile Yield Strength	ksi	Log-Normal	1.05	0.11	Ellingwood (1983)
Modulus of Elasticity	ksi	Log-Normal	1	0.07	Nowak et al (1994)
Unit Weight	pcf	Uniform	490**	503**	Liu and Weyers (1998)
Poisson's Ratio	-	Normal	1	0.05	Estes and Frangopol (2003)
Coefficient of Thermal Expansion	in/in/F	Normal	1	0.1	Adapted: FHWA (2011)

*Value is the standard deviation in units of the parameter.

**Parameter is uniformly distributed over the interval of the two values.

[^]Values are estimated from ACI 318 equation that related to compressive strength at 28 days parameter

- 'Adapted' means the value is not specified in reference, but parameter relates to other values given in reference.
- 'Estimated' means no reference to appropriate values was found, so the given values were assigned based on the range of typical values.

Table 3.2. Deterioration and professional factor parameters for bridge LR 50-0.2-17

Parameter	Units	Distribution Type	Statistics		Reference or Source of Bias and Variation Information
			Bias	Coefficient of Variation	
Environment					
Relative Humidity	-	Beta	1	0.4	Estimated
Deck Temperature at Casting	F	Normal	1	2*	^NOAA Database-Fort Collins, CO
Lowest Girder Temperature	F	Normal	1	10*	^NOAA Database-Fort Collins, CO
Deck Temperature Difference	F	Normal	1	5*	Estimated: Kennedy and Soliman (1987)
Time-to-Corrosion Initiation					
Surface Chloride Concentration	kg/m ³	Log-Normal	1	0.25	Stewart and Rosowsky (1998a)
Diffusion Rate Through Concrete	cm ² /s	Log-Normal	1	0.75	Stewart and Rosowsky (1998a)
Threshold for Corrosion Initiation	kg/m ³	Uniform	0.6**	1.2**	Stewart and Rosowsky (1998a)
Time-to-Corrosion Cracking					
Unit Weight of Rust	pcf	Uniform	219**	234.7**	Liu and Weyers (1998)
Mass of Iron to Mass of Rust Ratio	-	Uniform	0.523**	0.622**	Liu and Weyers (1998)
Equivalent Pore Thickness around Rebar	in	Normal	1.25	0.08	Adapted: Liu and Weyers (1998)
Corrosion Rate	μA/cm ²	Normal	1	0.2	Stewart and Rosowsky (1998a)
Pitting Corrosion Factor	-	Type I EVD	1	0.22	Turnbull (1993)
Concrete Cracking					
Crack Width	in	Normal	1	0.4	Stewart and Rosowsky (2003)
Professional Factors					
Shrinkage Model	-	Normal	0.99	0.129	Adapted: Goel et al (2007)
Creep Model	-	Normal	1.2	0.22	
Subsidence Cracking Model	-	Normal	1	0.02	Values for these factors are not available. Therefore, no bias is applied and variation is kept the same for all.
Corrosion Initiation Model	-	Normal	1	0.02	
Corrosion Cracking Model	-	Normal	1	0.02	

*Value is the standard deviation in units of the parameter.

**Parameter is uniformly distributed over the interval of the two values.

^Values fit to data collected from NOAA National Climatic Data Center. Station located in Fort Collins, CO. See section 3.5.2.

- 'Adapted' means the value is not specified in reference, but parameter relates to other values given in reference.
- 'Estimated' means no reference to appropriate values was found, so the given values were assigned based on the range of typical values.

While most of the parameters can be reported or adapted from the literature, some of this information is estimated due to scarce testing available for determining the appropriate values. For example, the variation chosen for the Poisson's ratio of concrete was chosen to encompass all possible values that are typical of concrete. Each parameter is modeled using a well-known CDF for which the relation between mean and standard deviation to distribution-specific parameters is known. Many distributions came from reported literature, but the distributions of the parameters that are estimated are either normal or chosen based on domain of the parameter, such as the relative humidity.

3.3 Incorporating Inspection Results into Model and Projecting the Future Condition

3.3.1 *Updating the Current Condition with Inspection Results for Delamination*

Objective four asks how inspection results change our knowledge of uncertainty in bridge deck cracking. Inspection results are also uncertain due to the precision and accuracy of the test, the quality of the equipment or inspector, and the environmental conditions surrounding the test site. This uncertainty can sometimes be quite large. While these results can be looked at independently from the model results, this is not the most efficient use of data. Since there are two sets of information available to describe the current condition, conclusions about the actual current condition can be made more certain by considering both the model output and the inspection results together. This is done through Bayesian updating.

The Bayesian updating is performed by using a discretization procedure of the domain of ADL and finding the combined probability of each bin. The distribution of the model data is set as the prior distribution for analysis, and is represented by a set of simulated points from the output of CDCPM. The variability of the inspection data is assumed to be a truncated normal, where the truncation prevents simulating values below 0% or above 100%.

The procedure for performing the Bayesian analysis is as follows:

1. The domain of ADL is discretized into bins, as shown in Figure 3.11. The bins are log-distributed on the sample space such that smaller bins occur close to zero, where the majority of sample points are expected to be.
2. A truncated normal distribution is created with a mean equal to the product of the bias factor and inspection result, and a coefficient of variation related to the inspection procedure performed.
3. For each bin, the percent of model samples in the bin is calculated and the probability that the inspection value is in the bin is calculated.
4. Applying Bayes' theorem, the probability the actual ADL falls within a bin range based on both data sets is calculated.
5. A simulated CDF of the posterior function is summing the probabilities at each bin with all bins lower in value.
6. A new set of random variables is generated from the simulated posterior CDF for ADL.

The result is a new sample set of variables based on knowledge from two sources.

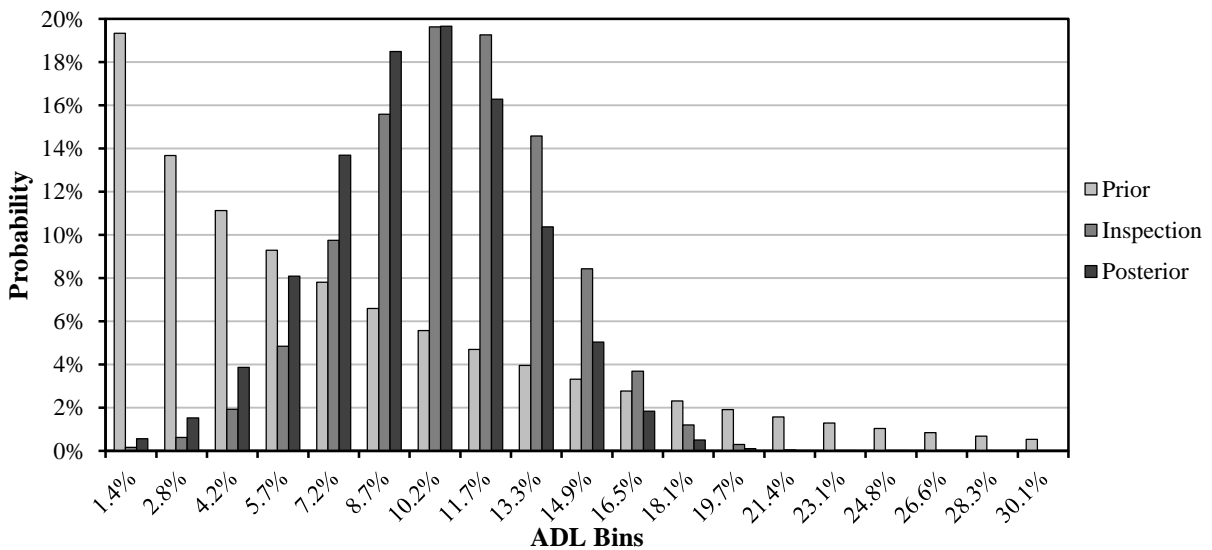


Figure 3.11. Visualization of Bayesian updating using bins

For this thesis, no actual inspections using NDE technology were conducted on this bridge. However, since each method is input as a bias and coefficient of variation in the model along with the inspection result, the effect of different NDE procedures are analyzed by evaluating a range of inspection bias and coefficients of variation using uncertainty forecast plots. These plots show how the inspection outcome will affect the knowledge of deck delamination after the Bayesian updating procedure.

3.3.2 Projecting the Future Condition Post-Inspection

The future condition can be determined by running CDCPM for the time of interest. However, this causes problems when the condition is to be updated using inspection results. These results cause discontinuities that the equations do not account for. Therefore, the future condition is determined by adjusting the model to the time when the updated percent deck area delaminated would be observed, whether this is greater than or less than the last model output. This term is referred to as the time error in analysis.

The time error is determined after the new set of ADL values is calculated from an inspection result. After each inspection update, the ADL is input into the chloride diffusion model and the time to this ADL is back-calculated. This time will be different from the time input in the model. The difference of the updated time from the model time is equal to the time error. For all future time simulations after the update, this time error is subtracted from the model time input. This ensures that future projections are based on the magnitude of the updated ADL, and not on where the model previously projected the condition to be.

3.4 Sensitivity Analysis for Vertical Cracking and Delamination

The first objective asks what parameters of the bridge deck contribute the most to uncertainty in cracking. This was done using a sensitivity analysis, which tests each parameter individually to see how the cracking output is affected. Once information on the uncertainty of the input parameters was known, a variance-based sensitivity study was conducted to see which parameter uncertainty most affected the ADL output uncertainty. This is done to identify which variables are controlling the uncertainty in the vertical cracking and delamination so that inspections can be geared to the causes of uncertainty instead of the cracking itself. If the variables that contribute most to cracking can be identified, then inspections can be geared toward these factors to reduce the uncertainty in cracking.

Variance-based sensitivity studies examine how the variance in the input parameters affect the variance in the output. All of the input parameters used in a specific model are shown in Table 3.3 below.

Table 3.3. Variable parameters used in both cracking models for sensitivity study

Vertical Cracking Model Input	Delamination Model Input
<p>Geometry</p> <ul style="list-style-type: none"> • deck thickness • flange thickness • volume-surface area ratio • rebar diameter • cover depth • spacing of longitudinal rebar • girder height • distance from girder centroid to deck soffit • cross-sectional area of girder • moment of inertia of girder <p>Material Properties</p> <ul style="list-style-type: none"> • concrete compressive strength • modulus of elasticity of concrete • tensile strength of concrete • weight of concrete • Poisson’s ratio of concrete • coefficient of thermal expansion of concrete • modulus of elasticity of steel rebar • coefficient of thermal expansion of steel rebar • modulus of elasticity of girder material • weight of girder material • coefficient of thermal expansion of girder material <p>Environmental Factors</p> <ul style="list-style-type: none"> • relative humidity • temperature at time of casting • maximum/minimum temperature during season • temperature difference in deck <p>Bias Factors</p> <ul style="list-style-type: none"> • bias in creep model • bias in shrinkage model 	<p>Geometry</p> <ul style="list-style-type: none"> • volume-surface area ratio • rebar diameter • cover depth • thickness of pore band around the rebar <p>Material Properties</p> <ul style="list-style-type: none"> • concrete compressive strength • modulus of elasticity of concrete • tensile strength of concrete • Poisson’s ratio of concrete • percent of fine aggregate in total aggregates • cement content • water content • aggregate content • concrete slump • unit weight of rebar steel • unit weight of rust product • mass ratio of rust product to steel <p>Chloride Diffusion/Corrosion Factors</p> <ul style="list-style-type: none"> • corrosion rate • pitting corrosion factor • surface chloride concentration by weight of mortar • chloride threshold for corrosion initiation at rebar • chloride diffusion rate through cement paste <p>Environmental Factors</p> <ul style="list-style-type: none"> • relative humidity <p>Bias Factors</p> <ul style="list-style-type: none"> • bias in creep model • bias in subsidence cracking model • bias in chloride diffusion model (Fick’s law) • bias in time-to-cracking model

The first-order sensitivity index (FOSI) was chosen for this analysis, which evaluates the level of influence each individual parameter uncertainty affects the overall output uncertainty. Each index is determined using a Monte Carlo-type simulation of the samples. In order to reduce the number of required samples needed for the index to converge, Latin Hypercube sampling is used to reduce the number of required runs, while preserving the accuracy of the output values. The estimation method proposed by Jansen (1999) is used herein to estimate the sensitivity index for every input parameter for each model. Jansen’s formula estimates the numerator of the first-order sensitivity index definition, and is presented in equation 26 below.

$$FOSI = V_{X_i} \left(E_{X_{\sim i}}(Y|X_{\sim i}) \right) = V(Y) - \frac{1}{2N} \sum_{j=1}^N \left(f(B)_j - f(A_B^{(i)})_j \right)^2 \quad (26)$$

- N = number of Monte Carlo simulations
- A, B = two $N \times k$ independent matrices of N simulated variables for k input parameters
- $f(B)_j$ = model output for simulated row j of input parameters from matrix B .
- $f(A_B^{(i)})_j$ = model output for simulated row j of the input parameters from matrix A , with column i of matrix B is substituted for column i of matrix A .

The FOSI is typically a value between 0 and 1. Each parameter is assigned a FOSI, and the higher the value of the FOSI, the larger the influence of that parameter uncertainty on the uncertainty of the output value. The FOSI for a particular parameter may also be dependent on the time of analysis. Therefore, the analyses will evaluate the FOSI for all input parameters listed in Table 3.3 at different times during the bridge's service life to examine which parameters are important at which times.

3.5 Determination of Parameter Values for Climate Analysis

The second objective asks how the climate surrounding the bridge affects the uncertainty in concrete deck cracking. This is answered by evaluating the input variables in CDCPM that a climate-dependent. Three classes of input parameters are identified: 1) humidity, 2) ambient seasonal temperatures, and 3) surface chloride concentration. Each parameter arises from different reasons, and therefore, the analysis of each parameter's effect on cracking is performed differently.

3.5.1 Humidity Parameters

Humidity plays a role in the amount of evaporation of pore water the concrete will experience. This evaporation will affect the drying shrinkage and creep rate of concrete over

time (Gardner & Zhao, 1993). Humidity is quantified as relative humidity, so it can only take on values between 0% and 100%. Also, actual humidity values vary greatly within a single day, and can usually encompass the entire range of possible values. Therefore, no location-specific information was gathered for humidity and the analysis was conducted by using multiple mean values in this range, each associated with a range of standard deviations. Due to the restriction on the range of values, the beta distribution is used to model the relative humidity. The mean values chosen are 40%, 60%, and 80%. The standard deviations chosen are 5%, 10%, and 20%. All nine possible combinations are examined.

3.5.2 *Temperature Parameters*

For evaluating the stress due to seasonal temperature fluctuations, representative values for the mean temperature during which the bridge deck was cast and the annual maximum and minimum temperatures are used with the linear temperature profile. These profiles are shown in Figure 3.12. The mean temperature is set as the initial temperature of the deck, T_0 , and the minimum temperature experienced by the deck is set as T_2 . The value from T_1 will take on the value of T_2 plus or minus a temperature differential between the top and bottom of the deck, dT . The positive value for dT occurs due to heating of the deck surface from the sun's radiation during the daytime (Kennedy & Soliman, 1987). The negative dT value occurs when the surface is suddenly drenched with rain or snow, which cools the top of the deck faster than the girder (Kennedy & Soliman, 1987). Table 3.4 below gives typical values for dT based on the season that will be being analyzed.

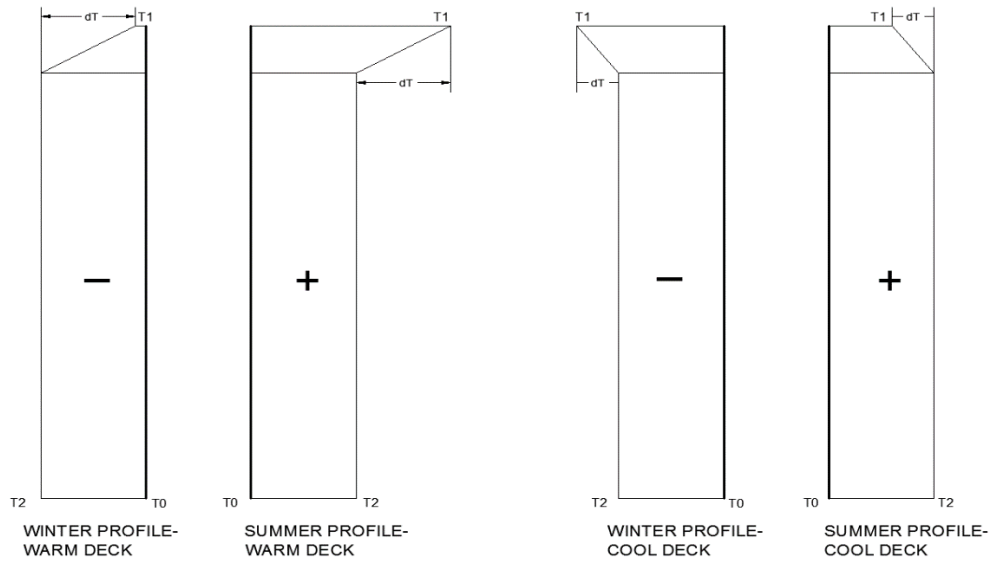


Figure 3.12. Four temperature profiles used in deck stress analysis

Table 3.4. Seasonal temperature differential from the bottom of the deck to the top of the deck (Kennedy & Soliman, 1987)

Season	Maximum Temperature Differential, dT [$^{\circ}F$]	Minimum Temperature Differential, dT [$^{\circ}F$]
Summer	40	-7.5
Winter	20	-7.5

The actual values for T_0 and T_2 are determined based on the region where the bridge is located. The magnitude of the temperature values and their variability from year to year is different depending on where the bridge is located. To determine the appropriate mean, standard deviation, and distribution type for T_0 and T_2 , annual mean and minimum temperature values were collected from four different climate centers during the years from 1931 to 2014, which is 84 data points. The centers were chosen based on their region in the United States and on the completeness of recorded data during the time frame. The four data stations are located in Fort Collins, CO, Ann Arbor, MI, Clemson, SC, and Santa Barbara, CA. Data on the maximum annual temperatures were also collected for the Fort Collins station only.

In order to determine the appropriate distributions for T_0 and T_2 , each data set was evaluated using probability plots. Probability plotting is one of the easiest visualizations of the

goodness-to-fit of a particular probability distribution to a set of data. When the data points of the set are plotted on the probability plot for a specific distribution, a straight line indicates that the distribution is a good model for this sample set. Also, the slope and intercept of the trend line gives an indication of the distribution parameters. It should be noted that this estimation is not the same as the method of moments or maximum likelihood estimation of distribution parameters. Using the coefficient of determination (or R-squared) value as calculated by Microsoft Excel, the goodness-to-fit of the linear trend line to the sample data can be compared between probability distributions.

The normal distribution and type I extreme value distribution of minimum values (Type I) are considered for each data set of minimum annual temperatures. The lognormal distribution was not considered due to the possibility of negative values for temperature. The Gumbel distribution is a popular model to describe the distribution of the maxima or minima of a set of data, so it may apply for the minimum annual temperature value, T_2 . Figure 3.13 below shows the probability plots for Fort Collins, CO for the minimum temperature. The other probability plots for other locations and for the Fort Collins, CO maximum and mean temperatures are shown in Figures A.1 to Figure A.5 in the Appendix.

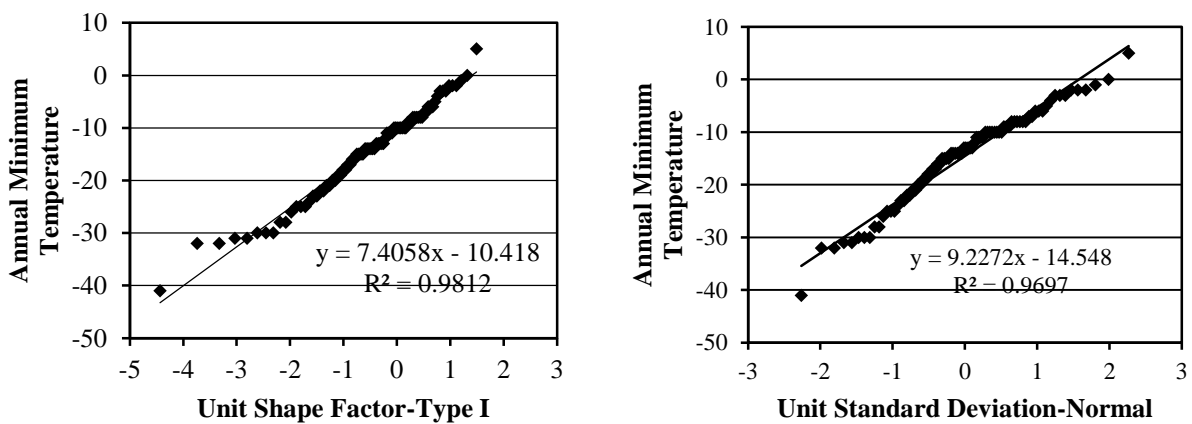


Figure 3.13. Probability plots of minimum annual temperature in Fort Collins, CO for Type I (left) and normal (right) distributions

Based on the R-squared value for each plot, the Type I distribution is the better model for the annual minimum temperature, and the normal distribution is the better fit for the mean temperature. Therefore, these are the distributions chosen to model temperature. The same logic is applied to the other locations and to the maximum temperature in Fort Collins. The parameters that are used to characterize each location annual minimum temperature are presented in Table 3.5 below.

Table 3.5. Mean, standard deviation, and Type I distribution parameters for annual minimum temperatures at various locations

Location	Fort Collins, CO	Santa Barbara, CA	Clemson, SC	Ann Arbor, MI
Mean	-14.7	32.9	10.5	-5.3
Standard Deviation	9.5	4.6	5.6	6.5
Shape Factor	7.4	3.6	4.3	5.1
Characteristic Extreme	-10.4	35.0	13.0	-2.3

3.5.3 Chloride Concentration Parameters

The build-up of chlorides on a deck surface is the result of the use of de-icing chemicals on the deck during the winter or the salt concentration in the air in marine environments. This concentration is variable during the season right at the surface, but at a very small depth below the top surface, the concentration will maintain some maximum value that stays constant at a depth of about 0.5 inches below the surface (Cady & Weyers, 1983). Cady and Weyers collected data on this maximum concentration for four state DOTs: Michigan, Kansas, Missouri, and California. The data is reported in Table 3.6 below.

Table 3.6. Chloride content statistics by % weight of mortar from various state DOTs (Cady & Weyers, 1983)

State	Bridges Inspected	Tests Performed	Chloride as Weight % of Mortar (%)	
			Average	Standard Deviation
Kansas	21	125	0.19	0.07
Michigan	13	42	0.27	0.14
California	21	44	0.29	0.18
Missouri	18	105	0.16	0.13
Totals:	73	316	0.20*	0.12**

*Weighted average

**'Pooled' standard deviation

States such as California have many different climates within one state, and may have many bridges located near the coastline, so this data has the highest average and standard deviation. The values are given as percent of the concrete mortar content. Therefore, the concentration is calculated as the sum of the weight of cement, water, and fine aggregate times the percentages given. Each concentration is analyzed using CDCPM to see the effect on the delamination of the concrete deck.

3.6 Use of Uncertainty in Inspection Planning

This section outlines the example scenarios for implementing the developed inspection plan. Three examples are provided: 1) comparison of proposed inspection plan to the actual inspection plan used on a bridge, 2) planning the timing and inspection method for a future inspection based on the latest inspection report, and 3) planning of inspection method for two bridges when inspection resources are scarce. These examples do not cover every scenario that may arise in inspection planning, but it will provide clarity into the decision-making process that accompanies inspection planning.

3.6.1 Analysis of Past Inspection Results Based on Model Prediction

This demonstration is done not only to validate the model’s prediction, but it also can help to draw conclusions on the appropriate timing of these inspections. The Larimer County Engineering Services division has records of all inspection reports on bridge LR 50-0.2-17 dating back to 1980. Inspections were available for every two-year span except 1982. Analysis of these inspection reports provided insight on not only the quantifiable condition state changes from inspection to inspection, but also on the quality of note taking and damage recognition for each inspection. The AASHTO CoRe elements were not used on this bridge until 1996, so reports before this included only very general assessments of the deck condition, and would be very difficult to compare directly to output from CDCPM.

Since 1996 is the first year of AASHTO CoRe elements in the inspection report, this is chosen as the starting point for the past inspection analysis. Using the model, a projection from 1996 to 2002 is made from this data, and this is compared to inspection reports done in 1998, 2000, and 2002. The six-year span is determined such that it is in line with the maximum allowable inspection interval suggested in NCHRP Report 780. The AASHTO CoRe element ratings and NBI ratings for this deck between 1996 and 2002 are summarized in Table 3.7 below.

Table 3.7. AASHTO CoRe element and NBI inspection ratings for LR50-0.7-17 from 1996 to 2002

Inspection Year	Inspection Month/Day	AASHTO CoRe Element Rating (1-5)	Estimated ADL Based on AASHTO Rating	FHWA NBI Rating (9-0)
1996	9/27	1	0%	7
1998	4/23	2	0% - 2%	6
2000	8/01	2	0% - 2%	7
2002	3/14	2	0% - 2%	6

In the notes from the inspections, hairline longitudinal cracks are observed in the deck from the underside for every inspection year, but no efflorescence or spalling was present, which

means that corrosion is not significant yet. Efflorescence is the result of salt deposits on the concrete surface that are left behind when the water evaporates from the concrete. AASHTO designates this as a smart flag, which is used to note deteriorated conditions not explicitly given in the CoRe elements. This Smartflag is designated as condition state 1 (out of 5 total condition states for this smart flag) in 1996, and is not explicitly given in the other inspection reports.

3.6.2 Predicting Future Inspection Strategy

The latest inspection on the Larimer County Bridge was performed in 2013, so this is the start year from which the next inspection will be planned. The inspection methods considered are chain drag, impact-echo, and ground-penetrating radar for deck delaminations. Timing, inspection effect on uncertainty, and cost (in terms of money and time to conduct inspection) are all considered when choosing the appropriate inspection plan.

The delamination evaluation starts with the ADL simulation output from CDCPM. The bias and coefficient of variation for each test method is estimated to represent information from ASTM standards, and research performed by Hesse (2013). Due to the presence of an asphalt overlay, the impact-echo and the chain drag methods are less effective and could have highly variable results (Yehia et al., 2007). These two methods will have augmented coefficients of variation, with a larger increase on the chain drag than the impact echo (Yehia et al., 2007). The minimum detectable delamination percentage is also taken into account. The GPR minimum detectable delamination is reported by Hing and Halabe (2010), the Impact-Echo value is reported by Sansalone and Streett (1997), and the chain drag value is estimated based on data reported by Maser (2004). The percentage is calculated as the area of the smallest detectable delamination divided by the total bridge area. Using approximate values as shown in Table 3.8

shows the bias, coefficient of variation, and smallest detectable delamination for all three methods as used in this analysis.

Table 3.8. Bias, standard deviation, and smallest detectable area values for various NDE inspections for delamination

Inspection Method:	Chain Drag	Impact-Echo	GPR
Bias	1.219	1.06	1.077
COV (%)	40	15	20
Smallest Detectable Delamination (in²)	50	(0.3*cover) ²	4
Smallest Delamination by ADL of LR50-0.2-17 (%)	0.028	0.00046	0.0022

The inspection report quantified the entire deck as being in condition state 1 in 2013 based on the AASHTO CoRe element rating, so no delamination is assumed from the initial visual inspection. Since the AASHTO rating has no range of ADL for condition state 1, the standard deviation of ADL in 2013 is also set to 0% ADL. A projection is then made for six years, and recommendations on the future timing and required inspection quality are made.

Due to the low initial delamination of the future prediction from the LR 50-0.2-17 inspection reports, another analysis is run as if the deck had more severe delamination. The goal of this is to see how an inspection would be planned for such a bridge deck. The same LR 50-0.2-17 concrete girder section is used in the analysis. After running a GPR inspection in 2013, the deck is considered to be in condition state 4 with a mean ADL of 18%. Using projections of the 90th percentile ADL and the standard deviation of ADL, inspection timing and method recommendations are made.

3.6.3 Inspection Decision between Two Decks

The following scenario is presented to investigate how the proposed inspection plan can be used to allocate scarce inspection resources to two different bridges. A city bridge inspection

planner has two bridge decks that require inspection in the next month. The planner is worried about the possibility of delamination in both decks, but neither bridge deck has ever had a delamination inspection performed before.

Both bridges are 40 feet simple-span bridges that experience moderate traffic during the day. One deck slab is 9-inches thick (Deck A) and the other is 8-inches thick (Deck B). The total area of deck A and deck B is 1600 ft² and 1200 ft², respectively. Deck A and Deck B are 30 years and 60 years old, respectively. Both decks are made with 5000 psi compressive strength concrete and the rebar is A36 in both cases. The girder type that is below the deck is irrelevant for delamination analysis in CDCPM. All corrosion parameters and environmental parameters are kept the same for both bridges. Table 3.9 shows the minimum detectable percent area delaminated for each test on each deck based on this information. Figure 3.14 below shows the design drawings for both decks.

Table 3.9. Minimum detectable ADL for each bridge deck for each inspection method

Inspection Method	Deck A (% ADL)	Deck B (% ADL)
Chain Drag	0.022	0.029
GPR	0.0017	0.0023

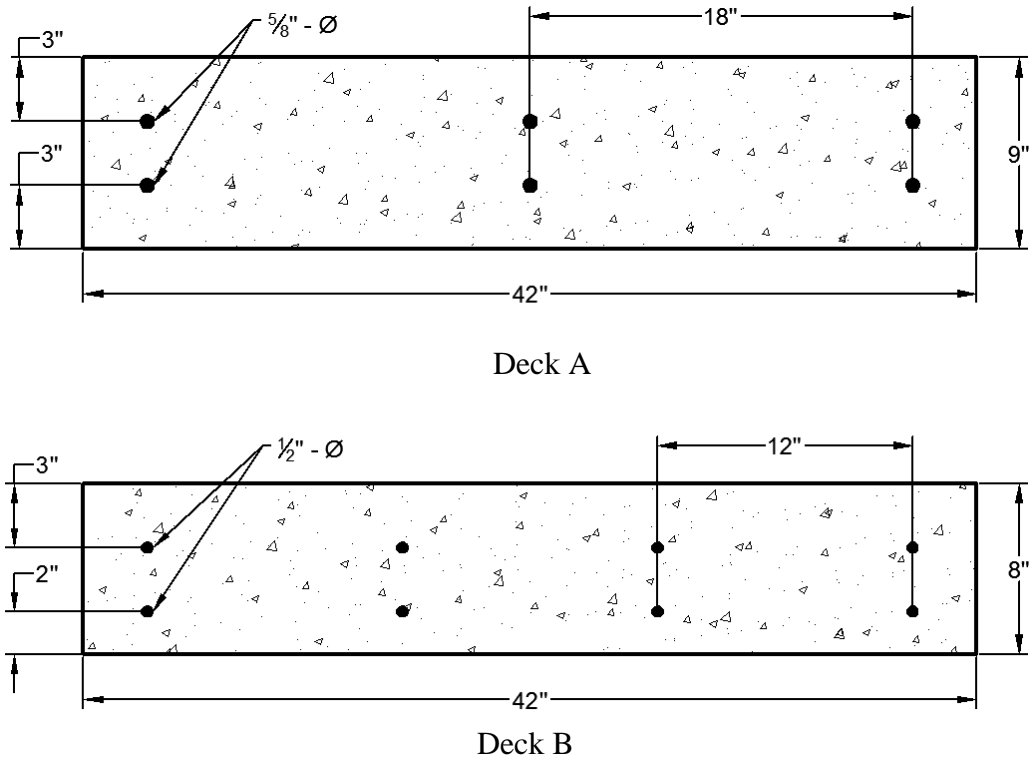


Figure 3.14. Design drawings of sample decks for inspection planning comparison

The planner has two inspection methods available to use on the decks, chain drag and ground penetrating radar (GPR). The chain drag test is easier and cheaper to run than the GPR. Also, the GPR method may require time to interpret the results that the chain drag does not need. The chain drag method does take time to run and can be tedious, but the results are instant once the inspection is completed. The GPR method is much more accurate than the chain drag method, as shown in Table 3.9. Due to the extra time needed for the GPR, the inspectors will only be able to perform it once during the month. Therefore, one bridge will have the delamination estimated by chain drag while the other is inspected by GPR.

The analysis plan is as follows:

- 1) Both decks were modeled in CDCPM, and the uncertainty in the current condition was determined assuming no previous maintenance on the deck.
- 2) Uncertainty forecast plots are developed for both decks using both inspections.

3) The decision on which inspection to run on each bridge can be made based on the plots.

Uncertainty forecast plots show the expected mean or standard deviation of the updated model based on the precision of the inspection method over a range of possible inspection results. This allows the planner to consider all possible outcomes of the inspection, and to compare different inspection methods of different precisions to see if the precision will make a difference in the updating. From this analysis, the plan of which bridge gets which inspection method can be made.

4. RESULTS AND ANALYSIS

4.1 Development of Uncertainty Forecast Plots

Before an inspection plan is developed, the effect of updating the current condition with inspection results is investigated. For delamination, the inspection results are incorporated with the ADL output of CDCPM using Bayesian Updating to arrive at the updated ADL from both pieces of information. First, CDCPM was run to establish the current condition of delamination as a set of sample ADL from simulations; this data set is the prior distribution in the Bayesian analysis. Table 4.1 below shows the statistics of the prior distribution for demonstration purposes. All analyses were conducted using 10,000 simulations and 5,000 bins, as described in section 3.4.

Table 4.1. Statistics of prior distribution created using CDCPM

Statistic		ADL (%)
Mean		8.77
Median		6.74
Standard Deviation		9.61
95% Confidence Interval Bounds	Lower	0.01
	Upper	34.6

A range of possible inspection results and precisions were considered. Inspection results between 1% and 50% ADL are considered. Precision is quantified by coefficient of variation, and the values considered are 0% (perfect inspection), 0.5%, 1%, 5%, 10%, 25%, and 50%. While most inspection methods would most likely have a precision greater than 15% (see Table 3.8), the smaller values are also considered to show the transition between a perfect inspection and more realistic inspection precisions. Every combination of inspection result and precision was analyzed, and the results are presented graphically. Figure 4.1 and Figure 4.2 below show

the updated mean ADL and standard deviation in ADL, respectively, based on the result of the inspection at different precision levels.

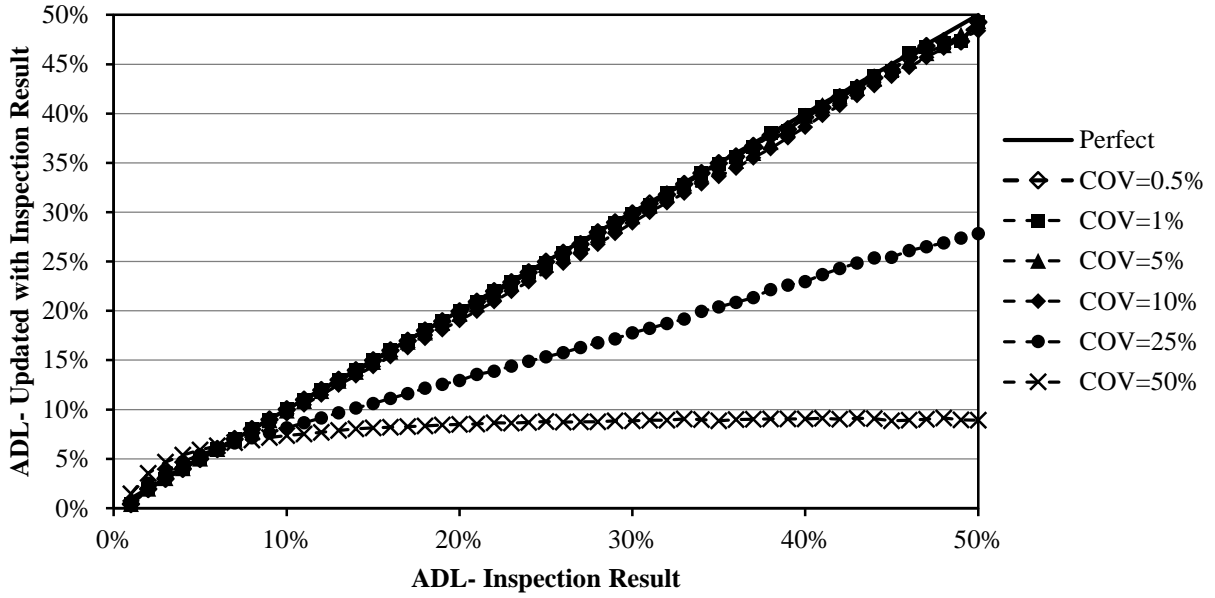


Figure 4.1. Uncertainty forecast plot for mean ADL based on inspection result for various levels of inspection precision

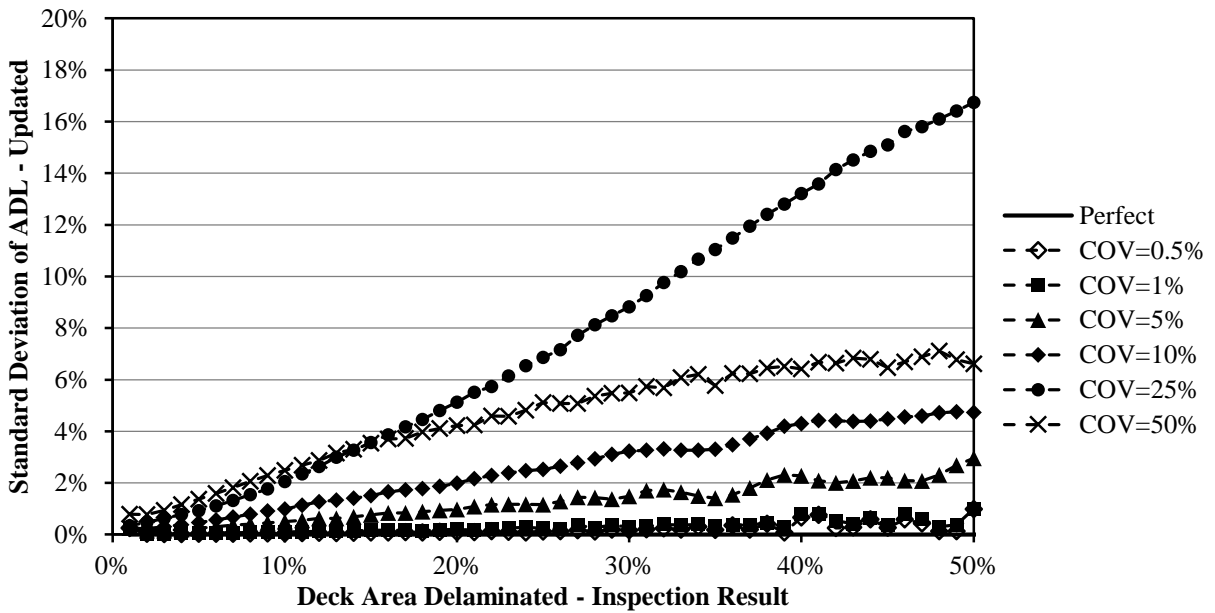


Figure 4.2. Uncertainty forecast plot for standard deviation of ADL based on inspection result for various levels of precision

Figure 4.1 and Figure 4.2 above show that the inspection result and the precision both play a role in what the updated ADL and uncertainty will be. In Figure 4.1, the mean value of the updated ADL is examined. As expected, a perfect inspection means that the updated ADL will take on the inspection value, regardless of the prior model prediction. In contrast, the updated ADL from the least precise inspection result of 50% coefficient of variation will take on the value of the prior distribution, which is 8.77% ADL. Precisions that are 10% or less generally give a good estimate of the actual ADL when compared to a perfect inspection.

The standard deviation of ADL shows that as the inspection result becomes larger, the standard deviation in ADL will also become larger. For more precise inspections, the updated uncertainty will level off at a particular value, which shows that inspection results above a particular value will all update to the same standard deviation of ADL. As the inspection coefficient of variation becomes very large, the updated standard deviation will level off close to the prior standard deviation. The 25% precision shows a special case where the inspection and prior distributions cover a wide range of possible ADL values, which actually widens the possible range of ADL and increases the standard deviation of ADL from the prior distribution. While such results are not likely, this possibility should be considered when the prior distribution has high variability.

Uncertainty forecast plots like the ones in Figure 4.1 and Figure 4.2 can be made for any inspection that is quantified by a bias and a coefficient of variation. This means that each line in the plot can represent a particular inspection method. Multiple inspection methods can then be plotted together to see how they compare both to each other and to limit criteria for knowledge of the current condition. Due to the usefulness of these plots in forecasting how the updated

knowledge will behave for a given inspection, they will be termed uncertainty forecast plots in this thesis.

4.2 Planning Inspections Using Uncertainty

The development of a bridge inspection plan using uncertainty in the knowledge of the bridge condition is presented and explained here. In order to showcase the methodology as clearly as possible, a plan is developed and examined for concrete bridge decks only. Using the output of CDCPM, the uncertainty in the bridge condition at any time can be modeled as a set of simulated data, from which a mean, standard deviation, and other statistical parameters can be calculated. This uncertainty can then be updated to include inspection results at any time, where the inspection result is also considered uncertain.

For either case, a maximum inspection interval of 6 years is assumed for each inspection plan established here. This is based on the maximum inspection interval from NCHRP Report 782 (Washer et al., 2014), as well as the maximum inspection interval used in European bridge inspection agencies (ASCE/SEI-AASHTO, 2009). However, CDCPM is capable of making projections beyond 6 years. Therefore, it would be reasonable to allow for longer inspection intervals based on the projection. The feasibility of inspection intervals over 6 years should be gaged by the comfort level from inspection agencies as well as the accuracy of CDCPM predictions over time.

The plans for both vertical cracking and delamination are developed and presented separately. The vertical cracking inspection plan is presented in one section, describing both inspection before cracks occur and after cracks occur. The delamination inspection plan is presented in two separate sections. The first section focuses on determining the time of the

inspection. The second section focuses on deciding the inspection method to perform based on uncertainty.

4.2.1 Planning Inspection for Vertical Cracking

The inspection plan for vertical cracking is broken into two parts: 1) inspection plan when cracks are not yet present on the bridge deck and 2) inspection plan when cracks have already been observed on the bridge deck. Before cracks are present on the bridge deck, CDCPM quantifies the probability of vertical cracking (p_{cr}) for the bridge deck, as well as projects the expected crack width and spacing once they occur. Together, this information can be used to plan bridge inspection timing before the cracks have formed. The framework for conducting inspections before cracks have formed is a risk-based approach using uncertainty. The probability of vertical cracking is the probability of occurrence, and the crack width and spacing are the consequences of crack formation. After vertical cracks have been observed, the inspection plan is dependent on the observed location and severity of cracking. CDCPM output is no longer useful because no reliable equation to describe post-crack development was found in research. Therefore, the inspection interval is based on the potential for further deterioration, such as delamination or spalling.

Before establishing the inspection plan, an example of the projection of probability of cracking with time is generated to understand the general trend in probability of cracking over time. This is done by projecting the p_{cr} for bridge LR 50-0.2-17 for 75 years, and this result is shown in Figure 4.3 below.

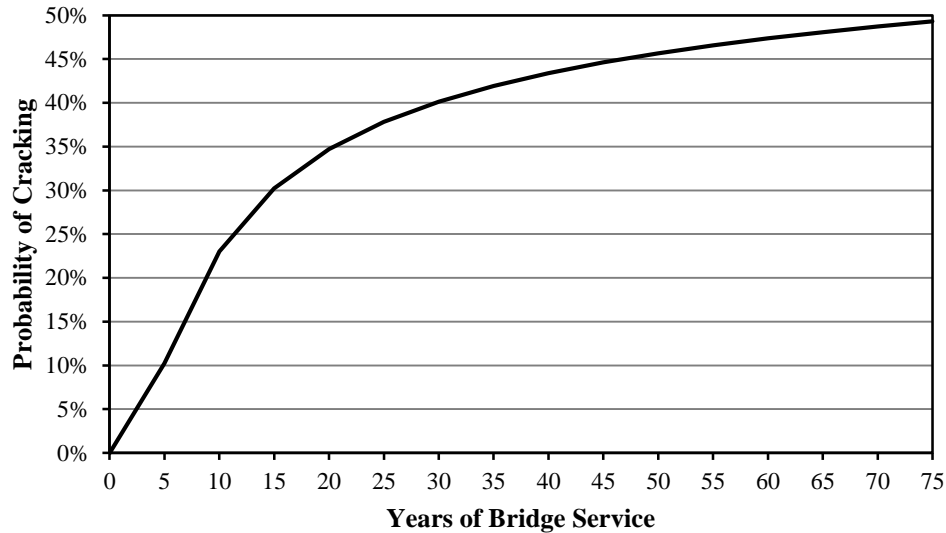


Figure 4.3. Probability of transverse cracking over the service life of a bridge in Fort Collins, CO

Figure 4.3 above shows that the probability of vertical cracking increases as the bridge ages. The probability increases at a quicker rate in the first 10 years, and then the rate of change of probability of cracking decreases as the bridge ages beyond 10 years. This plot will not predict the exact timing of vertical crack formation, but gives an indication of the probability of occurrence of the cracks. The timing of an inspection is based on this probability, with a higher probability of cracking indicating more frequent inspections should be required. This is done because a higher probability is the result of CDCPM predicting the applied tensile stress is closer to the tensile strength of the concrete. Inspections are conducted to find these cracks, and should be conducted when the probability of these cracks is greater.

Once the probability of crack occurrence is determined, the consequence of crack formation must be examined. The consequence is defined by the expected crack width and crack spacing. For this same bridge, the crack width and spacing is estimated using equations 24 and 25 from the methods section, and the results are shown in Table 4.2 below. The condition state definition from crack width and spacing is determined from AASHTO Smartflag 358, and the same definition is used in this inspection plan. These values are shown in Table 4.3.

Table 4.2. Statistical results of transverse crack width and spacing from CDCPM

Statistic		Crack Width [in]	Crack Spacing [ft]
Mean		0.012	1.69
Standard Deviation		0.0023	0.089
95% CI Bounds	Upper	0.015	1.83
	Lower	0.0085	1.55

Table 4.3. Condition states for crack width and spacing, from AASHTO Smartflag 358

Crack Width [W] (in)	Crack Spacing [S] (ft)			
	S > 10	6 < S ≤ 10	3 < S ≤ 6	S ≤ 3
W ≤ 1/32	1	1	2	3
1/32 < W ≤ 1/16	1	2	3	4
1/16 < W ≤ 1/8	2	3	4	4
1/8 < W	3	3	4	4

According to the output of CDCPM for expected crack width (0.012 inch) and spacing (1.69 feet) and comparing to the criteria in Table 4.3, the expected condition state of the cracks would be condition state 3. The bounds of the CI for this case occur completely within the condition state bounds in Table 4.3. Some analyses of other bridges may show that the CI bounds cover multiple condition states. When the CI bounds cover multiple condition states, the mean value from the analysis would be sufficient for defining a condition state because the data sets do not show much skew in the data. The condition state defined above is considered the consequence in the analysis.

The risk that a bridge will form vertical cracks is defined as a result of the occurrence and the consequence of vertical cracking. To combine both parts in developing a timing strategy, limits on the probability of cracking for different inspection intervals are defined based on the expected condition state of the cracks. The determination of inspection intervals for combinations of the occurrence and consequence are based off achieving the following goals:

- 1) Bridges that have a higher probability of cracking should be inspected more often.

- 2) Bridges that project to have more severe cracking (have a higher condition state) should be inspected more often. More severe cracking can lead to more serviceability concerns, and should be caught early.
- 3) Any bridge that has a probability of cracking greater than 50% should be inspected every 2 years. This will ensure that cracks can be caught early when they occur.
- 4) Since vertical cracking is typically not a threat to the structural integrity of the bridge, longer inspection intervals should be considered whenever possible to allow for inspections to focus on more crucial elements of the bridge.

Taking these goals into account, the following inspection intervals are proposed as shown in Table 4.4.

Table 4.4. Maximum inspection interval for vertical crack inspection

Probability of Cracking (p_{cr}) [%]	Expected Condition State (CS)			
	CS 1	CS 2	CS 3	CS 4
5	6	6	6	6
10	6	6	6	5
15	6	6	5	4
20	6	6	4	3
25	6	5	4	3
30	5	4	3	2
35	4	3	2	2
40	4	3	2	2
45	3	2	2	2
50	3	2	2	2

A maximum inspection interval of six years is chosen because this is the recommended maximum from NCHRP Report 780 (Washer et al., 2014). When using the above plot, the inspector should start by isolating the column for the expected condition state. Next, the probability of cracking should be identified from CDCPM for six years, and the maximum probability of cracking should be identified over this time span. When this value falls between two probabilities, the probability of cracking that is higher than the projected probability of

cracking should be used. The inspector can then read across and obtain the suggested time for the next inspection from the current time. When the probability of cracking exceeds the probabilities shown in Table 4.4, the inspection interval should be a maximum of every 2 years. As an example, if the bridge in question projects to have condition state 2 cracking, and CDCPM estimates a maximum probability of cracking of 22% in the next 6 years, the next inspection should be conducted in 5 years.

However, this is not the most efficient inspection system for bridges that have not cracked and show little increase in the probability of cracking over a 6-year projection. When CDCPM projects the same or a slight increase in probability of cracking, this means that the state of stress within the deck is not changing much. This occurs later in the service life of the bridge when shrinkage and creep strains in the deck have reached their maximum values. Therefore, inspecting a bridge often when the state of stress is not changing much makes little sense. To cater to such situations, an allowance for an extended interval is made for bridges that show little change in the probability of cracking over the 6-year projection. Table 4.5 below shows the allowable inspection interval extension based on the change in probability of cracking for the next 6 years of bridge service.

Table 4.5. Additional inspection time for bridges that show little increase in probability of occurrence

Difference in p_{cr} from current prediction to 6-year projection	Allowable addition to inspection interval
$1\% < \Delta p_{cr} \leq 2\%$	1 year
$\Delta p_{cr} \leq 1\%$	2 years

The values in Table 4.5 can be added to the inspection interval determined by the probability of cracking plot and the limits defined in Table 4.4. The total inspection interval should not exceed 6 years in any case. Using the projection in Figure 4.3 above, the bridge deck would be eligible for a 1 year addition to the inspection interval starting at year 35, assuming no

cracking has been observed before this time. This is the first time where a 6-year projection would show less than 2% increase in probability of cracking.

Once cracks have formed in the bridge deck, the probability of cracking inspection model would no longer apply for inspection timing. Therefore, the timing is based on the location of the cracks and the potential for causing more serious forms of deterioration such as delamination or spalling in the future. First, the actual condition state of cracking should be determined by measuring the crack width and average spacing. Then, the cracks should be investigated for their location relative to the rebar. Cracks that form directly over rebar would allow unimpeded ingress of chlorides to the rebar, which could initiate the corrosion reaction much sooner than if the chlorides diffused through the concrete. Evidence of efflorescence shows that conditions for corrosion initiation may be present, and staining indicates that active corrosion is occurring.

Figure 4.4 outlines the methodology for inspection timing for vertical cracking considering both before and after crack formation. This methodology follows the prior explanation.

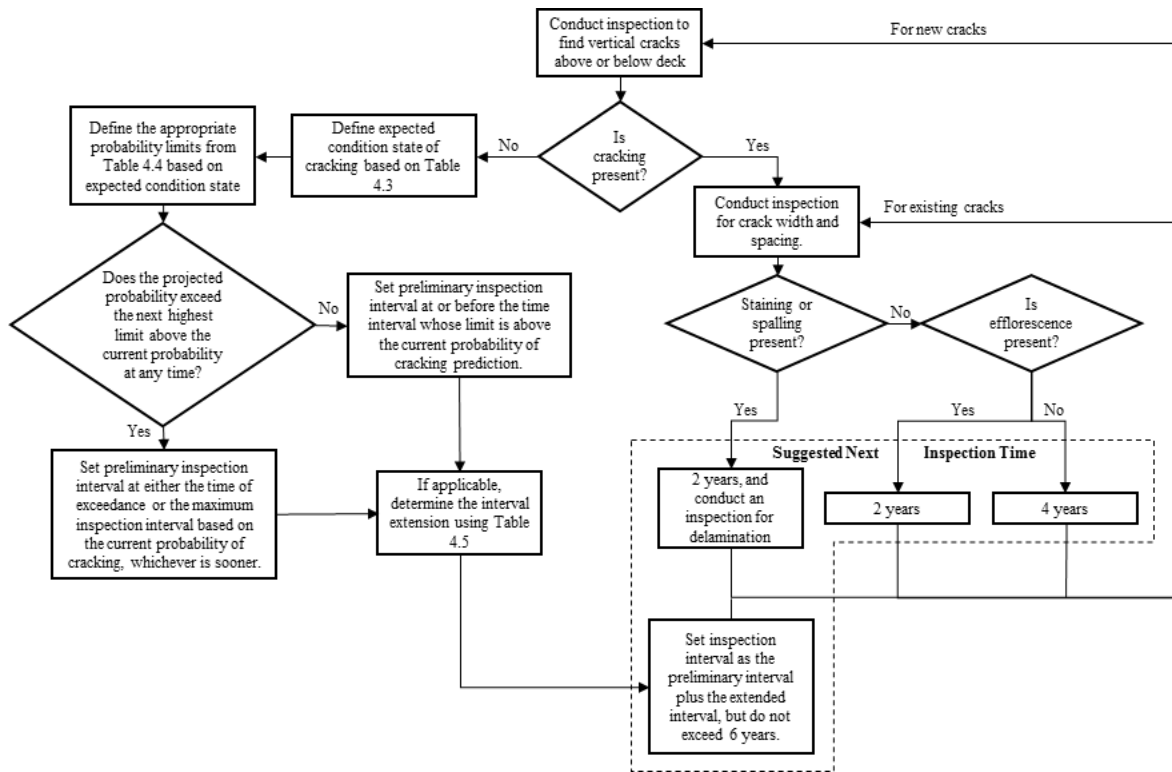


Figure 4.4. Flowchart of methodology for vertical crack inspection timing

Starting with an initial inspection, the flowchart will help to plan the next inspection time for vertical cracking in a concrete bridge deck. The methodology allows for a range of possible inspection times based on the risk of vertical cracking, and will ensure that the more at-risk bridge decks receive more frequent inspections than those that do not. This will aid in ensuring that knowledge of bridge deck conditions can be monitored and maintained in the most efficient manner.

4.2.2 Planning Inspection Timing for Delamination

Unlike the output of the vertical cracking model, the direct output from CDCPM is a set of simulated ADL values for delamination. While the analysis uses this data set in the calculations, this is not the most convenient way to represent the data. Therefore, ADL is represented as either a mean, standard deviation, a percentile value, or a confidence interval (CI). Each statistical value gives information on the data, and the use of multiple values provides a

more complete representation of data. The following results and discussion will use these statistical values to describe delamination.

When planning an inspection based on uncertainty in the delamination of the concrete bridge deck, it should achieve one or both of the following goals:

- 1) Reduce the spread, or uncertainty, in the predicted ADL.
- 2) Investigate if the condition state has changed when there is reasonable evidence that a change has occurred.

The spread, or uncertainty, in ADL output data is quantified by the standard deviation (SD), and limits are placed on the standard deviation to define when the output data is too uncertain. The probability of a condition state change is quantified as a percentile value. A percentile is defined by a percentage, and the percentile value is the ADL at which the specified percentage of simulated values falls at or below this value. For example, a 75th percentile ADL is the value of ADL at which 75% of simulations would fall at or below this value. Both the standard deviation limit and percentile are evaluated to find the appropriate values for inspection planning. The condition states are divided as shown in Table 4.6 below. These values are from the AASHTO CoRe element definitions for all condition states except condition state one, which is given 0.5% instead of 0% so that an allowance for uncertainty in the results can be made for condition state 1.

Table 4.6. Definition of condition states for deck delamination

Condition State	Maximum ADL for Condition State
1	0.5%
2	2%
3	10%
4	25%
5	100%

The next step in developing the methodology is to define the appropriate standard deviation limits for each condition state, and the percentile that should be used for all condition states. A target inspection interval between 2 years and 6 years is established for conducting inspections. This analysis was performed for a range of initial mean ADL and initial standard deviation of ADL values in all condition states. The analysis for determining the standard deviation for condition state 3 is presented below, and the other limits on standard deviation are presented later in Table 4.9. For condition state 3, three mean and three standard deviations of ADL are considered for initial conditions, and projections are made for 6 years. The means and standard deviations of ADL are chosen so that the mean ADL values cover multiple ranges within the condition state, and the standard deviations of ADL model possible values that would result from an inspection update for a bridge deck in condition state 3. The bridge for analysis is 50 years old at the initial time of analysis, because this time ensures that areas of the deck are corroding for the parameters used. Figure 4.5 below shows the 6 year projected standard deviation of ADL for all nine combinations of initial mean ADL (M) and initial standard deviation of ADL (SD).

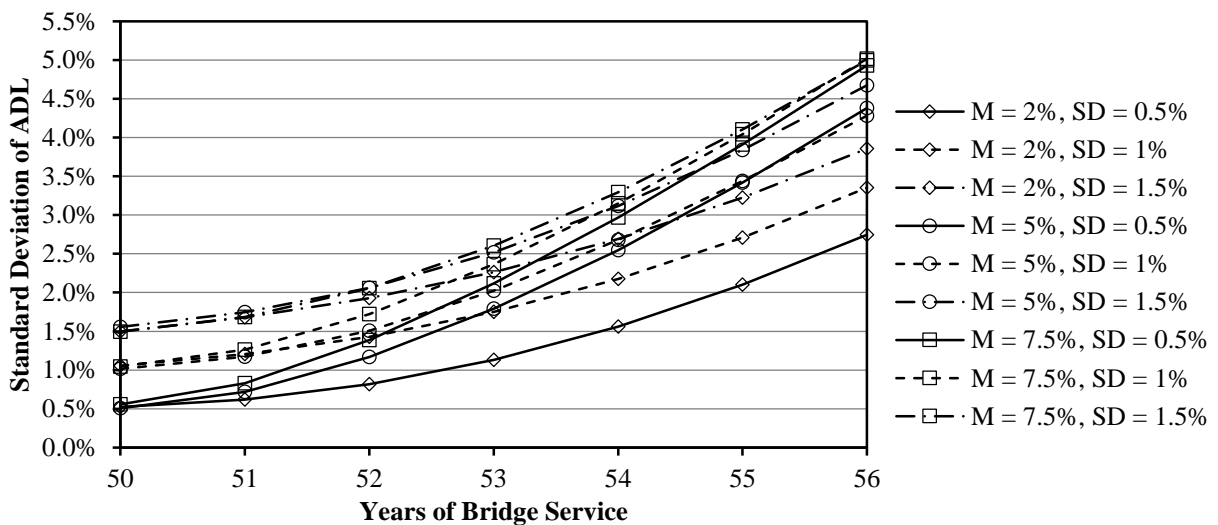


Figure 4.5. Projection of standard deviation of ADL for various initial mean and standard deviation values

Figure 4.5 shows that the initial mean ADL will determine the rate of change of the projected standard deviation of ADL over time. As the mean ADL is higher, the rate of change in ADL will also be higher. The rate of change of the standard deviation in ADL appears to not be affected by the initial standard deviation in ADL, with the range of initial standard deviations in ADL all changing at a similar rate for the same mean ADL. Therefore, the initial mean ADL is a better indicator of how the ADL spread will change over time than the standard deviation in ADL.

Three percentile values are investigated to use in the inspection plan: the 75th, 90th, and 95th percentiles. Each percentile is determined for the same nine combinations of mean and standard deviation of ADL as the standard deviation of ADL analysis. Figure 4.6 shows the results of this analysis for various initial mean values at an initial standard deviation of 1% ADL.

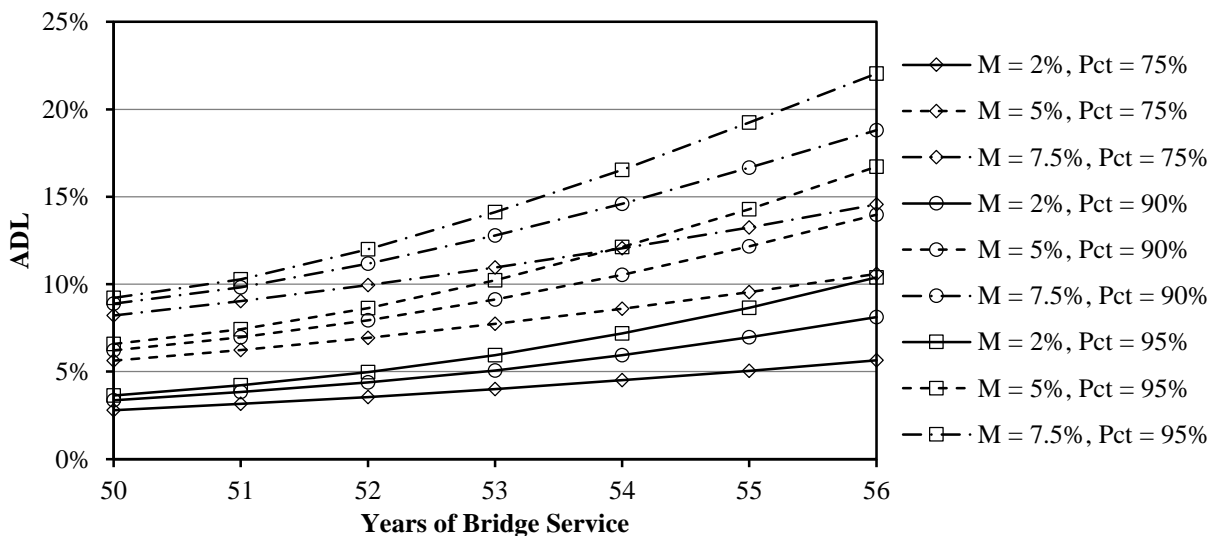


Figure 4.6. Projection of ADL for various mean and percentile values at 1% initial standard deviation

Again, the initial value of ADL makes a difference in the rate of change in the ADL over the 6 year projection. The choice of the percentile can have large difference in the projected ADL over time, with a difference of 5% ADL for the projection at six years for all initial mean ADL considered.

Using Figure 4.5 and three possible limits on the standard deviation of ADL, the inspection interval based on the spread is determined for condition state 3. Limits of 2%, 2.5% and 3% on the projection of standard deviation of ADL are considered because these values will yield reasonable inspection intervals. Standard deviation of ADL values above or below these values will yield inspection intervals of 6 years or 1 year in most cases, which does not provide for a variable inspection interval. When the majority of projected inspection intervals fall between 1 year and 6 years, this is referred to a full coverage of the target inspection intervals. The expected intervals are shown in Table 4.7 below. The inspection interval based on the percentiles are also presented in Table 4.8, The interval is determined by when the percentile plot in Figure 4.6 crosses the limit for condition state 3 shown in Table 4.6, which is 10% ADL.

Table 4.7. Inspection interval based on allowable spread in prediction at condition state 3

Initial Mean ADL	Initial Standard Deviation of ADL	Projected Standard Deviation of ADL Limit		
		2%	2.5%	3%
2%	0.5%	5	6	6
	1%	4	5	6
	1.5%	3	4	5
5%	0.5%	4	4	5
	1%	3	4	5
	1.5%	2	3	4
7.5%	0.5%	3	4	5
	1%	3	4	4
	1.5%	2	3	4

Table 4.8. Inspection interval based on probability of change in condition state from 3 to 4

Initial Mean ADL	Initial Standard Deviation of ADL	Percentiles of Sample ADL		
		75%	90%	95%
2%	0.5%	6	6	6
	1%	6	6	6
	1.5%	6	6	6
5%	0.5%	6	4	4
	1%	6	4	3
	1.5%	6	4	3
7.5%	0.5%	3	2	2
	1%	3	2	2
	1.5%	2	2	2

In order to decide which standard deviation of ADL limit and percentile is appropriate, the conditions under which inspection time should control are considered. When the initial mean ADL is low, the percentile inspection interval should not control in most cases over the spread because the expected rate of deterioration will not be fast enough to arrive at the next condition state in six years. In contrast, when the initial mean ADL is close to the condition state limit, the percentile inspection interval should control due to the high chance that the condition state will need to be changed in the next six years, and the percentile value is the indicator of the actual condition. Also, the appropriate limit should result in a range of inspection intervals, and not predict all intervals above 6 years or below 1 year. This will allow for full coverage of the target inspection intervals.

Based on the coverage of the range of target inspection intervals, the 3% standard deviation in ADL limit values have the poorest coverage of inspection intervals. The 75th percentile also has a large gap in the inspection interval between 5% and 7.5% initial mean ADL compared to the other percentiles considered. Of the remaining combinations, the 2.5% standard deviation of ADL limit and the 90th percentile ADL projection best address the goals described in the previous paragraph. The spread will control for all the 2% initial ADL projections and the

1.5% initial standard deviation of ADL for the 5% initial mean ADL projection. The 90th percentile projection will control for all 7.5% mean ADL projections, which is when the condition state change should be a concern. Therefore, these values are set as the limits for the inspection plan.

A similar analysis was conducted for other condition states. The 90th percentile ADL is used for all condition states. The standard deviation limit is different depending on the condition state considered because the severity of the allowable standard deviation in ADL is measured relative to the maximum ADL for each condition state. The results for each limit is shown in Table 4.9 below.

Table 4.9. Maximum standard deviation of ADL for each condition state

Condition State	Maximum Standard Deviation
1	0.5%
2	1%
3	2.5%
4	5%
5	5%

The standard deviation of ADL for condition state 5 is set at 5%, and could not be compared to the percentile study because no upper limit exists for this condition state. The 90th percentile ADL will no longer have an effect on inspection timing once in condition state 5. The complete inspection plan is described by the flowchart shown in Figure 4.7 below.

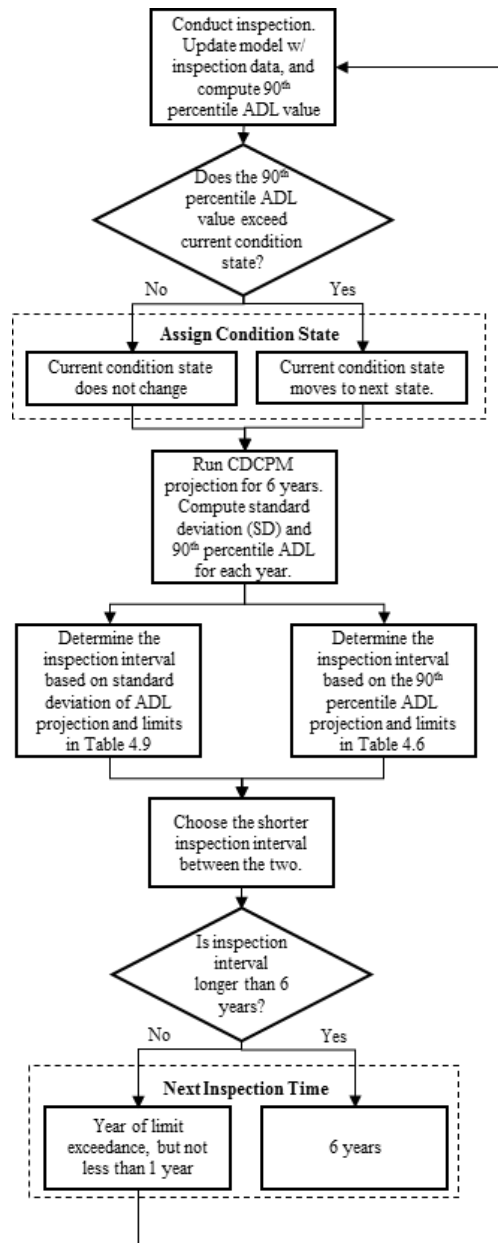


Figure 4.7. Flowchart of inspection timing plan for delaminations

The limit values established here are reasonable for the bridge analyzed here, but they have limitations in applicability to further inspection planning and in quantity of supporting evidence for the values selected. The range of applicability for all bridge decks can be improved by comparing to projections for multiple bridge decks of different thicknesses, reinforcement plans, cover depths, and chloride environments. Other types of corrosion enablers should also be investigated such as carbonate corrosion to compare how this deterioration may be different than

chloride-induced corrosion. A similar plan can be developed for other bridge components where the failure mode can be quantified and modeled based on input variables. Also, input from bridge inspectors and managers on their comfort level both in the spread of ADL and the percentile should be considered in establishing these limits. A survey of bridge inspection experts could gauge the required confidence each expert would require in the condition results in order to act on repairing a cracked or delaminated deck.

4.2.3 Planning Inspection Method for Delamination

After the timing of the inspection is established, the choice of which inspection method to run is determined. The inspection goal is defined by the limit violated that determined the inspection time in the first place. When the standard deviation limit has been reached, the knowledge about the condition of the bridge deck is too uncertain. If the percentile value reaches the condition state limit, there is a reasonable chance that the condition state has worsened since the last inspection. This will influence how the uncertainty in ADL is analyzed.

The inspection goal also defines which uncertainty forecast plot is most relevant for choosing an appropriate inspection method. The effect of an inspection method on the spread in the predicted ADL is best analyzed using an uncertainty forecast plot for the standard deviation of ADL. Likewise, the effect of an inspection method for establishing the condition state is best analyzed using an uncertainty forecast plot for the mean ADL. To investigate how uncertainty forecast plots can be used to choose an appropriate inspection method, two prior distributions are generated from CDCPM for demonstration purposes; one that has a high spread in data, but does not indicate a change in condition state and the other is more certain, but indicates the condition state may have worsened. Both prior distributions are generated by selecting the mean and standard deviation of a normally-distributed initial data set, and projecting the data for 10 years

to allow the representative skew in the data to develop so that the data set resembles an actual prior distribution. With a target mean and standard deviation of the data set in mind, the data that most closely achieves these target values is selected as the prior distribution. Table 4.10 below shows the mean, standard deviation, and percentile value for each prior distribution.

Table 4.10. Statistics for the high-spread and close to condition state change prior distributions

Statistics		High-Spread	CS Change
Mean		3.86%	9.77%
SD		3.42%	0.82%
90th Percentile		4.82%	10.22%
95% CI Bounds	Upper	12.32%	11.59%
	Lower	0.02%	8.47%

Uncertainty forecast plots are created for multiple coefficients of variation in inspections. The same precisions used in section 4.1 are use here for the demonstration. Figure 4.8 and Figure 4.9 show the updated standard deviation in ADL from the high-spread distribution and the updated mean ADL from the condition state change distribution, respectively. The range of inspection results considered in each case encompass the 95% CI for each prior distribution, which represent the most likely inspection results.

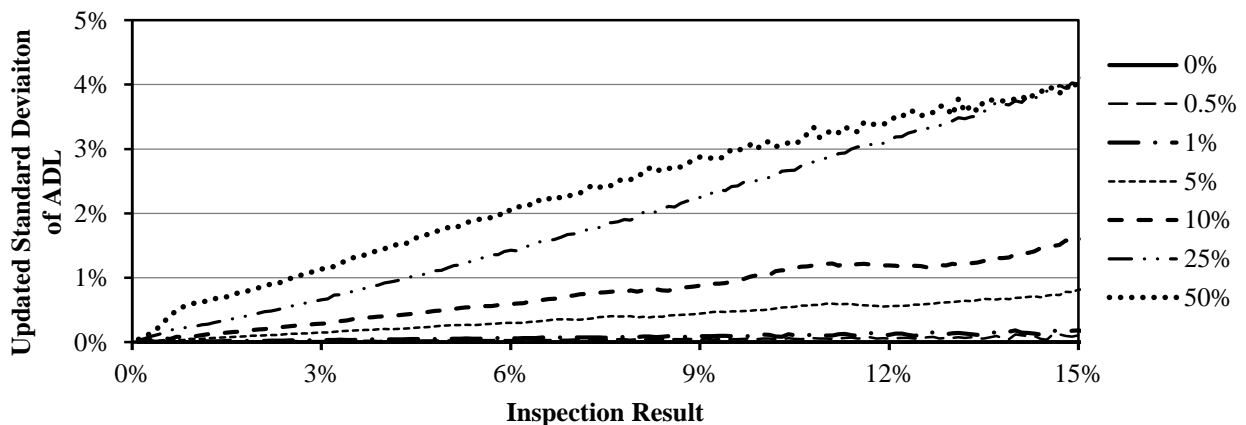


Figure 4.8. Updated standard deviation in ADL from the high-spread prior distribution for various inspection precisions

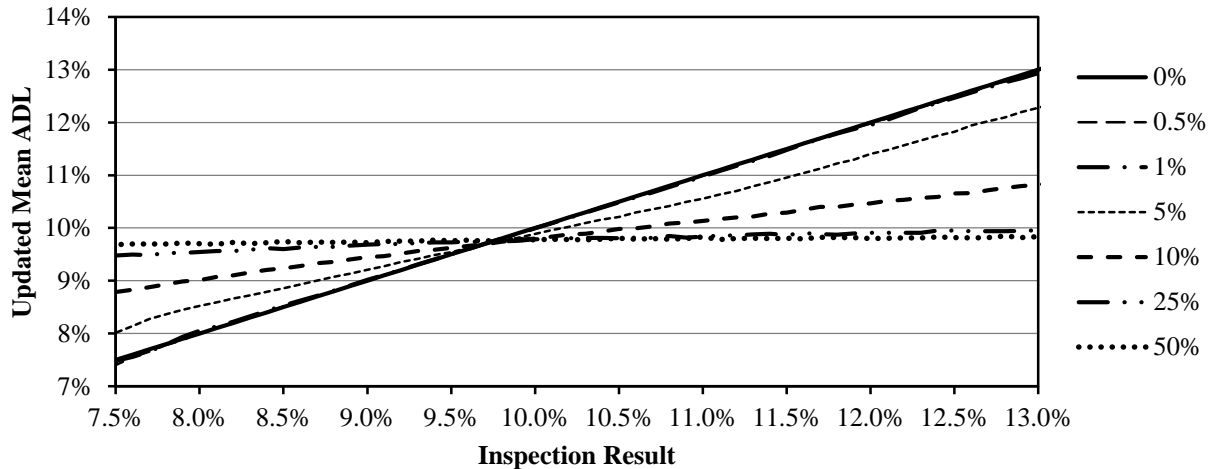


Figure 4.9. Updated mean ADL for the condition state change prior distribution for various inspection precisions

Figure 4.8 compares the inspection precisions for updating the standard deviation in ADL. The perfect inspection line actually follows the x-axis, since the updated standard deviation will be 0% ADL regardless of the inspection result. As less precise inspections are considered, the updated standard deviation will become more dependent on the result of the inspection. An appropriate inspection method based on uncertainty should be chosen based on the target standard deviation of ADL and the probability that a satisfactory result can be obtained. For example, if the target updated standard deviation is 1% ADL, and the 10% precision inspection is being investigated, an inspection result of 10% ADL or less will achieve the target standard deviation. The probability of getting such a result is 95.7% based on CDCPM output.

Figure 4.9 compares the inspection precisions to determine which will give the most accurate estimation of the condition state. The perfect inspection will give a definitive condition state based on the result. In contrast, the 50% precision result will be too uncertain to provide enough influence on the prior distribution to update the mean ADL. An appropriate inspection will be precise enough to provide an updated estimate close to the inspection result. For example, the 10% precision would require a result of at least 10.5% ADL to provide enough evidence to

change the condition state from 3 to 4. Any result below this will show either the condition state has not changed, or the condition state is still uncertain. For these cases, the updated standard deviation of ADL uncertainty forecast plot should be used as well to see how low a result is required to clearly define the ADL as condition state 3. The expected mean and standard deviation of ADL can be used to estimate the updated 90th percentile ADL from a normal distribution, which is the distribution used for inspection precision, and test if the result is sufficient to show the deck is still in condition state 3. If the result still shows no definitive condition state, the condition state should be moved to condition state 4 as a conservative representation on the bridge condition.

4.3 Effect of Uncertainty of Parameters on the Deterioration Model

The results given by CDCPM are highly dependent on the values specified for the input parameters, and how these parameters are modeled together. Accurate representation of the parameters will lead to a more dependable model for inspection planning. Since the above plan relies on the time that predictions reach particular limits, a poor representation could result in inspection being conducted either too often or too sparse. However, not every parameter has the same influence on the output. Therefore, this section will investigate which parameters affect CDCPM, and what can be done to improve CDCPM results through understanding the input parameters.

It should be noted these results are for the parameter coefficients of variation given in Table 3.1 and Table 3.2. If these are changed, the sensitivity index of that parameter also changes, and the indices of other parameters will also be affected.

4.3.1 Sensitivity Analysis of Vertical Cracking

The vertical cracking model is examined to see how the uncertainty in the input parameters affects the axial stress applied to the bridge deck. Since the final output value of probability of cracking does not have a variance associated with the parameter, the intermediate value of applied axial stress is used as the output in the analysis. This does neglect the concrete tensile strength in the analysis, but this parameter is already considered important because it is the only parameter used in the resistance of the limit state function. Due to the large number of parameters used in the analysis, only the most influential parameters are graphed in the following plots. Figure 4.10 shows the results of the sensitivity analysis for the first year of bridge service.

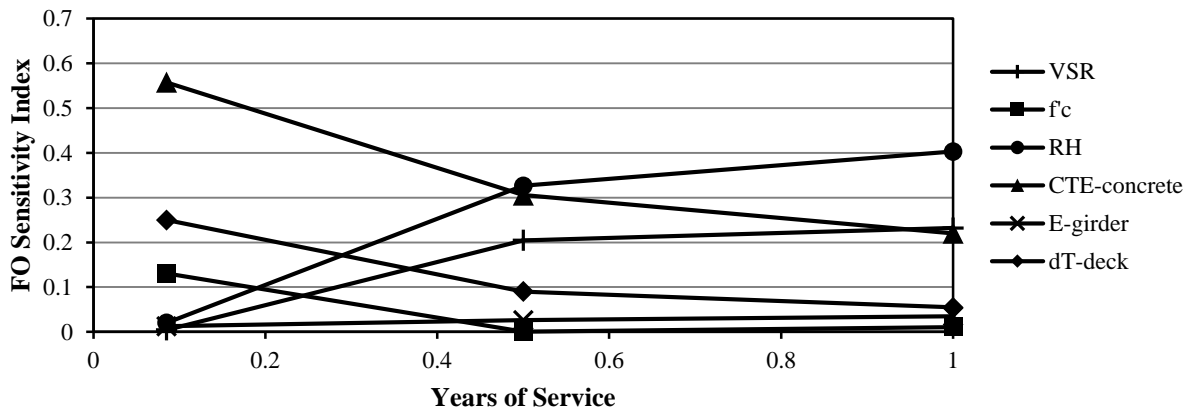


Figure 4.10. First-order sensitivity indices of the vertical cracking model for the first year of bridge service

Directly after curing, the coefficient of thermal expansion of the concrete in the deck has the greatest influence on uncertainty. This shows that the ambient air temperature is very important directly after curing in determining if a bridge deck will crack. As the first year of bridge service progresses, the relative humidity (RH) and volume to surface area ratio (VSR) inputs become more influential, and the concrete coefficient of thermal expansion is less influential. This shows that the shrinkage strain output of the shrinkage sub-model output is now the main contributor to deck cracking, as both parameters are key to that model.

For inspection planning, this indicates that running a visual inspection after one year of bridge service for vertical cracking may be useful in gaging the progress of shrinkage in the deck. Also, this indicates regions with high daily temperature changes may want to inspect for cracking shortly after curing. Figure 4.11 below shows the rest of the projection out to 50 years of bridge service.

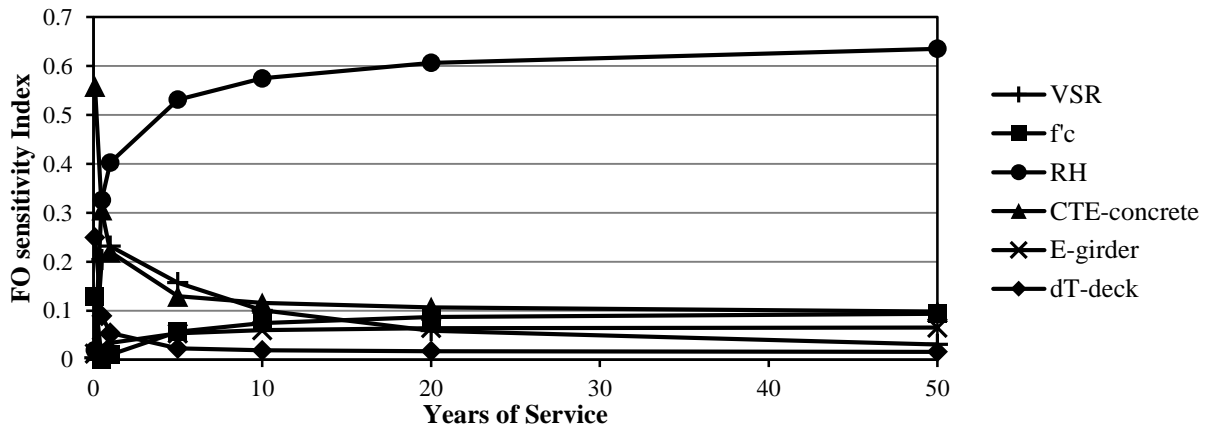


Figure 4.11. First-order sensitivity indices of the vertical cracking model projected for 50 years of service

The relative humidity becomes the sole important parameter in the analysis. This means that correct modeling of the relative humidity is key to an accurate representation of the applied tensile stress. The variability in relative humidity is a source of aleatoric uncertainty, which means it arises from the environment, and cannot typically be reduced. Therefore, accurate representation of this variability through statistical analysis of parameters, and seasonal representation of relative humidity may help to improve the predictions made by CDCPM for vertical cracking. The tensile strength is a source of epistemic uncertainty, which means it arises due to a lack of knowledge of the actual concrete used in the bridge deck. This uncertainty can be reduced through experimental testing, such as of concrete cores from the deck. While efforts to reduce uncertainty in other parameters could be made, it will not have much effect on the

uncertainty in axial stress applied, and therefore, little effect on probability of cracking predictions from CDCPM for the deck.

4.3.2 Sensitivity Analysis of Delamination

The delamination model is examined to see how the uncertainty in input parameters affects the ADL output. ADL is output as a set of simulated values from Monte Carlo simulation, for which a variance can be calculated. Therefore, ADL is the direct output in the sensitivity study. Again, a large number of parameters are used, so only the most influential ones are shown in the following plots. Figure 4.12 shows the results of the sensitivity analysis for the first 30 years of the bridge's service life.

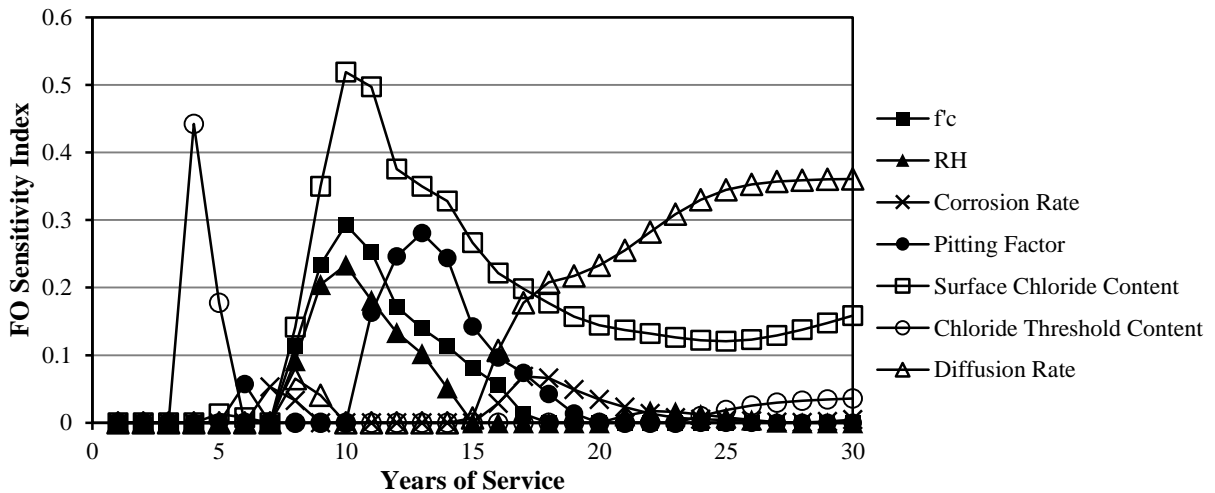


Figure 4.12. First-order sensitivity indices for the delamination model during the first 30 years of bridge service

The first key to understanding the results of Figure 4.12 is to realize that the average time-to-cracking from the corrosion initiation was 12.5 years, with a 95th percentile value of 21.3 years. The deck cannot delaminate unless a sufficient amount of corrosion product has built up to initiate cracking. Therefore, the ADL output at this time depends on the amount of corrosion build up. This is evidenced by the surface chloride content, pitting factor, concrete compressive strength (f'_c), and relative humidity all contributing to uncertainty in ADL during the first 20

years. The spike in the chloride threshold influence near year 5 of bridge service is the result of the simulation procedure, and should be disregarded in this analysis.

The uncertainty in values of the pitting factor and surface chloride content are epistemic uncertainty, while the uncertainty in compressive strength of concrete is aleatoric uncertainty. Drilling cores in the deck would allow for direct testing of the compressive strength by ASTM C39 (2015). Surface chloride content can be evaluated using a couple of possible tests outlined by ASTM (ASTM-C1152/C1152M, 2012; ASTM-C1218/C1218M, 2008). The pitting factor for corrosion may be more difficult to evaluate, but testing does exist to evaluate the probability of corrosion in embedded rebar (ASTM-C876-09, 2009). Relative humidity uncertainty was discussed in section 4.3.1 above, and can be dealt with in the same manner here.

After 20 years of service, the effect of delamination from diffusing chlorides starts to become apparent. There are only three real contributors to the corrosion-induced delamination of concrete decks: 1) diffusion rate, 2) surface chloride content, and 3) chloride threshold for corrosion initiation. All three parameters are used in the time-to-corrosion initiation sub model based on Fick’s second law of diffusion. The impact of these parameters is projected beyond 30 years of bridge service to 100 years in Figure 4.13 below.

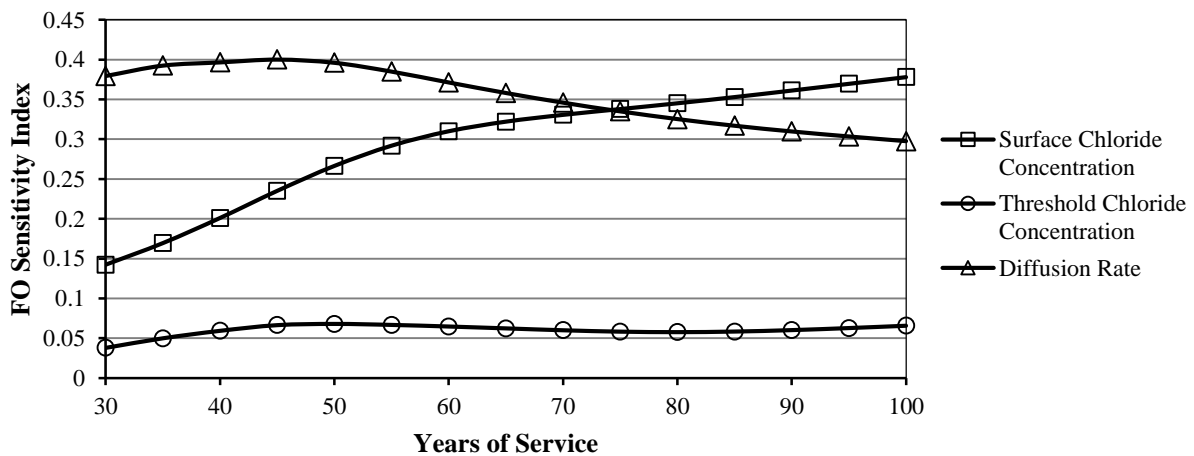


Figure 4.13. First-order sensitivity indices for the delamination model for years 30 to 100 of bridge service

From year 30 up to year 70 of bridge service, the uncertainty in the diffusion rate is the biggest contributor to uncertainty in ADL. After this, the uncertainty in surface chloride content again becomes the largest influence of uncertainty in ADL. The threshold chloride content for corrosion initiation plays a smaller role, but is still significant compared to the rest of the parameters, which are non-factors after 30 years.

According to Page et al (1981), this diffusion rate is dependent on the pore structure in the concrete, which is influenced by the chemical composition of the cement and the curing conditions. Two other factors investigated were the water to cement ratio and the temperature of the cement in service. Therefore, the uncertainty in the diffusion rate can be reduced through a better understanding of these factors. It may also be reduced through testing, such as running a concrete core sample through ASTM C1556 (2011), which determines the diffusion rate for concrete in saturated sodium chloride. The threshold chloride content has a small influence, and is dependent on the type of steel and the coating around the steel for protection.

4.3.3 Example: Climate Parameter Uncertainty

Effect of Relative Humidity on Vertical Cracking

According to the sensitivity study results shown in Figure 4.11, the relative humidity (RH) is a highly influential parameter in the vertical cracking model. RH is of less concern in the delamination model as explained in section 4.3.2, so it is not analyzed for delamination in this section. Three mean and three standard deviation values are investigated in this section. The mean values are 40%, 60%, and 80% humidity, and the standard deviations are 5%, 10%, and 20%, where all nine possible combinations are investigated. The most realistic standard deviations would be 10% to 20%, because humidity can vary greatly within a single day between day and night, and these values will capture that variability better. The analysis was carried out

with 2000 simulations for each time. Figure 4.14 and Figure 4.15 show the effect of various standard deviations and various mean values, respectively, on the p_{cr} of the concrete deck.

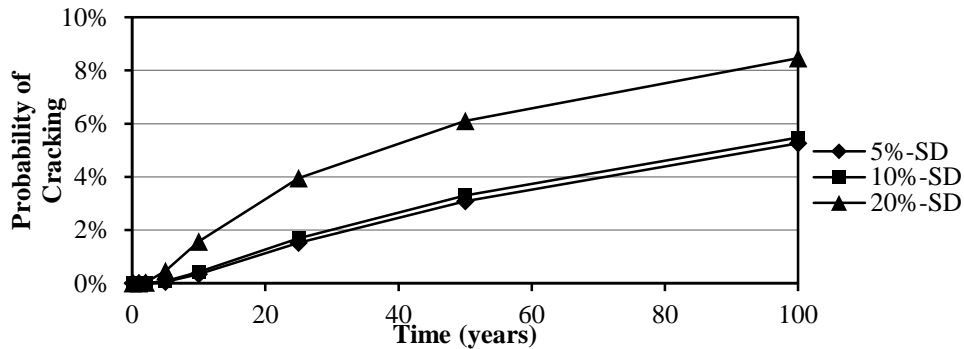


Figure 4.14. Probability of cracking at different standard deviations-60% mean relative humidity

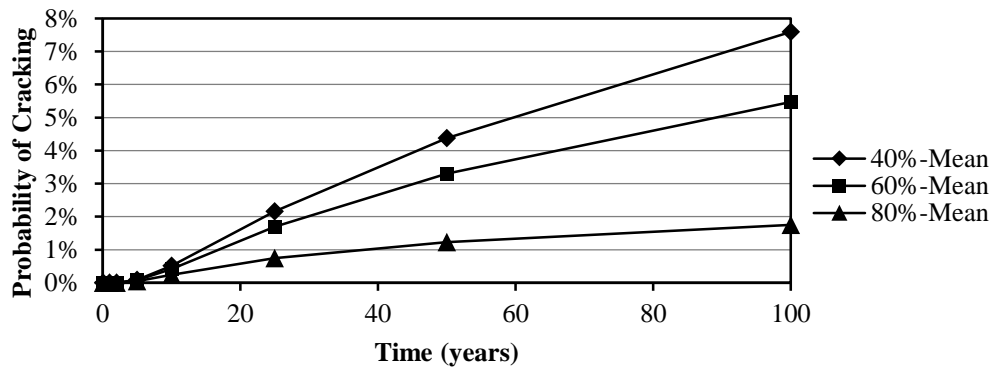


Figure 4.15. Probability of cracking at different mean values - 10% standard deviation

In computing the probability of cracking, the relative humidity affects both the creep and shrinkage behavior of concrete. Both figures above show that the expected probability of cracking increases with time. The probability of cracking will depend more on the mean value of relative humidity than the standard deviation. The higher probability of cracking values occur when the relative humidity is low, as shown in Figure 4.15. A high variability in relative humidity also results in a higher probability of failure, due to the higher possibility of low relative humidity.

The above plots show that regions that experience low relative humidity regularly, typically below 80%, will have a greater chance of transverse cracks occurring. Also, regions that experience a large range of relative humidity values throughout a year may also be

susceptible to transverse cracking. The uncertainty in relative humidity cannot be reduced because it is a source of aleatoric uncertainty, but CDCPM can be improved to better capture the uncertainty in the prediction. For short-term predictions, seasonal variability can be addressed if the value varies by season. Also, better models of the distribution can be obtained by collecting more data. Precise modeling of the uncertainty in relative humidity will strengthen the precision of the probability of cracking.

Effect of Temperature Variation on Vertical Cracking

Although the sensitivity index values of temperature used in CDCPM did not indicate that the parameters have much effect on axial stress, the coefficient of thermal expansion of concrete did, and this value serves as a bridge between the temperature and the induced strain in the concrete. Therefore, the magnitude of the temperature may be an influential factor on p_{cr} , even if the uncertainty is not. Temperature data for four different cities was collected, and fit to a probability distribution to input in CDCPM. The temperature analysis was performed with 2000 simulations. Table 4.11 and Table 4.12 below show the seasonal difference and the regional difference, respectively, in maximum tensile stress in the deck. Both plots show the state of stress when the deck top surface is warmer than the bottom surface.

Table 4.11. Seasonal maximum tensile stress in the deck for Fort Collins, CO from temperature sub model

Stress (psi)	Winter	Summer
Mean	87.2	93.4
90th Percentile	108.2	113.3
95th Percentile	114.7	121.1
97.5th Percentile	120.2	129.1

Table 4.12. Maximum tensile stress in winter for various locations from temperature sub model

Stress (psi)	Fort Collins, CO	Santa Barbara, CA	Clemson, SC	Ann Arbor, MI
Mean	87.2	71.3	81.5	83.5
90 th Percentile	108.2	88.1	99.8	101.7
95 th Percentile	114.7	92.6	105.4	108.5
97.5 th Percentile	120.2	97.5	110.3	115.1

All of the maximum stress values occurred at the bottom of the deck for daytime temperatures. As shown in Table 4.11, the maximum tensile stress is slightly larger in the summer than in the winter. The minimum annual winter temperature is most likely less than the temperature during curing, which would indicate that the most shrinkage would occur during the winter. However, the difference in the temperature within the deck appears to have a larger influence on the stress in the deck. According to Kennedy and Soliman (1987), the difference in the deck temperature is greater in the summer than in the winter during the daytime (see Table 3.4). The effect of this temperature on the probability of cracking at several geographic locations is shown in Figure 4.16 and Figure 4.17 below for both maximum and minimum temperature.

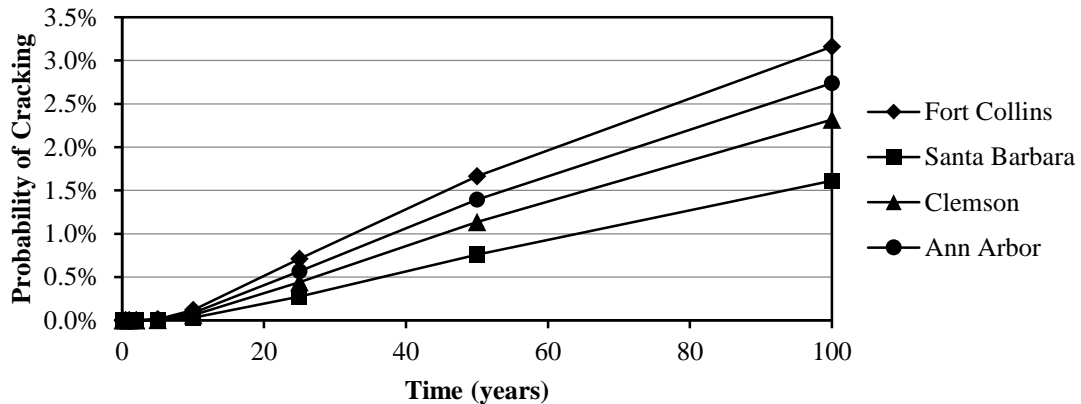


Figure 4.16. Probability of cracking comparison of various locations when deck surface is warmer than bottom in winter

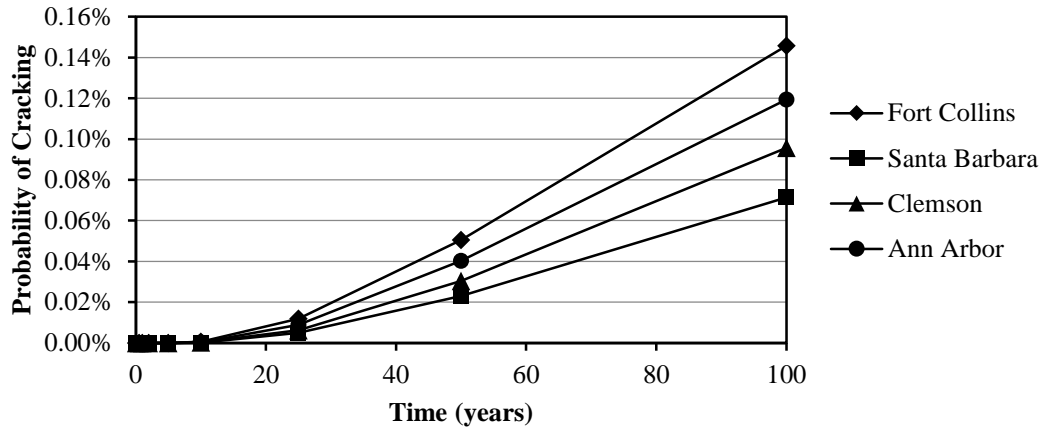


Figure 4.17. Probability of cracking comparison for various locations when the deck surface is cooler than bottom in winter

In both cases, Fort Collins, CO has the highest probability of cracking due to temperature. This is because Fort Collins has the largest differential between the mean and minimum annual temperature. Santa Barbara, CA had the lowest probability of cracking in both cases because the temperature difference is the smallest in a given year. The probability of cracking is also larger when the deck is warmer on top than cooler on top.

The above analysis of temperature in different locations implies that the magnitude of the temperature differential for different regions plays a small role in the probability of transverse cracking. The difference in the probability of cracking between regions is small over the 100 years analyzed, which means that decisions on inspection planning would most likely not be dependent on the temperature in the region.

Effect of Surface Chloride Content Variation on Delamination

Surface chloride content buildup on a bridge deck may arise from use of de-icing salts or from salt in the atmosphere near the coastline. Using data collected by Cady and Weyers (1983) from multiple state DOT concrete core samples, the mean and standard deviation of the chloride content near the deck surface for four states was reported. The surface chloride analysis was

conducted using 2500 simulations. Figure 4.18 and Figure 4.19 below show the percentile ADL output and the standard deviation of ADL output, respectively, over time for the states of Kansas, Michigan, California, and Missouri.

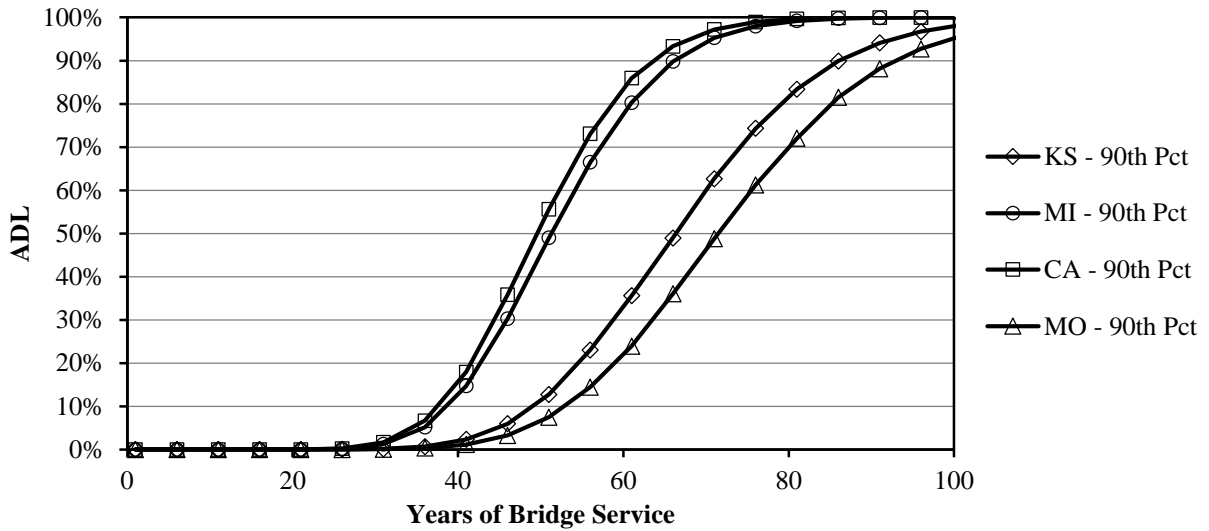


Figure 4.18. 90th percentile ADL projection based on surface chloride content levels for various states

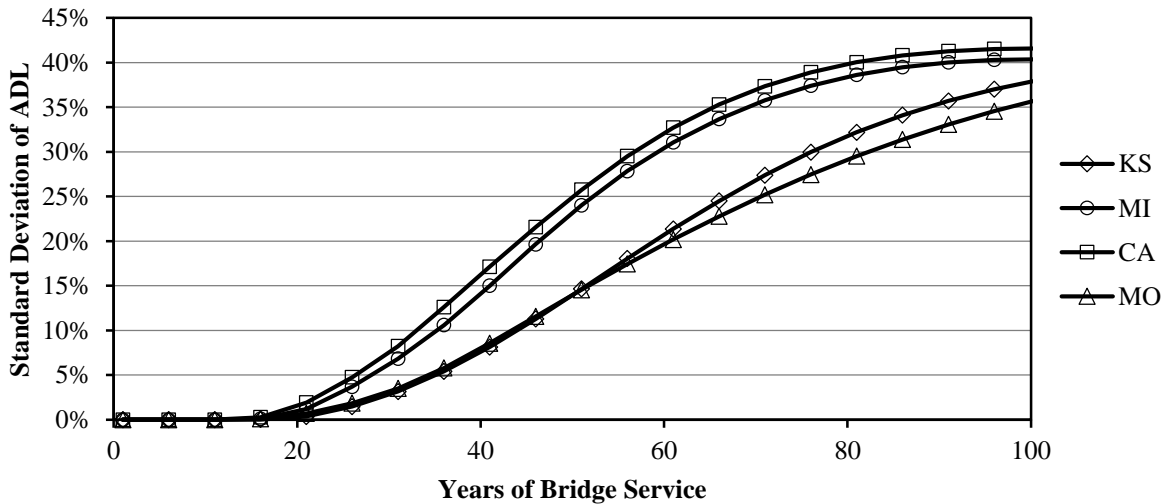


Figure 4.19. Projected standard deviation of ADL based on surface chloride content levels for various states

Both California and Michigan show the highest 90th percentile and standard deviation of ADL once delamination has initiated, while Kansas and Missouri project lower values. Due to the high mean surface chloride content for California and Michigan, CDCPM will project a higher rate of change of ADL, which leads to shorter inspection intervals.

Within the limits for 90th percentile ADL and standard deviation of ADL set in Table 4.6 and Table 4.9, respectively, the timing could vary greatly depending on which state the bridge is located. Between the standard deviation of ADL limit and the 90th percentile limit, the standard deviation limit will dictate the timing of the first delamination inspection. Using the standard deviation values shown in Figure 4.19 and the standard deviation limit of 0.5% ADL as shown in Table 4.9, the first delamination inspection based on spread would be conducted on the bridge in California in year 17 of bridge service. In contrast, the latest first inspection for delamination would be for the bridge in Missouri in year 22 of bridge service for the same standard deviation limit. Therefore, the surface chloride content variability alone can have at least a 5 year difference in when the first delamination inspection is conducted.

The variability in surface chloride content is a source of aleatoric and epistemic uncertainty. The aleatoric uncertainty arises in the surface chloride content being different at different locations on the bridge deck. The epistemic uncertainty arises from how the value is quantified, and this uncertainty can be reduced. The values used above represent multiple cores from multiple bridges across the state. This leads to a lack of knowledge in the surface chloride content in any particular bridge, and the uncertainty is therefore high. However, if data on the surface chloride content can be obtained for the bridge of interest, the uncertainty in surface chloride content can be reduced. Figure 4.20 below shows the effect of different coefficients of variation (COV) of surface chloride content on the spread in ADL.

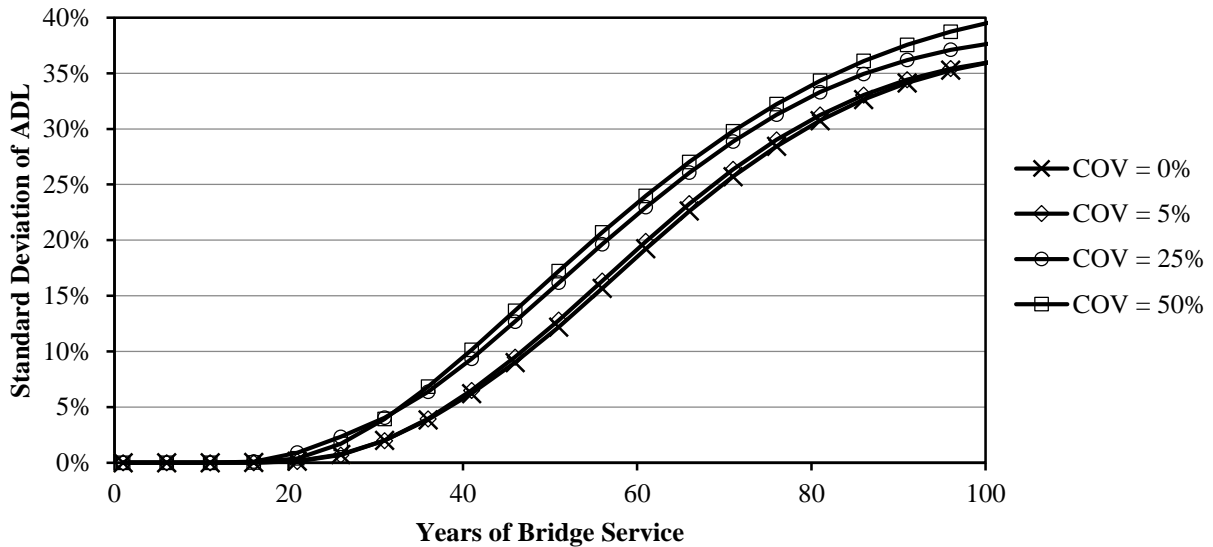


Figure 4.20. Comparison of variability in surface chloride content on the standard deviation of ADL

As shown in Figure 4.20, the standard deviation of ADL output can be decreased when the amount of surface chloride content is reduced. The 5% COV shows little deviation from a certain knowledge of the surface chloride content, which indicates that the uncertainty in the surface chloride content is no longer a major influence on the standard deviation of ADL at or below 5%, while the 25% and 50% COV show an increase in the standard deviation of ADL. The ability to reduce the uncertainty to this level is limited by the aleatoric uncertainty from the distribution of chlorides on the deck area. Also, not all of the epistemic uncertainty can be eliminated due to variability in testing and the inability to sample every part of the deck area. Data on the surface chloride content should be recorded for each bridge in order to reduce the uncertainty in the bridge condition, and to possibly prolong the time to the next inspection due to a more complete knowledge of the bridge condition. Also, this model can be improved if the amount of surface chloride content can be adjusted based on snowfall in a region. This will provide a better estimate for chlorides that come from de-icing salt application on the deck.

4.3.4 Establishing Important Parameters for Individual Bridges

The above variance-based sensitivity analysis on parameters will work for any mechanistic model that results in a single quantifiable parameter that can be characterized by a variance. This study should be conducted whenever the variability in any influential parameter is reduced. This will then identify how the influence of the other parameters has changed, and if any new parameter emerges as an influential parameter. This could become a time-consuming task when many bridges are considered; however, the influential parameters may be the same in most cases if the same parameter variability is applicable to multiple bridges in the bridge system. For example, bridges made of the same concrete that experience the same seasonal temperatures may have similar diffusion coefficient for chlorides. Considering that this parameter is influential in determining delamination uncertainty when the bridge is over 30 years old, one sensitivity study could be conducted to evaluate the level of influence for both bridges.

Once the most influential parameters are identified, each should be classified as aleatoric, epistemic, or a combination of both. For aleatoric uncertainty, the model or distribution used for the parameter should be given more attention in order to ensure the most correct representation of the field conditions. Epistemic uncertainty may be reduced through inspection or experimentation for some cases. Other cases of epistemic uncertainty may require more involved models without simplification or research into the mechanisms that determine a particular parameter. These avenues may be advantageous in reducing the number of inspections required later in a bridge's service life, and in some cases, could provide more cost-effective alternatives to reducing uncertainty than running an inspection on deck delamination.

4.4 Inspection Planning Scenario Analyses

How can the proposed inspection plan for delamination be implemented? This is examined using a few scenarios. First, the inspection plan proposed in this thesis is compared directly with the current inspection plan in use in Colorado. The differences in how inspections are timed and conducted are noted, and the advantages and disadvantages of each are weighed. Next, the proposed inspection plan is used to project the next inspection time and method for the same bridge based on the latest available inspection report. Lastly, the delamination inspection plan is used to effectively allocate resources in an example scenario between two bridge decks.

4.4.1 Past Inspection Analysis on Larimer County Bridge LR 50 - 0.2 - 17

Starting with the inspection report from 1996, CDCPM is used to project the next six years. Projections are made for both the steel and concrete girder-supported decks, which will henceforth be referred to as steel girder section and concrete girder section, respectively. Since no information on the reinforcement in the concrete girder section could be found, the variability of the steel reinforcement geometry was raised for this section. The rebar diameter has a coefficient of variation of 5%, the rebar cover depth has a standard deviation of 0.6 inches, and the longitudinal rebar spacing standard deviation was set to 1 in. The inspection reports from 1998, 2000, and 2002 are then compared with the output of CDCPM. The inspection recommendations are compared to the actual inspections performed, and the advantages and disadvantages of each plan are discussed. Figure 4.21 and Figure 4.22 below show the projections of the standard deviation of ADL and 90th percentile ADL value, respectively, for the time from 1996 to 2002. The analysis assumes the deck is not delaminated as of 1996 as indicated in the inspection report (see Table 3.7).

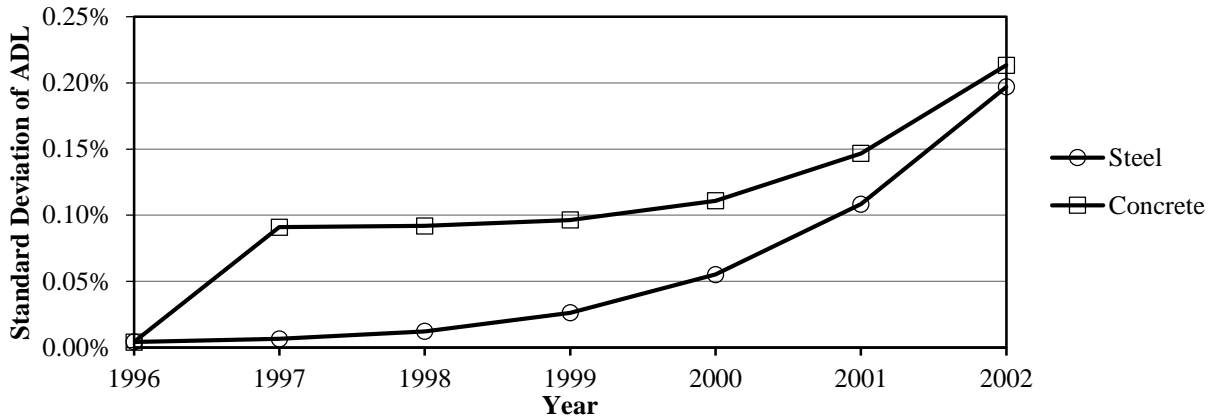


Figure 4.21. Projection of standard deviation of ADL for bridge LR 50-0.2-17 from 1996 to 2002

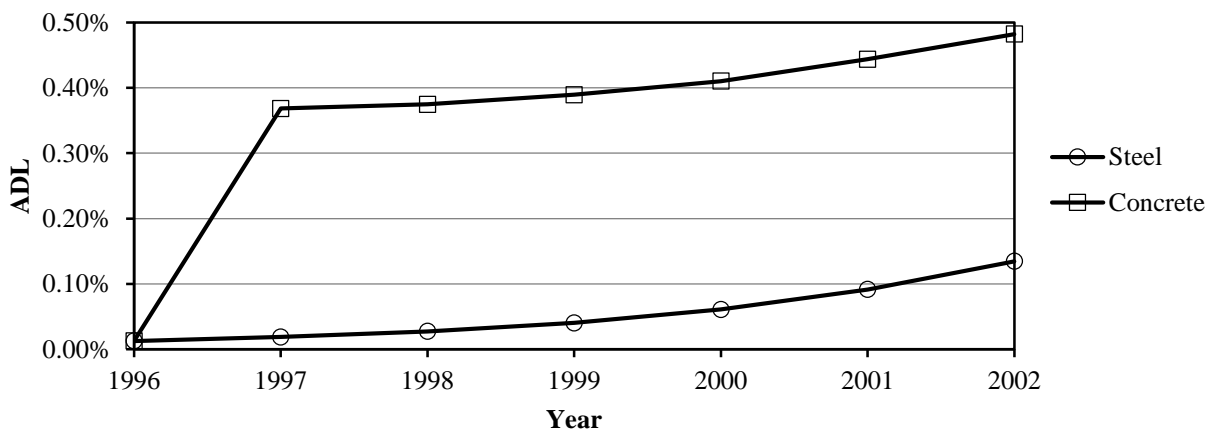


Figure 4.22. Projection of 90th percentile ADL value for bridge LR 50-0.2-17 from 1996 to 2002

The concrete girder section shows a higher 90th percentile and standard deviation of ADL projection than the steel section. This may be due to the age of the bridge deck, or the uncertainty in the steel reinforcement. As time progresses, the standard deviations of ADL approach similar values in 2002. The 90th percentile ADL values stay separated.

When both of these plot are applied to the inspection timing plan outlined in Figure 4.7, neither the percentile nor standard deviation limits are reached in these six years. This would indicate that an inspection is not required for delamination until 2002. The percentile value for the concrete girder section does get close to the limit to remain in condition state 1 in 2002, so the uncertainty forecast plot for mean ADL should be used in determining the inspection method for this time. The steel girder section does not project to reach either limit. In this case, either or

both uncertainty forecast plots should be used, depending on which goal is more important to the bridge manager.

When the CDCPM output is compared to the actual inspection reports, reasonable results are obtained, and evidence that the inspections could have been conducted at longer intervals is present. Starting with the 1998 inspection report, the AASHTO CoRe element condition state for the deck was downgraded from 1 to 2, which means that the delaminated area is less than 2% of the total deck area. The AASHTO CoRe element definition of condition states 1 and 2 are slightly different than the definition of the condition states in Table 4.6 in that AASHTO condition state 1 is zero percent delaminated and condition state 2 is between 0% and 2% ADL. While the condition state did worsen in 1998 according to inspection reports, the reported range does encompass the values projected by the 90th percentile ADL from CDCPM. All subsequent inspections also show condition state 2, which indicates the condition remains steady. CDCPM reflects this in the 90th percentile ADL value having only a small change in this time period. This suggests that CDCPM does provide a good projection, and that the inspections run in 1998 and 2000 for delamination may not have been needed in the inspection planning methodology presented in this thesis.

4.4.2 Future Inspection Plan on Larimer County Bridge LR 50 - 0.2 – 17

Starting with the latest inspection report available for the Larimer County Bridge in 2013, CDCPM and uncertainty forecast plots are used to plan the next inspection time and method. Using the inspection plan presented in Figure 4.7, the timing of the next inspection is determined. Three possible inspection methods for delamination are considered: 1) chain drag, 2) impact-echo (I-E), and 3) ground penetrating radar (GPR). Figure 4.23 and Figure 4.24 below shows the 6-year projection of standard deviation of ADL and percentile ADL for the concrete

girder section based on 0% delaminated in 2013 with no standard deviation, as reported in the inspection report.

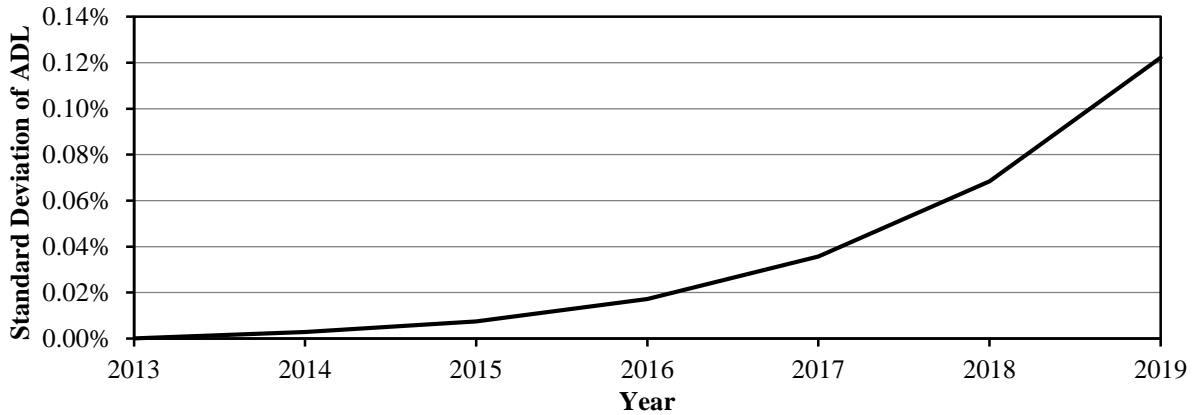


Figure 4.23. Projected standard deviation of ADL for bridge LR 50-0.2-17

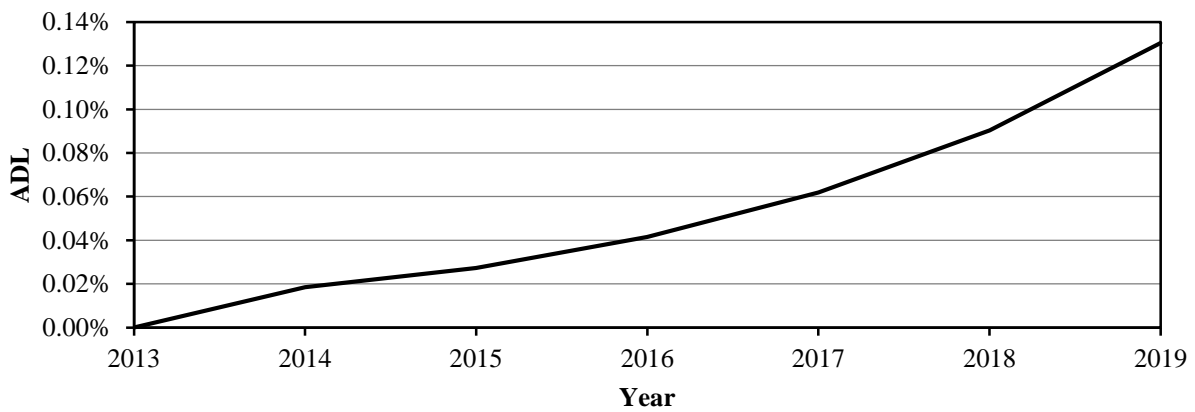


Figure 4.24. Projected 90th percentile ADL for bridge LR 50-0.2-17

When the projections shown above are compared to their appropriate limits for condition state 1 (Table 4.6 and Table 4.9), neither limit will be reached in the next 6 years. Therefore, the next inspection should be conducted in 2019. Since the chance of the deck changing condition states in the next 6 years is small, the inspection will focus on reduction the spread in ADL.

Figure 4.25 below shows the uncertainty forecast plot for the standard deviation of ADL in 2019 for the three inspection methods considered.

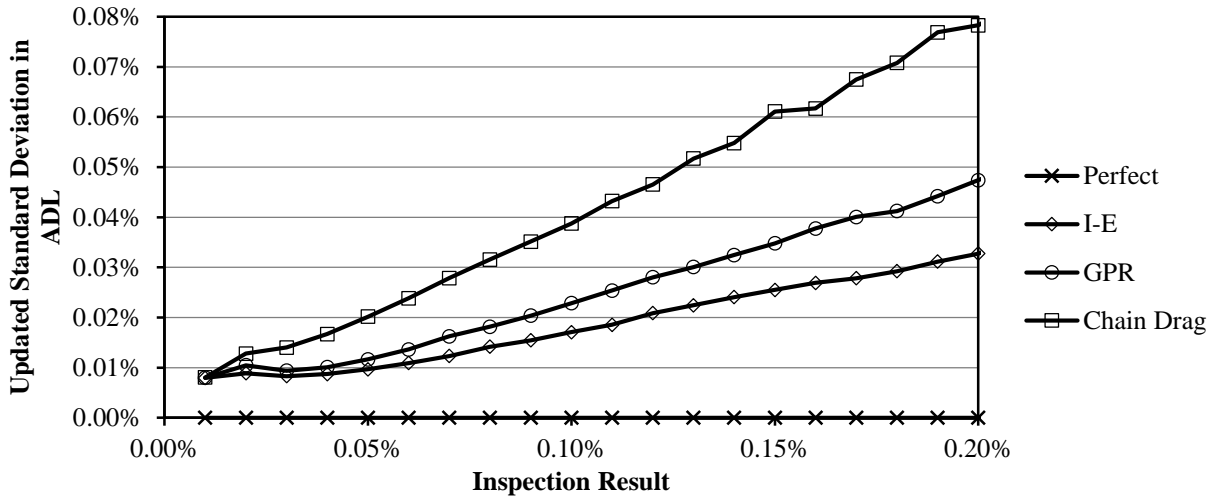


Figure 4.25. Uncertainty forecast plot of the updated standard deviation in ADL for various inspection methods in 2019

According to Figure 4.25, all three inspection methods considered will succeed in keeping the standard deviation below the limit of 0.5%. Therefore, from an uncertainty standpoint, any of the above methods are reasonable methods to use for this inspection. When considering the cost of equipment, the chain drag method would be the best choice. Other considerations include the time to conduct inspection, difficulty in interpreting results, and disruption of traffic to perform the inspection.

In order to investigate inspection planning for severely delaminated decks, a deck in condition state 4 is analyzed in the same manner as done above. Table 4.13 shows the initial distribution parameters of the bridge condition in 2013.

Table 4.13. Initial ADL statistics for severely delaminated deck

Statistic		Value
Mean		18%
Standard Deviation		3.6%
90 th Percentile ADL		22.08%
95% CI Bounds	Upper	25.06%
	Lower	10.94%

From this distribution, CDCPM is used to project the standard deviation of ADL and the 90th percentile ADL values for the next six years. Figure 4.26 shows the projection of the standard deviation of ADL, and Figure 4.27 shows the 90th percentile ADL projection.

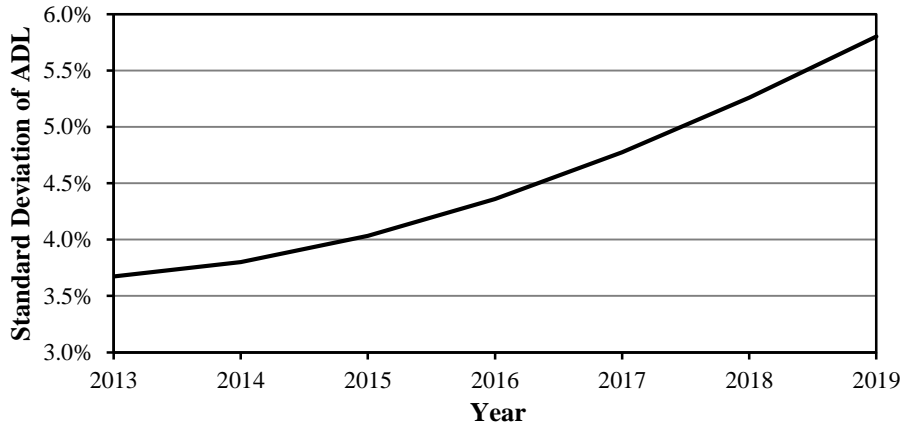


Figure 4.26. Standard deviation of ADL projection for severely delaminated bridge deck

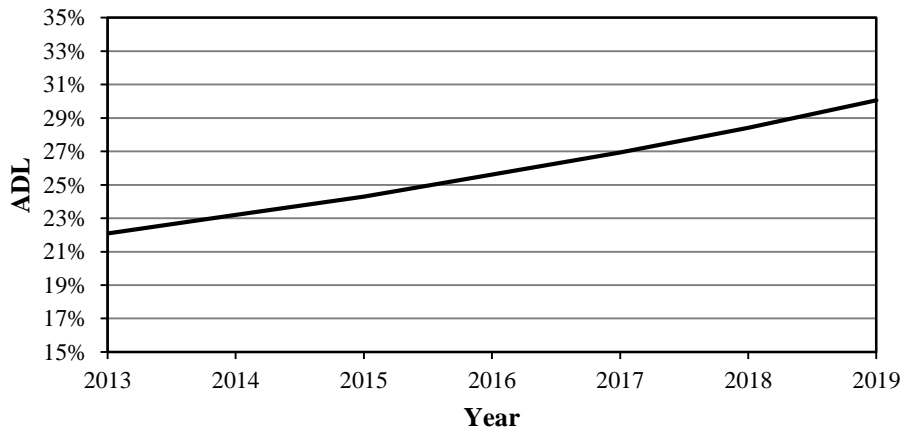


Figure 4.27. 90th percentile ADL projection for severely delaminated bridge deck

Both sets of data are compared to the limits established in Table 4.6 and Table 4.9. For condition state 4, the maximum standard deviation of ADL is 5% and the maximum ADL is 25%. The next inspection based on standard deviation of ADL should be conducted in 2018, while the next inspection based on the 90th percentile ADL should be conducted in 2016. Since the 90th percentile gives the shorter interval, this inspection method will control. This means the goal of the next inspection is to see if the condition state has changed from 4 to 5 in year 2016.

Using the simulated ADL from year 2016, an uncertainty forecast plot of the mean ADL is created for the same inspection methods used before; chain drag, I-E, and GPR. This plot is shown in Figure 4.28 below.

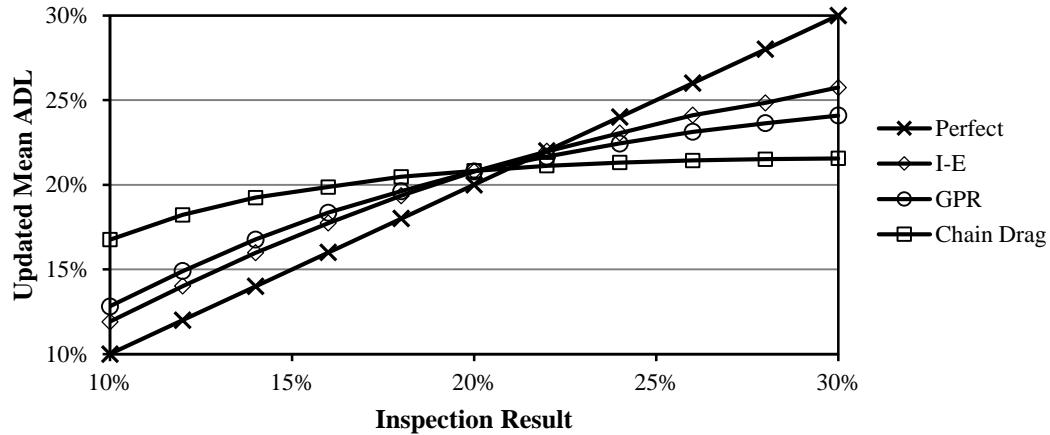


Figure 4.28. Uncertainty forecast plot of the mean ADL for the severely delaminated concrete deck

According to the uncertainty forecast plot in Figure 4.28, neither the chain drag nor GPR methods are accurate enough to provide a good update of the mean. The I-E method will provide enough evidence to change the condition state to 5 if a result greater than 28.1% is obtained. The probability of obtaining such a result based on the prior distribution in 2016 is only 3.9%. However, of the available options, the impact-echo method is the best option from an uncertainty standpoint. To improve the effectiveness of this procedure, the ways to reduce the variability in the result should be examined, such as using more experienced inspectors. However, this plot is also limited by the understanding of precision of NDE methods, and it is possible that these methods are more precise for the high ranges of ADL experienced here. Through further research on NDE precision, the estimation of the uncertainty forecast plot can be improved to give a better decision tool for planning inspection methods.

4.4.3 Inspection Planning for Two Bridge Decks

Two different bridge decks are compared in order to plan the allocation of inspection resources for each bridge. The scenario is described in section 3.6.3. For the two decks, one can receive a GPR delamination test, while the other can receive a chain drag test. Neither deck has received a delamination inspection before, so CDCPM projected the prior distribution from the beginning of the deck's service life. Table 4.14 below shows the mean, standard deviation, 90th percentile, and 95% confidence interval bounds for each deck for the current time as determined from CDCPM delamination output.

Table 4.14. Statistics of the two concrete bridge deck at the current time

Statistic (% ADL)	Bridge Deck	
	A	B
Mean	0.471	11.4
Standard Deviation	3.75	23.5
90th Percentile ADL	0.194	44.7
Upper Bound- 95% CI	2.84	91.9
Lower Bound-95% CI	0	0

The older deck, deck B, shows a much more uncertain delamination condition than deck A. Deck A shows the mean ADL is greater than the 90th percentile value, which indicates a large amount of skew in the data, and this also shows why the mean ADL is not a good indicator of the projected condition. The mean and 90th percentile ADL values for both decks are above the minimum detectable ADL for each test shown in Table 3.9. This indicates that either method should be capable of detecting the existence of delamination in either bridge.

In order to investigate how possible inspection results would affect the updated uncertainty in the bridge deck, uncertainty forecast plots were developed for the mean and standard deviation of the updated data for each inspection, as well as the line for the perfect inspection. All of the plots are shown for the range of inspection results that are within a 95% confidence interval from the model, which are the most likely inspection results. The goal is to

find an inspection that will give an accurate estimate of the current condition while also providing a significant reduction in uncertainty for the model. The plots of the mean updated ADL for both decks are shown in Figure 4.29 and Figure 4.30 below.

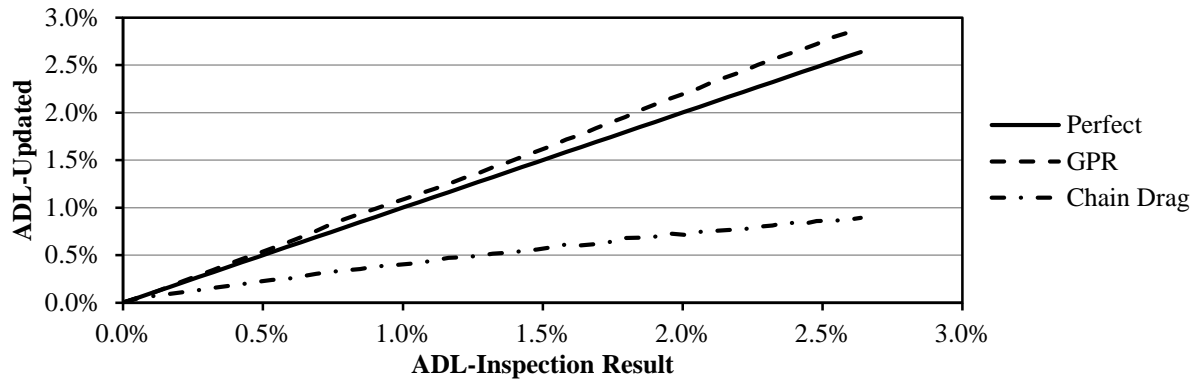


Figure 4.29. Uncertainty forecasting plot for the mean updated ADL – Deck A

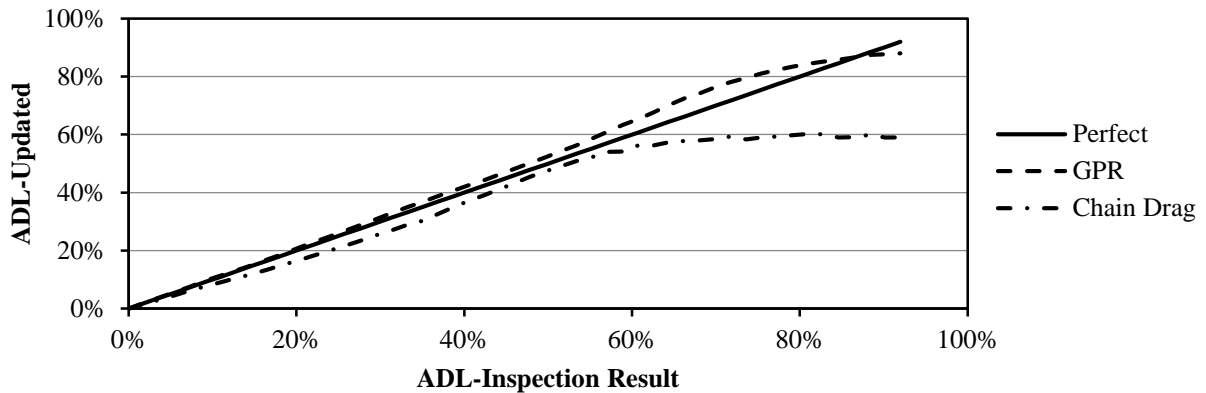


Figure 4.30. Uncertainty forecasting plot for the mean updated ADL – Deck B

Both of the plots show that the updated mean ADL will be lower than the inspection result for the chain drag method, but the updated ADL result from the GPR method will be near-identical to the inspection result. As seen with the chain drag method, updating tends to weigh the model prediction heavier when the inspection results are not reliable. Figure 4.31 and Figure 4.32 below show the uncertainty forecasting plots for the updated standard deviation of ADL.

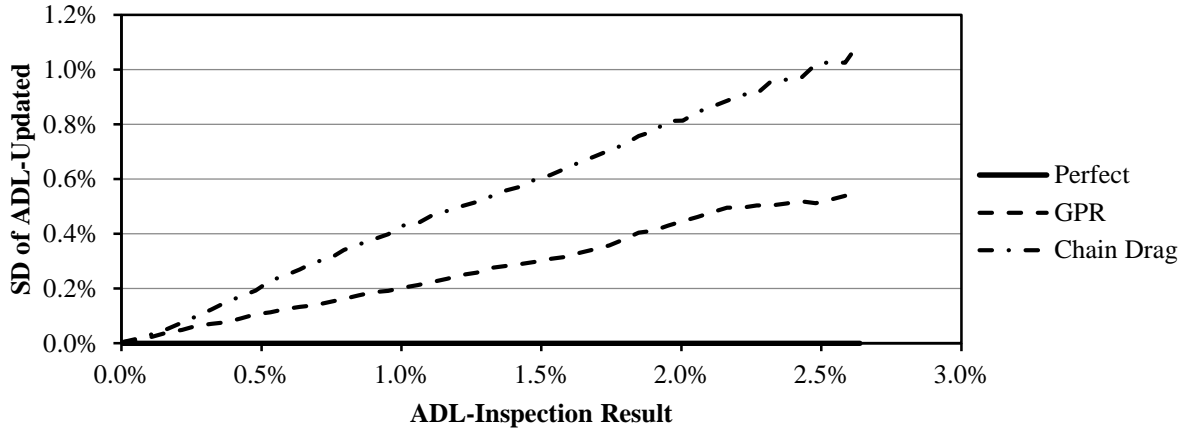


Figure 4.31. Uncertainty forecasting plot for the standard deviation of updated ADL – Deck A

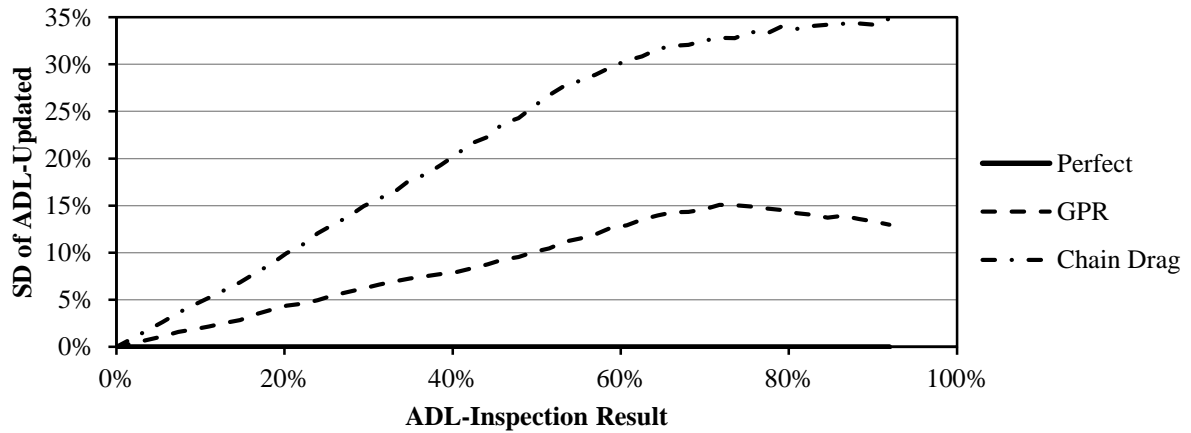


Figure 4.32. Uncertainty forecasting plot for the standard deviation of updated ADL – Deck B

As a reminder, the perfect inspection plots along the x-axis in Figure 4.31 and Figure 4.32, because there will be no standard deviation in ADL regardless of inspection result. As expected, the chain drag method will yield a higher standard deviation in the updated ADL than the GPR test will. For bridge deck B, the uncertainty in the updated ADL could be large if the inspection yields a high amount of deck delaminated. For bridge deck A, both methods will most likely reduce the uncertainty in ADL.

Regarding the standard deviation requirement for the output, the target updated standard deviation in ADL should be different for each bridge. Deck A shows a mean and a 90th percentile ADL within condition state one, so this is the expected condition state. According to Table 4.9,

the standard deviation should be reduced at or below 0.5% ADL. Deck B shows no clear condition state according to the statistical data. However, the standard deviation should not be more than 5% for any condition state, so 5% will be the standard deviation limit for deck B.

Although neither inspection procedure appears to be a good method for evaluating deck B after reviewing Figure 4.32, the evaluation of the probability of obtaining a satisfactory inspection result shows that a successful inspection is much more likely. Using the samples of the prior distribution for each deck, the probability of obtaining a sufficient result is evaluated as the percentile of the maximum inspection result that will lower the standard deviation of ADL below 5% ADL. The maximum sufficient result can be pulled from Figure 4.32. The maximum sufficient result for the GPR method is 22.1%, for which there is an 83.9% probability of obtaining this result or less. The maximum sufficient result for the chain drag method is 8.1%, for which there is a 74.8% probability of obtaining this result or less. According to the prior distribution, both methods have a good chance of obtaining a sufficient result from an inspection.

The updated mean value of the output ADL will be near perfect for any result from either method on deck B that falls within the considered range of condition state ratings (less than 25% ADL). The updated mean ADL for deck A would be different depending on the inspection method chosen. The GPR method is accurate enough to give a near-perfect update to the model, while the chain drag method is not accurate enough, and the updating procedure would weigh the prior model with more influence. This shows that the effect of running a chain drag method for deck A will not give much new information on the condition.

Considering the analysis above, a decision on the appropriate inspection method for each bridge can be made. Since both inspection methods would provide a near-perfect mean ADL value for deck B, and the probability of getting an inspection result that would sufficiently lower

the uncertainty in the condition in is close for both methods, the chain drag method is recommended for deck B. This would allow the GPR method to be run on deck A, and the resulting uncertainty would very likely be low, which could in turn allow a longer time between inspection intervals. Since the uncertainty in the condition of deck B is high, any test that gives a reliable result would greatly improve our knowledge of the current condition. This would be the most efficient use of the available inspection procedures for the decks considered.

4.5 Implementing Inspection Plan for Use by Bridge Management Agencies

The proposed inspection framework is a reasonable plan for bridge owners to use to plan inspection timing and method for their system's concrete bridge decks. While the analysis using CDCPM is unique to each bridge, many parameters are likely to remain the same for most bridges within the management system. Such parameters may include climate-related parameters if the bridges are located in the same region, material parameters if the same materials are used, and model bias parameters if the same deterioration models are used. Other parameters such as bridge geometry require only input of the bridge dimensions, because the variability is determined from generally accepted values from literature. With only a few parameters that change for a particular bridge, new predictions would be easy to make for each bridge.

For implementation of this inspection plan by bridge owners for an entire bridge, subsequent prediction models should be developed for all critical components of a bridge. This would include models for deterioration such as fatigue of steel girders, cracking of concrete columns, and scour of abutments among others. The models can be developed by researching the causes of the deterioration, representing these processes through mechanistic models developed by theory and experiment, and running them under a Monte Carlo simulation framework.

Condition state limits can be established to provide guidance on maintenance actions for each component, similar to the CoRe element system used by AASHTO (2014).

The uncertainty-based inspection plan can also be used for the agency's entire bridge network, and would provide added benefits over the current bridge inspection system. The scenario with inspections for two bridge decks in section 4.4.3 highlighted that uncertainty can be used as a basis for allocating inspection resources within a system. As a bridge network involves many bridges, the use of UFP's would be even more critical in managing inspection resources. Mechanistic modeling of different bridge components will identify the specific components that require inspections, which would allow inspections to be component-specific. Another effect of component-specific inspections is that inspection teams can be focused on particular parts of the bridge. For instance, an inspection team can be designated as a bridge deck inspection team, and they are responsible for conducting NDE and visual inspections for all bridge decks within a system. Another benefit of this is that each team will become experts in their assigned bridge part, which can lead to reduced uncertainty and higher consistency between inspection results for the bridge deck within a system.

This uncertainty-based inspection plan will also have some challenges in implementing the variable inspection timing for components. The inconsistency in the timing and method of inspection from one simulation to the next can lead to difficulty in forecasting inspection budgets for the bridge system. Depending on the results of an inspection plan, it would be possible that many bridges would require inspections on the same component in the same year, which would lead to logistical and monetary problems on the inspection agency for that year, while the component-specific inspection team would have little work during the other years. However, this uncertainty-based inspection method defined the maximum allowable inspection interval, which

means that inspections could be run a year in advance. This would spread out the inspection workload, and lower the annual cost, of inspections for the component. For example, if 50 bridge decks are projected to require a delamination inspection in 5 years, while only 10 bridge decks require a delamination inspection in 4 years, some of the inspections for the 5-year projection group can be moved to 4 years so that the work load is more even in each year. The flexibility of the inspection time in this way can also allow bridge agencies to control the number of bridge decks that require inspections in each year, which in turn will allow for a more predictable budget each year, while ensuring that inspections are still being conducted only when needed.

5. CONCLUSIONS

5.1 Summary

An extensive literature review was conducted to gain a better understanding of the current approach to bridge inspection planning in the United States, and to determine the current research being done toward implementing a risk-based inspection approach. It was determined that the current system has multiple ways of quantifying the condition of bridge deck, but there are inconsistencies in the quality of reporting and the interpretation of the system. The literature review also was done to understand the current mechanistic models in use for modeling different processes that affect concrete bridge deck cracking and delamination, and the inspection methods available to investigate delaminations. Concrete drying and thermal shrinkage, dead load, and creep were considered to affect vertical transverse cracking, while subsidence, creep, and corrosion of embedded rebar affect delamination.

A computer model, CDCPM, was developed to analyze uncertainty in the bridge deck for the current condition, and to project the future condition. Using CDCPM, separate inspection plans for the evaluation of vertical cracking and delamination in concrete bridge decks is developed. The model is also evaluated under a sensitivity study to identify the most influential parameters to the uncertainty in the deck condition. Once identified, the management of these influential parameters is discussed to either reduce the uncertainty, or to improve the modeling of these parameters. Demonstrations are then conducted to showcase how CDCPM and the inspection plan for delamination can be used in bridge planning scenarios. The inspection plan is first compared to a past inspection plan for a real bridge and the efficiency of the past inspection plan compared to the proposed plan is discussed. The future plan for a single bridge is developed

for both timing and inspection method. A final scenario that uses the proposed plan to plan inspections for two bridges under limited resources is also explored.

5.2 Contributions to Bridge Inspection and Maintenance Practice

Based on the information researched in this thesis, the following conclusions can be drawn about bridge inspection planning:

- 1) The current bridge inspection program in the United States does not provide the most efficient timing for inspections.
- 2) An inspection plan is developed based on uncertainty in the current condition and projections of uncertainty to manage when inspections are conducted and what methods are used in the evaluation. This plan allows for longer inspection times, and provides a means to selecting inspection methods when resources are scarce.
- 3) The sources of uncertainty in concrete deck cracking are identified for different times in the bridge's service life. Recommendations on how these sources can be managed effectively is presented.
- 4) Climate-related parameters are identified and evaluated to explore how climate affects bridge deck deterioration under an uncertain analysis. Both actual climate data and theoretical values are used, and recommendations on the management of climate-related parameters are made.
- 5) Through use of CDCPM, uncertainty forecast plots, and the proposed inspection plan, examples of different management scenarios is made. This provides the groundwork for extension to system-level management using uncertainty, as well as development of similar inspection plans for other components of a bridge.

5.3 Further Research

The research presented here attempts to set the groundwork for the use of mechanistic models in bridge inspection planning under an uncertainty analysis. Possible topics that should be explored further based on this research are:

- 1) Research other mechanistic models, and explore how each different model affects the cracking and delamination of the concrete deck. Only one time-to-corrosion cracking and chloride diffusion model were considered for delamination in this study. Other models available should be explored to see if they help to reduce the uncertainty in the current condition, and then can be used to improve CDCPM.
- 2) The current model does not include uncertainty in low-probability events that would have a major consequence on the bridge, such as the impact loading from a vehicle striking the girder of an overpass bridge. Although not likely, it would severely change the condition of the bridge.
- 3) Since freeze-thaw cycles do cause cracking in concrete bridge decks, research should continue to explore how this cracking occurs, and how it can be modeled so that it can be implemented in an uncertainty analysis similar to the one presented in this thesis. The freeze-thaw model should also be implemented in combination with the other concrete sub models used in this thesis.
- 4) A similar methodology could be implemented for other deterioration modes such as freeze-thaw of concrete, fracture resistance of steel members, and strength capacity limit states of girders and columns to determine inspection timing and method for other bridge components.

- 5) Further studies should be conducted on the quantification of various NDE inspection precisions and bias, and how the quality of running the method affects these values. Accuracy estimates for different methods, as well as knowledge of how accuracy can be improved through quality control, should increase the effectiveness of the inspection methodology presented in this thesis.
- 6) The possibility of expanding the maximum inspection interval beyond 6 years should be investigated. Depending on the performance of CDCPM, the projection accuracy for times over 6 years can be verified, and the extension of inspections for times greater than six years can be made.
- 7) The implementation of this inspection plan for an entire bridge system should be investigated further. Expanding the concepts introduced in section 4.4.3 and section 4.5, the management of inspections for multiple bridges and limited resources will require careful analysis and planning not seen on an individual bridge basis.
- 8) Other bridge components should be analyzed in a similar framework. Once uncertainty analysis programs, such as CDCPM, are developed for all bridge components, a complete uncertainty-based inspection plan can be used for all bridge inspection management.

6. REFERENCES

- AASHTO. (1994). Manual for Condition Evaluation of Bridges *MCE-1*. Washington, DC: American Association of State Highway and Transportation Officials.
- AASHTO. (1997). Guide for commonly Recognized (CoRe) Structural Elements *CORE-1*. Washington, DC: American Association of State Highway and Transportation Officials.
- AASHTO. (2012). LRFD Bridge Design Specifications, Customary U.S. Units. Washington, DC: American Association of State Highway and Transportation Officials.
- AASHTO. (2014). Manual for Bridge Evaluation (2nd Edition) with 2011, 2013 and 2014 Interim Revisions. Washington, DC: American Association of State Highway and Transportation Officials.
- Al-Manaseer, A., & Lakshmikantan, S. (1999). Comparison between current and future design code models for creep and shrinkage. *Revue française de génie civil*, 3(3-4), 39-59.
- Allam, S. M., Shoukry, M. S., Rashad, G. E., & Hassan, A. S. (2012). Crack width evaluation for flexural RC members. *Alexandria engineering journal*, 51(3), 211-220.
- ASCE/SEI-AASHTO. (2009). White Paper on Bridge Inspection and Rating. *Journal of Bridge Engineering*, 14(1), 1-5. doi:10.1061/(ASCE)1084-0702(2009)14:1(1)
- ASTM-C39. (2015). Standard Test Method for Compressive Strength of Cylindrical Concrete Specimens. West Conshohocken, PA: ASTM International.
- ASTM-C876-09. (2009). Standard Test Method for Corrosion Potentials of Uncoated Reinforcing Steel in Concrete. West Conshohocken, PA: ASTM International.
- ASTM-C1152/C1152M. (2012). Standard Test Method for Acid-Soluble Chloride in Mortar and Concrete. West Conshohocken, PA: ASTM International.
- ASTM-C1218/C1218M. (2008). Standard Test Method for Water-Soluble Chloride in Mortar and Concrete. West Conshohocken, PA: ASTM International.
- ASTM-C1383. (2010). Standard Test Method for Measuring the P-Wave Speed and the Thickness of Concrete Plates Using the Impact-Echo Method. West Conshohocken, PA: ASTM International.
- ASTM-C1556. (2011). Standard Test Method for Determining the Apparent Chloride Diffusion Coefficient of Cementitious Mixtures by Bulk Diffusion. West Conshohocken, PA: ASTM International.
- ASTM-D4788. (2013). Standard Test Method for Detecting Delaminations in Bridge Decks Using Infrared Thermography. West Conshohocken, PA: ASTM International.

- ASTM-D6087. (2008). Standard Test Method for Evaluating Asphalt-Covered Concrete Bridge Decks Using Ground Penetrating Radar. West Conshohocken, PA: ASTM International.
- Azizinamini, A., Power, E. H., Myers, G. F., Ozyildirim, H. C., Kline, E., Whitmore, D. W., & Mertz, D. R. (2014). Design Guide for Bridges for Service Life. Washington, D.C.: National Academy of Sciences.
- Barnes, C. L., & Trottier, J.-F. (2000). Ground-penetrating radar for network-level concrete deck repair management. *Journal of Transportation Engineering*, 126(3), 257-262.
- Basheer, P. A. M., Chidiact, S. E., & Long, A. E. (1996). Predictive models for deterioration of concrete structures. *Construction and Building Materials*, 10(1), 27-37.
- Bayes, T., & Price, R. (1763). An essay towards solving a problem in the doctrine of chances. by the late rev. mr. bayes, frs communicated by mr. price, in a letter to john canton, amfrs. *Philosophical Transactions (1683-1775)*, 370-418.
- Bazant, Z. P. (1972). *Prediction of concrete creep effects using age-adjusted effective modulus method*.
- Bazant, Z. P., & Baweja, S. (1995a). Creep and shrinkage prediction model for analysis and design of concrete structures-model B3. *Materials and Structures*, 28, 357-365.
- Bazant, Z. P., Chern, J. C., Rosenberg, A. M., & Gaidis, J. M. (1988). Mathematical Model for Freeze-Thaw Durability of Concrete. *Journal of the American Ceramic Society*, 71(9), 776-783.
- Bazant, Z. P., & Kim, S.-S. (1979). Approximate relaxation function for concrete. *Journal of the Structural Division*, 105(12), 2695-2705.
- Bazant, Z. P., & L'Hermite, R. (1988). *Mathematical modeling of creep and shrinkage of concrete*: Wiley Chichester.
- Bazant, Z. P., & Oh, B. H. (1984). *Deformation of progressively cracking reinforced concrete beams*.
- Bazant, Z. P., & Baweja, S. (1995b). Justification and refinements of model B3 for concrete creep and shrinkage 1. statistics and sensitivity. *Materials and Structures*, 28(7), 415-430.
- Beck, J. L., & Au, S.-K. (2002). Bayesian updating of structural models and reliability using Markov chain Monte Carlo simulation. *Journal of Engineering Mechanics*, 128(4), 380-391.
- Bhide, S. B., & Collins, M. P. (1989). Influence of axial tension on the shear capacity of reinforced concrete members. *ACI Structural Journal*, 86(5).
- Bolukbasi, M., Mohammadi, J., & Arditi, D. (2004). Estimating the Future Condition of Highway Bridge Components Using National Bridge Inventory Data. *Practice Periodical*

- on Structural Design and Construction*, 9(1), 16-25. doi:10.1061/(ASCE)1084-0680(2004)9:1(16)
- Cady, P. D., & Weyers, R. E. (1983). Chloride penetration and the deterioration of concrete bridge decks. *Cement, concrete and aggregates*, 5(2), 81-87.
- Carreira, D., & Branson, D. (1982). Prediction of creep, shrinkage, and temperature effects in concrete structures. *ACI Special Publication*, 76.
- CDOT. (1998). Pontis Bridge Inspection Coding Guide.
- CEB-FIP. (1993). *CEB-FIP Model Code 1990: Design Code*: T. Telford.
- Cesare, M. A., Santamarina, C., Turkstra, C., & Vanmarcke, E. H. (1992). Modeling bridge deterioration with Markov chains. *Journal of Transportation Engineering*, 118(6), 820-833.
- Chan, K., Saltelli, A., & Tarantola, S. (1997, 1997). *Sensitivity analysis of model output: variance-based methods make the difference*. Paper presented at the Winter Simulation Conference.
- Chen, F., & Qiao, P. (2014). Probabilistic damage modeling and service-life prediction of concrete under freeze–thaw action. *Materials and Structures*, 1-15.
- Cho, T. (2007). Prediction of cyclic freeze–thaw damage in concrete structures based on response surface method. *Construction and Building Materials*, 21(12), 2031-2040.
- Clear, K. C. (1974). *Time to corrosion of reinforcing steel in concrete slabs*.
- Cornell, C. A. (1969). A probability-based structural code*. *ACI Journal Proceedings*, 66.
- Dakhil, F. H., Cady, P. D., & Carrier, R. E. (1975). *Cracking of fresh concrete as related to reinforcement*.
- Davis-McDaniel, C., Chowdhury, M., Pang, W., & Dey, K. (2012). Fault-Tree model for risk assessment of bridge failure: case study for segmental box girder bridges. *Journal of Infrastructure Systems*, 19(3), 326-334.
- Ellingwood, B., & Galambos, T. V. (1983). Probability-based criteria for structural design. *Structural Safety*, 1(1), 15-26.
- Emmons, R. H. (1993). *Concrete Repair and Maintenance Illustrated. Problem Analysis, Repair Strategy, and Techniques*.
- Enright, M. P., & Frangopol, D. M. (1999). Condition prediction of deteriorating concrete bridges using Bayesian updating. *Journal of Structural Engineering*, 125(10), 1118-1125.

- Estes, A. C., & Frangopol, D. M. (2003). Updating bridge reliability based on bridge management systems visual inspection results. *Journal of Bridge Engineering*, 8(6), 374-382.
- Everett, D. H. (1961). The thermodynamics of frost damage to porous solids. *Trans. Faraday Soc.*, 57, 1541-1551.
- Fagerlund, G. (1977). The critical degree of saturation method of assessing the freeze/thaw resistance of concrete. *Materials and Structures*, 10(4), 217-229.
- FHWA. (1995). Recording and Coding Guide for the Structure Inventory and Appraisal of the Nation's Bridges. Washington, DC: Federal Highway Administration.
- FHWA. (2011). Portland Cement Concrete Pavements Research.
- FHWA. (2012). Errata Sheet-Recording and coding Guide for the Structure Inventory and Appraisal of the Nation's Bridges. Washington, DC: Federal Highway Administration.
- FHWA. (2014). Specification for the National Bridge Inventory Bridge Elements. Washington, DC.
- Gardner, N. J., & Lockman, M. J. (2001). Design provisions for drying shrinkage and creep of normal-strength concrete. *ACI Materials Journal*, 98(2).
- Gardner, N. J., & Zhao, J. W. (1993). Creep and shrinkage revisited. *ACI Materials Journal*, 90(3).
- Gavin, H. P., & Yau, S. C. (2008). High-order limit state functions in the response surface method for structural reliability analysis. *Structural Safety*, 30(2), 162-179.
- Gergely, P. (1981). Role of cover and bar spacing in reinforced concrete. *ACI Special Publication*, 72.
- Goel, R., Kumar, R., & Paul, D. K. (2007). Comparative study of various creep and shrinkage prediction models for concrete. *Journal of materials in civil engineering*, 19(3), 249-260.
- Graybeal, B. A., Phares, B. M., Rolander, D. D., Moore, M., & Washer, G. (2002). Visual inspection of highway bridges. *Journal of nondestructive evaluation*, 21(3), 67-83.
- Hadidi, R., Ala Saadeghvaziri, M., & Thomas Hsu, C. T. (2003). Practical tool to accurately estimate tensile stresses in concrete bridge decks to control transverse cracking. *Practice Periodical on Structural Design and Construction*, 8(2), 74-82.
- Hasofer, A. M., & Lind, N. C. (1974). Exact and invariant second-moment code format. *Journal of the Engineering Mechanics division*, 100(1), 111-121.

- Hesse, A. (2013). *Using Expert Opinion to Quantify Accuracy and Reliability of Nondestructive Evaluations on Bridges*. (Master of Science), Colorado State University, Fort Collins, Colorado.
- Hing, C., & Halabe, U. (2010). Nondestructive Testing of GFRP Bridge Decks Using Ground Penetrating Radar and Infrared Thermography. *Journal of Bridge Engineering*, 15(4), 391-398. doi:10.1061/(ASCE)BE.1943-5592.0000066
- Igusa, T., Buonopane, S., & Ellingwood, B. (2002). Bayesian analysis of uncertainty for structural engineering applications. *Structural Safety*, 24(2), 165-186.
- Issa, M. A. (1999). Investigation of cracking in concrete bridge decks at early ages. *Journal of Bridge Engineering*, 4(2), 116-124.
- Jansen, M. J. W. (1999). Analysis of variance designs for model output. *Computer Physics Communications*, 117(1), 35-43.
- Kennedy, J., & Soliman, M. (1987). Temperature Distribution in Composite Bridges. *Journal of Structural Engineering*, 113(3), 475-482. doi:10.1061/(ASCE)0733-9445(1987)113:3(475)
- Kobayashi, K., Kaito, K., & Lethanh, N. (2010). Deterioration forecasting model with multistage weibull hazard functions. *Journal of infrastructure systems*, 16(4), 282-291.
- Krauss, P. D., & Rogalla, E. A. (1996). *Transverse cracking in newly constructed bridge decks*.
- Kyle, N. L. (2001). Subsidence cracking of concrete over steel reinforcement bar in bridge decks.
- Lancaster, T. (1992). *The econometric analysis of transition data*: Cambridge university press.
- Li, L., Sun, L., & Ning, G. (2014). Deterioration Prediction of Urban Bridges on Network Level Using Markov-Chain Model. *Mathematical Problems in Engineering*, 2014.
- Lichtenstein, A. G. (1993). The silver bridge collapse recounted. *Journal of performance of constructed facilities*, 7(4), 249-261.
- Litvan, G. G. (1976). Frost action in cement in the presence of de-icers. *Cement and Concrete Research*, 6(3), 351-356.
- Liu, Y., & Weyers, R. E. (1998). Modeling the time-to-corrosion cracking in chloride contaminated reinforced concrete structures. *ACI Materials Journal*, 95(6).
- Ma, F.-Y. (2012). *Corrosive Effects of Chlorides on Metals, Pitting Corrosion*: InTech.
- Maierhofer, C., Reinhardt, H.-W., & Dobmann, G. (2010). *Non-Destructive Evaluation of Reinforced Concrete Structures, Volume 2 - Non-Destructive Testing Methods*: Woodhead Publishing.

- Maser, K. (2004). Active Heating infrared thermography for detection of subsurface bridge deck deterioration. *TRB, Washington, DC*.
- Maser, K. R., & Roddis, W. M. K. (1990). Principles of thermography and radar for bridge deck assessment. *Journal of transportation engineering*, 116(5), 583-601.
- Mazzotti, C., & Savoia, M. (2003). Nonlinear Creep Damage Model for Concrete under Uniaxial Compression. *Journal of Engineering Mechanics*, 129(9), 1065-1075. doi:10.1061/(ASCE)0733-9399(2003)129:9(1065)
- Melchers, R. E. (1999). Structural reliability analysis and prediction.
- Melchers, R. E., & Melchers, R. E. (1999). Structural reliability analysis and prediction.
- Mirza, S. A., MacGregor, J. G., & Hatzinikolas, M. (1979). Statistical descriptions of strength of concrete. *Journal of the Structural Division*, 105(6), 1021-1037.
- Mishalani, R., & Madanat, S. (2002). Computation of Infrastructure Transition Probabilities Using Stochastic Duration Models. *Journal of Infrastructure Systems*, 8(4), 139-148. doi:10.1061/(ASCE)1076-0342(2002)8:4(139)
- Moore, M., Phares, B. M., Graybeal, B., Rolander, D., & Washer, G. (2001). *Reliability of visual inspection for highway bridges, volume I: Final report*. Retrieved from
- Morcous, G. (2006). Performance Prediction of Bridge Deck Systems Using Markov Chains. *Journal of Performance of Constructed Facilities*, 20(2), 146-155. doi:10.1061/(ASCE)0887-3828(2006)20:2(146)
- Moses, F. (1996). *Bridge Evaluation Based on Reliability*.
- Nasrollahi, M., & Washer, G. (2014). Estimating Inspection Intervals for Bridges Based on Statistical Analysis of National Bridge Inventory Data. *Journal of Bridge Engineering*.
- Nowak, A. S., Yamani, A. S., & Tabsh, S. W. (1994). Probabilistic models for resistance of concrete bridge girders. *ACI Structural Journal*, 91(3).
- Page, C., Short, N. R., & El Tarras, A. (1981). Diffusion of chloride ions in hardened cement pastes. *Cement and concrete research*, 11(3), 395-406.
- Pantazopoulou, S. J., & Papoulia, K. D. (2001). Modeling cover-cracking due to reinforcement corrosion in RC structures. *Journal of Engineering Mechanics*, 127(4), 342-351.
- Penttala, V. (1998). Freezing-induced strains and pressures in wet porous materials and especially in concrete mortars. *Advanced cement based materials*, 7(1), 8-19.
- Phares, B., Washer, G., Rolander, D., Graybeal, B., & Moore, M. (2004). Routine Highway Bridge Inspection Condition Documentation Accuracy and Reliability. *Journal of Bridge Engineering*, 9(4), 403-413. doi:10.1061/(ASCE)1084-0702(2004)9:4(403)

- Phares, B. M., Rolander, D. D., Graybeal, B. A., & Washer, G. A. (2001). Reliability of visual bridge inspection. *Public Roads*, 64(5).
- Powers, T. C., & Helmuth, R. A. (1953). Theory of volume changes in hardened portland-cement paste during freezing (Vol. 32).
- Prozzi, J. A., & Madanat, S. (2003). Analysis of experimental pavement failure data using duration models. *University of California Transportation Center*.
- Ramey, G., Wolff, A., & Wright, R. (1997). DOT Management Actions to Enhance Bridge Durability/Longevity. *Practice Periodical on Structural Design and Construction*, 2(3), 125-130. doi:10.1061/(ASCE)1084-0680(1997)2:3(125)
- Rens, K., Nogueira, C., & Transue, D. (2005). Bridge Management and Nondestructive Evaluation. *Journal of Performance of Constructed Facilities*, 19(1), 3-16. doi:10.1061/(ASCE)0887-3828(2005)19:1(3)
- Robelin, C.-A., & Madanat, S. M. (2007). History-dependent bridge deck maintenance and replacement optimization with Markov decision processes. *Journal of Infrastructure Systems*, 13(3), 195-201.
- Roberts, R. (2015). Inside the Bridge Inspection Toolbox: Ground Penetrating Radar Yields Benefits. *Structure Magazine*, 28-30.
- Russel, H. G., & Larson, S. C. (1989). Thirteen years of deformations in water tower place. *ACI Structural Journal*, 86(2).
- Ryan, T. W., Mann, J. E., Chill, Z. M., & Ott, B. T. (2012). Bridge Inspector's Reference Manual: Federal Highway Administration.
- Saltelli, A., Annoni, P., Azzini, I., Campolongo, F., Ratto, M., & Tarantola, S. (2010). Variance based sensitivity analysis of model output. Design and estimator for the total sensitivity index. *Computer Physics Communications*, 181(2), 259-270.
- Sansalone, M., & Carino, N. J. (1989). Detecting delaminations in concrete slabs with and without overlays using the impact-echo method. *ACI Materials Journal*, 86(2).
- Sansalone, M., & Streett, W. B. (1997). Impact-echo: nondestructive testing of concrete and masonry: Bullbrier Press Jersey Shore, PA.
- Scherer, W., & Glagola, D. (1994). Markovian Models for Bridge Maintenance Management. *Journal of Transportation Engineering*, 120(1), 37-51. doi:10.1061/(ASCE)0733-947X(1994)120:1(37)
- Scott, M., Rezaizadeh, A., Delahaza, A., Santos, C. G., Moore, M., Graybeal, B., & Washer, G. (2003). A comparison of nondestructive evaluation methods for bridge deck assessment. *NDT & E International*, 36(4), 245-255.

- Setzer, M. J. (1999). Micro ice lens formation and frost damage (pp. 1-15).
- Sommer, A. M., Nowak, A. S., & Thoft-Christensen, P. (1993). Probability-based bridge inspection strategy. *Journal of Structural Engineering*, 119(12), 3520-3536.
- Stewart, M. G., & Rosowsky, D. V. (1998a). Time-dependent reliability of deteriorating reinforced concrete bridge decks. *Structural Safety*, 20(1), 91-109.
- Stewart, M. G., & Rosowsky, D. V. (1998b). Structural safety and serviceability of concrete bridges subject to corrosion. *Journal of Infrastructure systems*, 4(4), 146-155.
- Turnbull, A. (1993). Review of modelling of pit propagation kinetics. *British Corrosion Journal*, 28(4), 297-308.
- Val, D. V., & Melchers, R. E. (1997). Reliability of deteriorating RC slab bridges. *Journal of structural engineering*, 123(12), 1638-1644.
- Von Bahr, B. (1965). On the convergence of moments in the central limit theorem. *The Annals of Mathematical Statistics*, 808-818.
- Vu, K. A., & Stewart, M. G. (2005). Predicting the likelihood and extent of reinforced concrete corrosion-induced cracking. *Journal of structural engineering*, 131(11), 1681-1689.
- Washer, G., Nasrollahi, M., Applebury, C., Connor, R., Ciolko, A., Kogler, R., . . . Forsyth, D. (2014). *Proposed Guideline for Reliability-based Bridge Inspection Practices*.
- Watanabe, T., Morita, T., Hashimoto, C., & Ohtsu, M. (2004). Detecting voids in reinforced concrete slab by SIBIE. *Construction and building materials*, 18(3), 225-231.
- Yehia, S., Abudayyeh, O., Nabulsi, S., & Abdelqader, I. (2007). Detection of common defects in concrete bridge decks using nondestructive evaluation techniques. *Journal of Bridge Engineering*, 12(2), 215-225.
- Zadeh, L. A. (2006). Generalized theory of uncertainty (GTU)—principal concepts and ideas. *Computational Statistics & Data Analysis*, 51(1), 15-46. doi:10.1016/j.csda.2006.04.029

7. APPENDIX

Table A.1. NBI condition rating statistical evaluation (Graybeal et al., 2002)

Bridge	Element	Average Rating	SD	Min Rating	Max Rating	Mode Rating	# of Inspectors	Reference Rating (NDEVC)
B251	Superstructure	5.9	0.78	4	8	6	49	5
	Substructure*	6.1	0.79	3	7	6	49	6
	Deck	5.8	0.81	3	7	6	49	5
B101A	Superstructure	4.2	0.77	2	6	4	49	4
	Substructure	4.3	0.76	3	6	4	49	4
	Deck	4.9	0.94	2	7	5	48	4
B111A	Superstructure	4.6	0.86	2	7	5	49	4
	Substructure	5.5	0.77	4	7	5, 6	48	5
	Deck	5.2	0.92	3	7	6	49	4
B543	Superstructure	5.3	0.88	4	7	5	44	5
	Substructure	6.1	0.89	4	8	6	47	6
	Deck	4.8	0.94	2	6	5	48	5
B544	Superstructure	5.8	0.72	4	7	6	48	6
	Substructure	5.3	0.83	3	7	5	47	6
	Deck	4.5	0.74	3	6	5	48	4
Route 1	Superstructure	6.7	0.66	5	8	7	49	7
	Substructure	7.2	0.57	6	8	7	49	8
	Deck	7.1	0.53	6	8	7	49	7
Van Buren	Superstructure*	6.8	0.64	6	9	7	24	7
	Substructure	6.7	0.62	6	8	7	24	8
	Deck	5.8	0.92	4	7	5	24	7**

*This condition rating did not pass the χ^2 test. This means the condition rating does not follow a normal distribution, which is assumed for all condition rating categories.

**This condition rating was determined without conducting a deck sounding survey for delamination detection. If this was performed, the reference rating would be a 5.

Compatibility Equations-Variables

- ε = strain at the location indicated (in/in)
- κ = curvature at the location indicated (1/in)
- F = longitudinal contact force between the slab and girder (lbs)
- Q = internal bending moment in the composite slab and girder (in-lbs)
- Fr_i = bond force in rebar level i (lbs)
- E_{aa} = age-adjusted effective modulus of elasticity of concrete (psi)
- E_{gir} = modulus of elasticity of the girder material (psi)
- E_{rebar} = modulus of elasticity of the steel reinforcement (psi)
- μ_c = Poisson's ratio of concrete
- b_c = concrete slab width (in)
- t_c = concrete slab thickness (in)
- c_{gir} = distance from girder centroid to the deck soffit (in)
- A_{gir} = cross-sectional area of the girder (in²)
- I_{gir} = moment of inertia of the girder (in⁴)
- dr_i = cover depth of rebar level i (in)
- nr = number of rebar layers
- Ar_i = total cross-sectional area of reinforcement level i (in²)
- α_c = coefficient of thermal expansion of the concrete (in/in/F)
- α_{gir} = coefficient of thermal expansion of the girder material (in/in/F)
- α_{rebar} = coefficient of thermal expansion of the steel reinforcement (in/in/F)
- T_o, T_1, T_2 = temperature profile (F) [see Figure 3.2 on page 55]
- Tr_i = temperature at the level of rebar I (F)

Compatibility Equations-Uniform Deck Temperature Profile

Equation 1-Strain Compatibility at Deck-Girder Interface

$$\varepsilon_{c-bot} = \frac{2(1 - \mu_c^2)}{E_{aa}b_c t_c^2} \left[-3 \left(Q + \sum_{i=1}^{nr} (dr_i Fr_i) \right) + t_c \left(2F + \sum_{i=1}^{nr} (Fr_i) \right) \right] + \alpha_c (1 + \mu_c) (T_1 - T_0)$$

$$\varepsilon_{gir-top} = \frac{-1}{E_{gir}} \left(\frac{F}{A_{gir}} + \frac{c_{gir}^2 F}{I_{gir}} + \frac{c_{gir} Q}{I_{gir}} \right) + \alpha_{gir} (T_2 - T_0)$$

Equation 2-Curvature Compatibility at Deck-Girder Interface

$$\kappa_{c-bot} = \frac{6(1 - \mu_c^2)}{E_{aa}b_c t_c^3} \left[-2 \left(Q + \sum_{i=1}^{nr} (dr_i Fr_i) \right) + t_c \left(F + \sum_{i=1}^{nr} (Fr_i) \right) \right]$$

$$\kappa_{gir-top} = \frac{c_{gir} F + Q}{E_{gir} I_{gir}}$$

Equation 3-Strain Compatibility at Rebar [solve for each layer of rebar (i=1...n) present]

$$\varepsilon_{c-rebar} = \frac{1 - \mu_c^2}{E_{aa}b_c} \left[\left(\frac{6}{t_c^2} - \frac{12dr_i}{t_c^3} \right) \left(Q + \sum_{i=1}^{nr} (dr_i Fr_i) \right) + \left(\frac{6dr_i}{t_c^2} - \frac{2}{t_c} \right) F \right. \\ \left. + \left(\frac{6dr_i}{t_c^2} - \frac{4}{t_c} \right) \sum_{i=1}^{nr} (Fr_i) \right] + \alpha_c (1 + \mu_c) (T_1 - T_0)$$

$$\varepsilon_{rebar} = \frac{Fr_i}{Ar_i E_{rebar}} + \alpha_{rebar} (Tr_i - T_0)$$

Compatibility Equations- Linear Deck Temperature Profile

Equation 1-Strain Compatibility at Deck-Girder Interface

$$\varepsilon_{c-bot} = \frac{2(1 - \mu_c^2)}{E_c b_c t_c^2} \left[-3 \left(Q + \sum_{i=1}^{nr} (dr_i Fr_i) \right) + t_c \left(2F + \sum_{i=1}^{nr} (Fr_i) \right) \right] + \alpha_c (1 + \mu_c) (T_2 - T_0)$$

$$\varepsilon_{gir-top} = \frac{-1}{E_{gir}} \left(\frac{F}{A_{gir}} + \frac{c_{gir}^2 F}{I_{gir}} + \frac{c_{gir} Q}{I_{gir}} \right) + \alpha_{gir} (T_2 - T_0)$$

Equation 2-Curvature Compatibility at Deck-Girder Interface

$$\kappa_{c-bot} = \frac{6(1 - \mu_c^2)}{E_c b_c t_c^3} \left[-2 \left(Q + \sum_{i=1}^{nr} (dr_i Fr_i) \right) + t_c \left(F + \sum_{i=1}^{nr} (Fr_i) \right) \right] + \frac{\alpha_c (1 + \mu_c)}{t_c} (T_2 - T_1)$$

$$\kappa_{gir-top} = \frac{c_{gir} F + Q}{E_{gir} I_{gir}}$$

Equation 3-Strain Compatibility at Rebar [solve for each layer of rebar (i=1...n) present]

$$\varepsilon_{c-rebar} = \frac{1 - \mu_c^2}{E_c b_c} \left[\left(\frac{6}{t_c^2} - \frac{12 dr_i}{t_c^3} \right) \left(Q + \sum_{i=1}^{nr} (dr_i Fr_i) \right) + \left(\frac{6 dr_i}{t_c^2} - \frac{2}{t_c} \right) F \right.$$

$$\left. + \left(\frac{6 dr_i}{t_c^2} - \frac{4}{t_c} \right) \sum_{i=1}^{nr} (Fr_i) \right] + \alpha_c (1 + \mu_c) \left[\frac{dr_i}{t_c} (T_2 - T_1) + T_1 - T_0 \right]$$

$$\varepsilon_{rebar} = \frac{Fr_i}{Ar_i E_{rebar}} + \alpha_{rebar} (Tr_i - T_0)$$

GL 2000 Model for Shrinkage Strain

$$\varepsilon_{sh} = \varepsilon_{sh-u} \beta(h) \beta(t)$$

$$\varepsilon_{sh-u} = 1000K \left(\frac{4350}{f_{cm28}} \right)^{1/2} * 10^{-6}$$

$$\beta(h) = 1 - 1.18h^4 > 0$$

$$\beta(t) = \left(\frac{t - t_c}{t - t_c + 97(v/s)^2} \right)^{1/2}$$

- f_{cm28} = mean concrete compressive strength at 28 days of curing (psi)
- K = coefficient depending on cement type
- h = relative humidity of the surrounding environment, as a decimal
- t = time after concrete pour (days)
- t_c = age of concrete as drying commenced, after curing (days)
- v/s = volume to surface area ratio of concrete member (in)

GL 2000 Model for Creep Compliance

$$f_{cmt} = f_{cm28} \left[\frac{t^{3/4}}{a + bt^{3/4}} \right]$$

$$E_{cmt} = 500,000 + 52,000\sqrt{f_{cmt}}$$

- f_{cmt} = mean concrete strength at time t (psi)
- E_{cmt} = concrete modulus of elasticity at time t (psi)
- a, b = coefficients depending on cement type

$$J(t, t') = \frac{1}{E_{cmt'}} + \frac{\varphi_{sp}}{E_{cm28}}$$

$$\varphi_{sp} = \Phi(t_c) \left[2 \left(\frac{(t - t_c)^{0.3}}{(t - t_c)^{0.3} + 14} \right) + \left(\frac{7}{t'} \right)^{0.5} \left(\frac{t - t_c}{t - t_c + 7} \right)^{0.5} \right. \\ \left. + 2.5(1 - 1.086h^2) \left(\frac{t - t'}{t - t' + 97(v/s)^2} \right)^{0.5} \right]$$

$$t' = t_c: \Phi(t_c) = 1$$

$$t' > t_c: \Phi(t_c) = \left[1 - \left(\frac{t' - t_c}{t' - t_c + 97(v/s)^2} \right)^{0.5} \right]^{0.5}$$

- $J(t, t')$ = creep compliance (1/psi)
- t' = time of first load application since first pour (days)
- φ_{sp} = specific creep coefficient
- $E_{cmt'}$ = mean concrete modulus of elasticity at time of loading (psi)
- E_{cm28} = mean concrete modulus of elasticity at 28 days (psi)

Probability Plots-Annual Minimum Temperatures

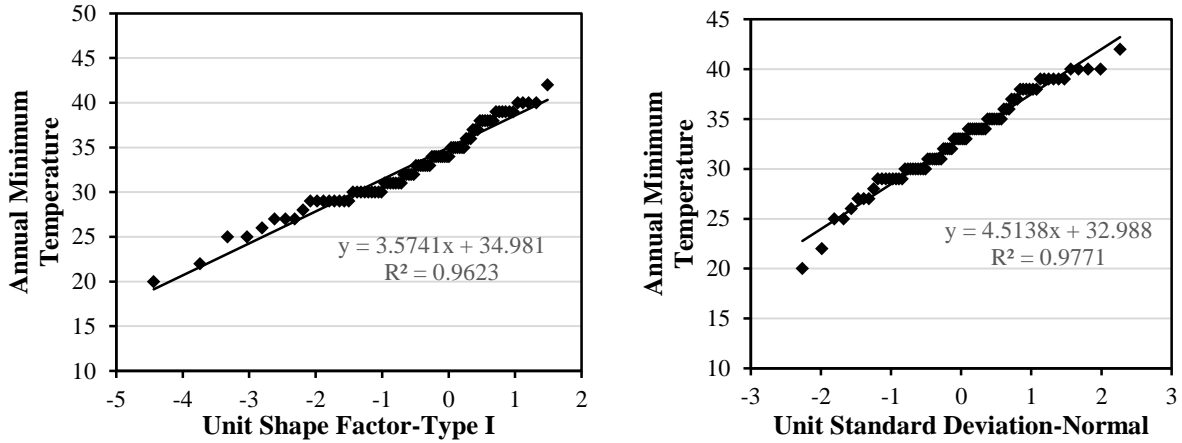


Figure A.1. Probability plots of annual minimum temperatures for Santa Barbara, CA-Type I (left) and normal (right)

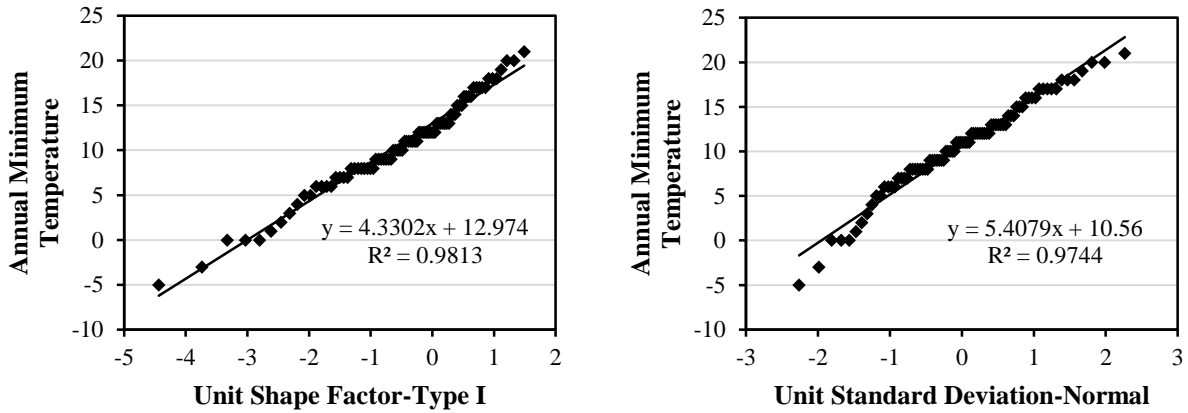


Figure A.2. Probability plots of annual minimum temperatures for Clemson, SC-Type I (left) and normal (right)

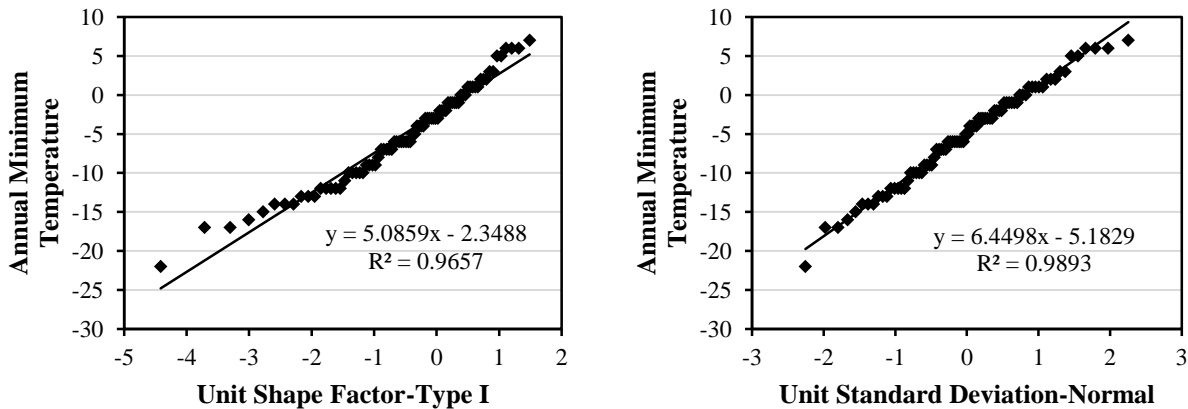


Figure A.3. Probability plots of annual minimum temperature for Ann Arbor, MI-Type I (left) and normal (right)

Probability Plots-Annual Maximum Temperature

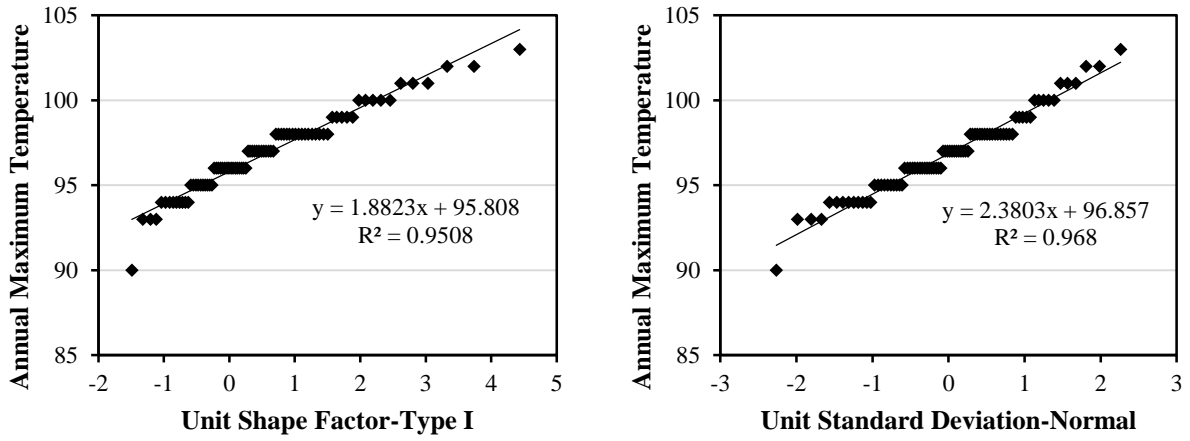


Figure A.4. Probability plots of annual maximum temperature in Fort Collins, CO-Type I (left) and normal (right)

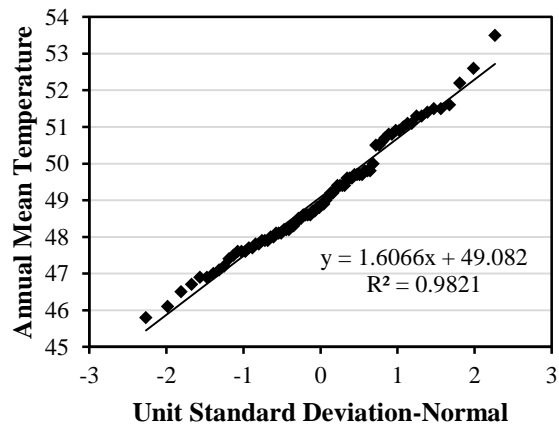


Figure A.5. Probability plot of annual mean temperature in Fort Collins, CO-normal